Motor Control in the Mesencephalic Locomotor Region: Implications for Action Diversification and Deep Brain Stimulation

Inauguraldissertation

zur Erlangung der Würde eines Doktors der Philosophie

vorgelegt der Philosophisch-Naturwissenschaftlichen Fakultät

der Universität Basel von

Manuel João Neves Ferreira Pinto

von Portugal

2022

Genehmigt von der Philosophisch-Naturwissenschaftlichen Fakultät
auf Antrag von

Fakultätsverantwortliche und Dissertationsleiterin: Prof. Dr. Silvia Arber

Korreferent: Prof. Dr. Pico Caroni

Basel, 22/06/2021

Dekan: Prof. Dr. Marcel Mayor

To my Catarina, with whom I share the pleasure of locomoting through life.

Para a minha mãe Helena, por tudo.

Em memória dos meus avós Maria Teresa e Carlos.

Em memória do meu mestre Tiago Henriques Coelho.

Table of Contents

Acknowledgments

"*If I have seen further, it is by standing on the shoulders of Giants.*"

Sir Isaac Newton

Letter to Robert Hooke, 1675

The work I developed during my PhD, as all other career related endeavors, is due to the outstanding support and contribution of the many persons who crossed my path, to whom I am eternally grateful. This section is my attempt at an impossible task: thanking all the Giants who lent me their shoulders throughout the journey.

I am especially grateful to my mentor Silvia Arber, for accepting me as a PhD student, for believing I could be a neuroscientist and for teaching me how to be one. I thank Silvia for all the inspiring scientific discussions, the encouragement and for always being an enthusiast of my ideas. Her passion for science and critical thinking are contagious. Working in her Lab was a true privilege and an amazing experience that I will fondly look back on throughout my life.

I am also in eternal debt to all the Arber Lab members. Our scientific discussions, experiments together and everything they taught me contributed decisively to my growth as a scientist and the execution of this thesis. On this note, it would be unfair not to highlight Harsh Kanodia, Antonio Falasconi, Markus Sigrist and Soledad Esposito for their outstanding contribution for the MLR project. To all of you, my deepest and sincere thank you. While working in the Arber Lab, I had the opportunity to be embedded in the amazing institutes Biozentrum and FMI, where I

had excellent technical support from the diverse facilities and was exposed to highly stimulating scientific discussions, brilliant minds and a friendly environment. I am grateful to every single person that crossed paths with me during the amazing years I worked at these institutes. I am particularly thankful to my thesis committee members Pico Caroni and Botond Roska, for significantly contributing to scientifically enrich my work.

The road that led me to being a PhD student was at least as important as the years I spent in Basel for the conclusion of this thesis. First and foremost, I thank my family for making me the person I am today and for always encouraging and supporting me throughout my life, particularly during my period away in Switzerland. I thank Catarina, my girlfriend, my best friend, my partner in life, for making me feel like Superman when I have her by my side, for helping me carry the heaviest of burdens or sharing the most joyful moments; ever since I've met her I see the world in brighter colors, and what an incredible feeling it is to love her and to know she loves me. I couldn't have done this without her unconditional support. I thank my mother Helena for always being there for me, for all the love and education, for supporting and unconditionally cheering me in every circumstance. I thank my aunt Ana Maria and my grandmother Maria Teresa who I also consider as mothers; together with my mother, they were the first important women in my life; they gave me the tools to navigate through life with a constant desire to reach further and further in the pursuit of my dreams. My major goal is to make the three of them proud. Everything I do is a reverberation of the impact they had on me since birth and, for that, I will be eternally grateful. I thank my grandfather Carlos for showing me the gift of making everyone around us happy and, especially, for giving me the most important advice I received in my life (he knows what it was). I thank my aunt Lurdes for always being there for

me and for showing me the value of unconditional family dedication. I thank my cousins Pedro, João Miguel and João Pedro for being authentic brothers to me; we share our virtues and have each other's backs. I thank my uncle João for everything he has done for me, from sharing infinite moments of suffocating laughter to stimulating my passion for science.

My path during medical school at the Faculty of Medicine of the University of Porto (FMUP) was crucial for my clinical education but also stimulated me to pursue a scientific career. At FMUP, I was fortunate to meet many inspiring people who helped shape my interest in research. I must first thank Prof. Dr. Tiago Henriques Coelho, the most prominent person in my evolution as a physician-researcher, for being an extraordinary mentor during my time as a researcher at the Physiology Department. Prof. Tiago was initially my Physiology teacher (a brilliant one), then the best research supervisor I could ask for at FMUP, and later a true friend. I will always look up to him as an extraordinary example of how to reconcile surgical, scientific and teaching careers. He was brilliant in all the three fields and if I am ever half as good as he was, I will feel accomplished. Tiago departed too soon, but I will always owe him an infinite debt of gratitude for all the encouragement through the awesome and the hard moments, for always supporting my ideas and projects and inspiring and propelling me to broaden my horizons. I am also perpetually grateful to Prof. Dr. Adelino Leite Moreira, head of the Physiology Department, for stimulating the model of the physician-researcher at the Department, for giving me the amazing opportunity to be inserted in such an environment, for showing me the incredible advantages of cultivating scientific reasoning in clinical and surgical practice and for always supporting me and investing in me as a scientist. I am also grateful to every person who worked with me for so many years at the Physiology Department, particularly

Daniel Gonçalves, Ana Filipa Silva, Rita Ferreira, Nádia Gonçalves, among so many other amazing colleagues. Still at FMUP, I fondly thank Prof. Dr. Raquel Soares for giving me my first opportunity to participate in a research project, during my first year of medical school at the Biochemistry Department. When I accepted to work with her, I had absolutely no idea that I was taking the very first step of an absolutely fascinating path through the world of science and where that road would take me! I must also thank Prof. Dr. Manuel Barbosa and my neuroanatomy teachers for instigating in me the passion for the nervous system and neurosciences which would turn out to be crucial a few years later when I chose the path I wanted for my life.

I am also grateful to the GABBA program for considering me worthy of the amazing opportunity to conduct my PhD abroad. I thank all the Coordinating Committee, especially Prof. Dr. Manuel Sobrinho Simões and Prof. Dr. Fátima Carneiro, who I particularly admire and treasure. I am also grateful to Rui Costa and Albino Oliveira Maia for taking the time and interest to talk to me and advising me on my career choices. I also thank the GABBA community and especially my colleagues from the 18th edition, for the fantastic months we spent together discussing science or just having fun.

I also have an immeasurable debt of gratitude to Prof. Dr. Rui Vaz for allowing me to postpone my medical career to pursue a full-time PhD, encouraging me throughout the journey and creating space for my scientific projects. I also extend my gratitude to all the physicians, nurses and technical staff of the Neurosurgery Department and Neurosurgery Operating Theater at Hospital São João, who received me with open arms when I started my residency and quickly made me feel a part of the team. I highlight my residency supervisor, Dr. Osvaldo Sousa, as well as my fellow residents, for their essential role in integrating me.

I must also thank my truest friends, not only for the happy childhood and adulthood we share, but also for being such a positive influence while I was developing my personality. I feel extraordinarily lucky to have met them and to count on their friendship and support (some for over 20 years). Although it is extremely ungrateful not to mention them all, I absolutely have to especially thank my friend Delfim, with whom I shared countless adventures and projects through elementary and high school, medical school, GABBA, YES Meeting, research, among so many other endeavors.

Every person mentioned, and many more, were instrumental to the development of this thesis. Thank you all!

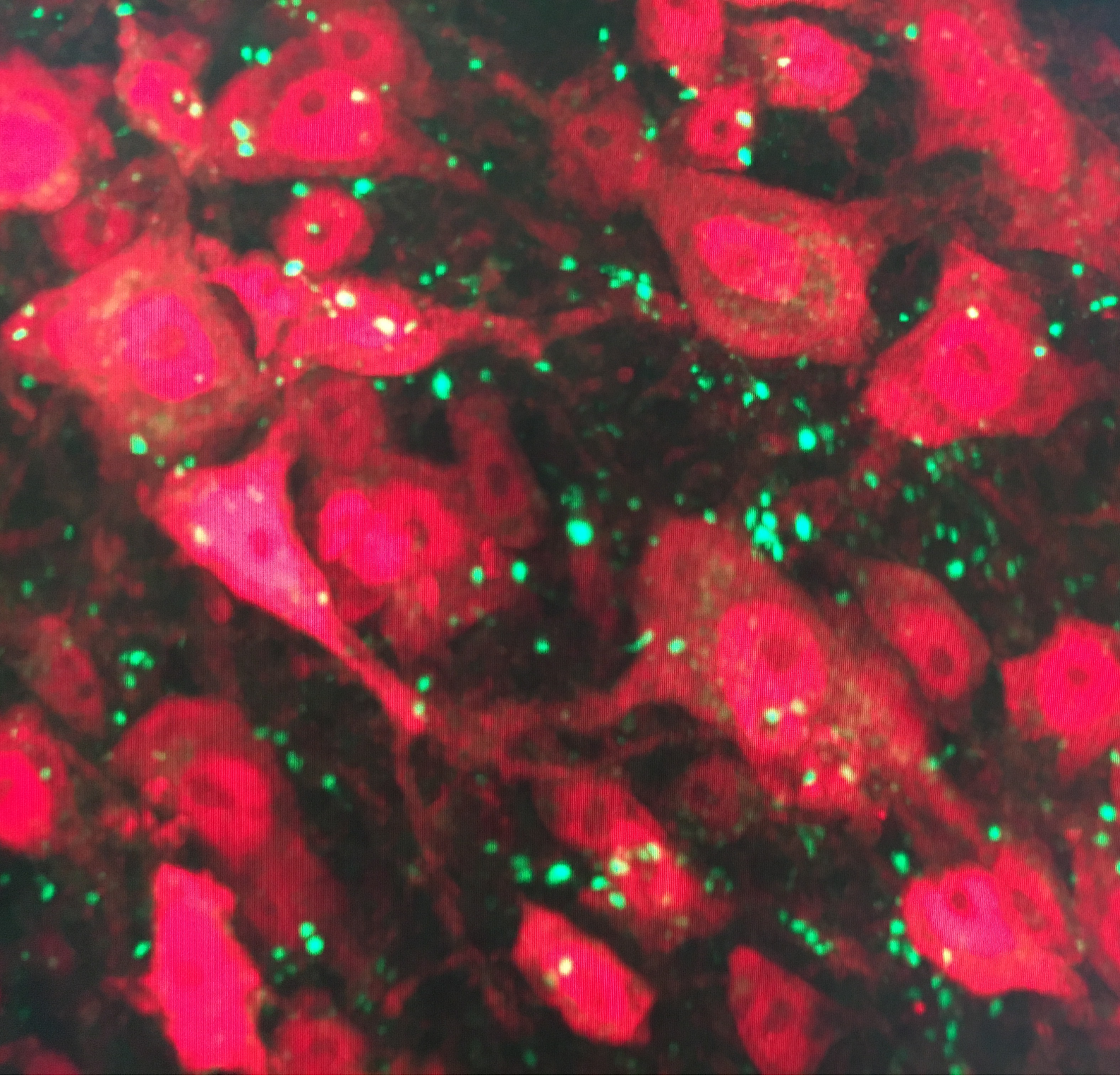

Summary

The brainstem is an evolutionarily conserved structure in vertebrate species, holding motor centers for the execution of diverse movements essential for the animal's life, including breathing, orofacial movements permitting nutrient consumption, posture and locomotion. Understanding the organization of motor programs controlling such behaviors and their specific recruitment according to external context and internal needs is an elemental quest in Neuroscience.

In the present dissertation, I discuss the brainstem as a continent for neuronal circuitry regulating movement control, at the interface between action-selection forebrain circuits and caudal executive centers in the spinal cord. After an introductory chapter, covering the main topics on the physiology of brainstem locomotor circuits, their possible dysfunction in Parkinson's Disease and potential relevance as therapeutic targets for deep brain stimulation, I present a review of the current knowledge on supraspinal circuits controlling locomotion selection (and the contextual aspects it entails, such as exploratory, appetitive and escaping) and execution (aligned with the required specific parameters, like speed, limb coordination, postural adjustments and directionality). In a third section, experimental work is presented, describing two glutamatergic subpopulations within the mesencephalic locomotor region (MLR), a spinal cord-projecting and a substantia nigra-projecting population, that segregate not only by projection-specificity but also by tuning to different behaviors and different consequences of their optogenetic manipulation. Using viral vector tools in intersection with mouse genetics, we devised experimental strategies to create local, retrograde and systemic entry-points to these specific neuronal subpopulations. Such access allowed us to map their anatomical organization within the MLR and their axonal projection patterns, to record their *in vivo* activity using micro-endoscopic calcium imaging, as well as to optogenetically manipulate them. We

concluded that the spinally-projecting population regulates body length and, consequently, postural adjustments during behavior, while the substantia nigra-projecting neurons preferentially encode the forelimb movements reaching and grooming and impinge on the basal ganglia circuitry to shape its motor output. The significance of these findings for the fields of MLR basic research and clinical application of PPN-DBS are discussed in the final chapter.

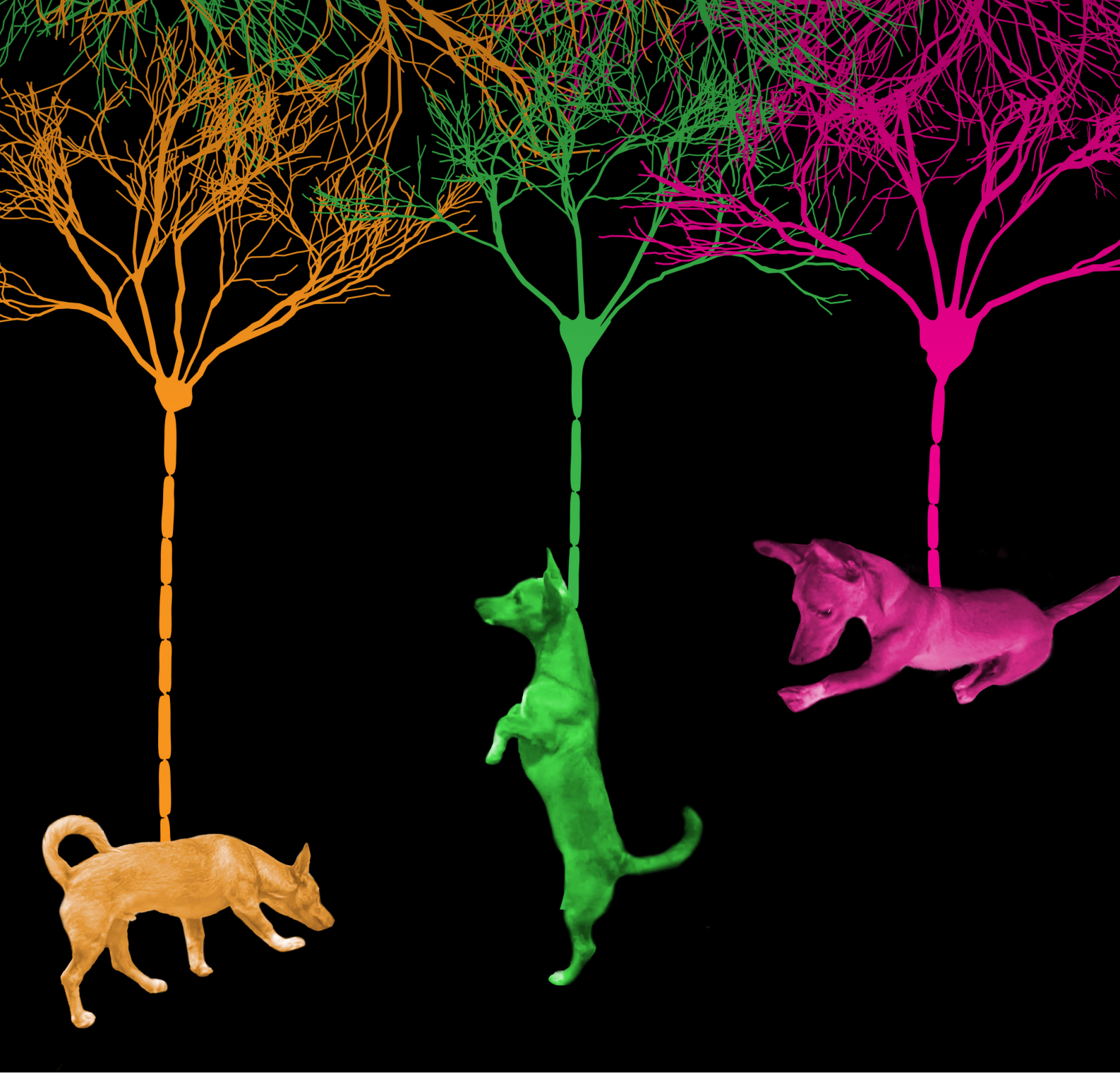

Section 1:
Introduction

Locomotion is the motor system's solution to translocate the body in terrestrial animals. The development of a locomotor system allows animals to interact with the outside world, moving towards matters of interest such as food, water, warmth and mating or away from unpleasant or potentially threatening environments. Understanding the neuronal network guiding the selection and execution of locomotion is a prominent field in Neuroscience. Considering motor control in general, the final execution of a motor action requires the concerted activity of neuronal populations residing across diverse locations within the central nervous system (CNS) (Arber and Costa, 2018). Dedicated structures are concerned with planning the motor action, evaluating contextual factors obtained from sensory information (visual, auditory, proprioceptive, nociceptive, among others), memory from past experiences, and computing internal needs (such as hunger, thirst, fear); at the same time, executive centers integrate this information and ensure that specific neuronal populations are recruited in order to generate the desired movement, when to initiate and when to stop it and how vigorous it should be.

Regarding locomotion, evidence from seminal studies reveals that the brainstem holds crucial circuitry commanding its execution, as decerebrated cats submitted to CNS transection at a pre-collicular, post-mammillary level ("the mesencephalic cat") maintain the ability to generate properly coordinated, full-body locomotion with adequate posture (Bard and Macht, 1958). These primordial findings demonstrated that there are neuronal populations within the brainstem capable of recruiting the spinal cord circuitry required for locomotion and postural adjustments, independently of forebrain structures including the thalamo-cortico-basal ganglia circuits. Although the mesencephalic cat displayed properly coordinated gait across the 4 limbs, the locomotion phenotype was described as "machine-like" in the sense

that it was a stereotyped behavior, and animals were unable to adapt to unexpected perturbations on the ground or integrate visual cues for visuomotor coordination during locomotion (Grillner, 1975; Mori et al., 1983; Shik and Orlovsky, 1976). In fact, motor planning and preparatory activity are believed to rely on cortical circuits, communicating with thalamic and brainstem centers (Bretzner and Drew, 2005; Drew et al., 2008; Drew and Marigold, 2015; Svoboda and Li, 2018).

The Enigmatic Mesencephalic Locomotor Region

The observations on the mesencephalic cat propelled the search for locomotion eloquent regions in the brainstem. By applying electrical stimulation to map the cat brainstem, Shik and colleagues described a region in the mesencephalon where electrical stimulation elicits properly coordinated, full-body locomotion (Shik et al., 1966) at a wide range of gaits and speeds that scale with stimulation frequency (Shik and Orlovsky, 1976). This region was named the mesencephalic locomotor region (MLR) and, ever since its description, historical research on supraspinal control of locomotion has been intrinsically connected with the study of the MLR. After the first descriptions in the cat, evidence for the existence of the MLR in several vertebrate species, including lamprey, rodents, non-human primates and humans, has been presented (Grillner et al., 1997; Le Ray et al., 2011), suggesting that this structure, like many locomotion-related regions, has been highly conserved throughout the evolution of vertebrates (Alam et al., 2011).

Following the first report of the MLR, many studies attempted to define the neuronal substrate for the locomotion-promoting response. In fact, having been mapped with electrical stimulation, the definition of MLR is not an anatomical, but a functional one, lacking both fine anatomical resolution or cell-type/neurotransmitter-

identity precision and so, the true neuronal identity of the MLR has been an ongoing subject of debate. The locomotion-responsive area encompasses a vast mesencephalic region bordered laterally by the lateral lemniscus, medially by the periaqueductal gray (PAG), dorsally by the superior and inferior colliculi and ventrally by the decussation of the superior cerebellar peduncles. The most reported candidates described in electrical and chemical stimulation studies are the pedunculopontine nucleus (PPN), the more dorsally located cuneiform and pre-cuneiform nuclei (CNF and pre-CNF) as well as the mesencephalic reticular formation (mRT) between and adjacent to them (Depoortere et al., 1990; Garcia-Rill and Skinner, 1987; Jordan, 1998; Mori et al., 1989; Roseberry et al., 2016; Shik and Orlovsky, 1976; Shik et al., 1966; Sinnamon, 1993; Skinner and Garcia-Rill, 1984). These nuclei comprise intermingled populations of glutamatergic and GABAergic neurons, and the PPN also contains cholinergic neurons (Martinez-Gonzalez et al., 2011; Wang and Morales, 2009).

While seminal studies did not resolve the anatomical definition of the locomotion-promoting nuclei and neurons, the development of viral and genetic tools to interrogate brain circuits opened the possibility to answer these long-lasting questions. Recent studies employing cell type-specific optogenetic manipulations have elegantly dissected neurotransmitter-defined populations within the mouse MLR and represent remarkable progress towards the understanding of this complex region and its critical role as a supraspinal regulator of locomotion (Caggiano et al., 2018; Capelli et al., 2017; Josset et al., 2018; Lee et al., 2014; Roseberry et al., 2016). Importantly, they identified glutamatergic neurons as the source of the locomotion promoting response and implicate CNF in the execution of high-speed locomotion. However, discrepancies regarding the role of glutamatergic PPN neurons in

locomotion persist, demonstrating that the MLR holds further layers of complexity that cannot be fully resolved with neurotransmitter-specificity alone, calling for additional entry points to interrogate their function. Section 2 of this dissertation reviews recent studies employing genetic access to MLR subpopulations (and other supraspinal centers implicated in locomotion control), emphasizing the different functions that have been attributed to neurotransmitter-identified neurons and exploring ongoing controversies on MLR organization. Section 3 depicts a new experimental approach, combining neurotransmitter and axonal projection specificities in order to explore anatomical and functional diversity within the MLR. Of note, we describe further anatomical and functional segregation within glutamatergic MLR subpopulations which contribute to resolve ongoing debate on MLR function and to the comprehension of its complex role in motor control, far beyond locomotion.

Integrating the MLR in the Global Network of Locomotion Control

According to the current model, the MLR receives diverse input from upstream structures providing contextual information, including the basal ganglia output nuclei *substantia nigra pars reticulata* (SNr) and internal *globus pallidus* (GPi), the subthalamic nucleus (STN), the cerebral cortex, the PAG, the superior colliculus, among other identified structures (Caggiano et al., 2018; Martinez-Gonzalez et al., 2011; Roseberry et al., 2016; Ryczko and Dubuc, 2013), and broadcasts the locomotion signal by activating caudal reticulospinal neurons which will, in turn, recruit spinal cord circuits that promote behavioral execution (Caggiano et al., 2018; Capelli et al., 2017). By receiving information from various sources and having privileged access to downstream targets, it is believed that the MLR controls the execution of locomotion under different contexts, such as cognitively-selected exploratory

locomotion as well as primary appetitive (predatory) and defensive (escaping) forms of locomotion (Caggiano et al., 2018; Jordan, 1998; Ryczko and Dubuc, 2013; Sinnamon, 1993). In fact, different channels within the MLR seem to be dedicated to execution of specific modes of locomotion, a concept that is further explored in Section 2. Briefly, evidence demonstrates that glutamatergic CNF neurons orchestrate high-speed, synchronous-gait locomotion in the context of escaping behavior, while for the glutamatergic PPN, one study points towards a role in low-speed, alternating gait locomotion in the context of exploratory activity (Caggiano et al., 2018), while another study finds locomotion-inhibiting responses with activation of glutamatergic PPN neurons (Josset et al., 2018). Additionally, glutamatergic MLR neurons also contact several rostral regions, such as the basal forebrain and the ventral tegmental area (VTA) and modulate locomotion-related brain processing (Lee et al., 2014; Yoo et al., 2017), ensuring a proper and integrated mobilization of the central nervous system during the execution of the complex full-body behavior that is locomotion. Section 3 explores a specific pathway from the MLR to the basal ganglia and its role in the regulation of motor control.

MLR disfunction as a potential therapeutic target for Parkinson's disease

The importance of the MLR in locomotion control that stemmed from electrical mapping studies has also triggered the interest of the clinical community studying Parkinson's disease (PD). This neurodegenerative disorder leads to the loss of dopaminergic neurons in the substantia nigra compacta causing a deficit of dopamine in the striatum and throughout the basal ganglia (Albin et al., 1989; Dauer and Przedborski, 2003; DeLong, 1990). This is believed to strongly impact the normal physiology of the basal ganglia action selection circuits causing the motor symptoms

rigidity, bradykinesia, difficulties in initiating, stopping and switching between motor programs. However, the motor symptoms go beyond muscle tone and movement speed and transition problems, with some PD patients experiencing severe axial symptoms such as postural instability and gait impairment, with frequent episodes of freezing, that can lead to falls and severe morbidity. While bradykinesia and rigidity significantly improve with pharmacological dopamine signal enhancement and deep brain stimulation of the STN, postural and gait symptoms are particularly refractory to the current therapeutic strategies (Ferraye et al., 2010), suggesting that perturbation of other circuits beyond dopaminergic signaling could be implicated in their genesis. In fact, PD does not solely affect the SNc but produces a global neurogenerative process across the brain, particularly in the brainstem (Braak et al., 2002; Goedert, 2015). Given the significant role in locomotion control attributed to the MLR, the scientific community raised the possibility that gait symptoms could be caused by malfunction at the MLR level. This hypothesis was further boosted by studies documenting cholinergic PPN neuron loss in PD (Hirsch et al., 1987) and that PD patients with gait symptoms had more severe degeneration of cholinergic PPN neurons than PD patients without locomotion problems (Karachi et al., 2010). These two findings together were sufficient to boost the pursuit of the PPN as a target for DBS in patients with gait impairment, in an attempt to treat this symptom.

The first PPN implantations were described in 2005 (Mazzone et al., 2005; Plaha and Gill, 2005) and since then, accumulated experience with PPN-DBS has produced unconvincing results overall (Golestanirad et al., 2016; Wang et al., 2017; Yu et al., 2020). There are still ongoing debates on multiple issues not yet resolved (Garcia-Rill et al., 2019), such as the exact location to target, with some studies suggesting that the CNF should be the target instead of the PPN (Chang et al., 2020;

Ferraye et al., 2010), the best stimulation parameters, potential side effects and specific patient features to be considered when defining candidates for this procedure. A possible explanation for the disappointing outcome of PPN-DBS is the inadequate knowledge on the basic neurobiology of this region, whose high complexity could not be dissected with the previous methodologies of electrical or chemical manipulations applied locally in a region with distinct neuronal populations residing in close proximity. Only with the development of the recent technology for dissecting neuronal circuits with cell-type, projection and genetic specificity can we access and interrogate specific neuronal populations in order to better understand the neuronal control of locomotion and movement in general that is encoded in the PPN and the global MLR region.

The present dissertation addresses the ongoing questions regarding the neuronal control of movement at the level of the MLR. In Section 2, I review historical and recent literature concerning supraspinal circuits controlling locomotion orchestration; unresolved topics are discussed and potential entry points to study them are proposed. Section 3 describes experimental work contributing to elucidate the complexity of MLR circuitry organization. Our results implicate the classically defined MLR region in motor control functions far beyond locomotion. This complexity is explained by segregated neuronal populations residing in close proximity within the MLR, but with distinct connectivity maps and activity patterns during behavior. In the final Section, I further discuss these findings in light of the current literature and present my view on their potential impact in resolving the ongoing controversies at two different dimensions: the basic scientific community studying the organization of motor control circuits as well as the clinical community trying to target neuronal circuits to treat movement disorders such as PD.

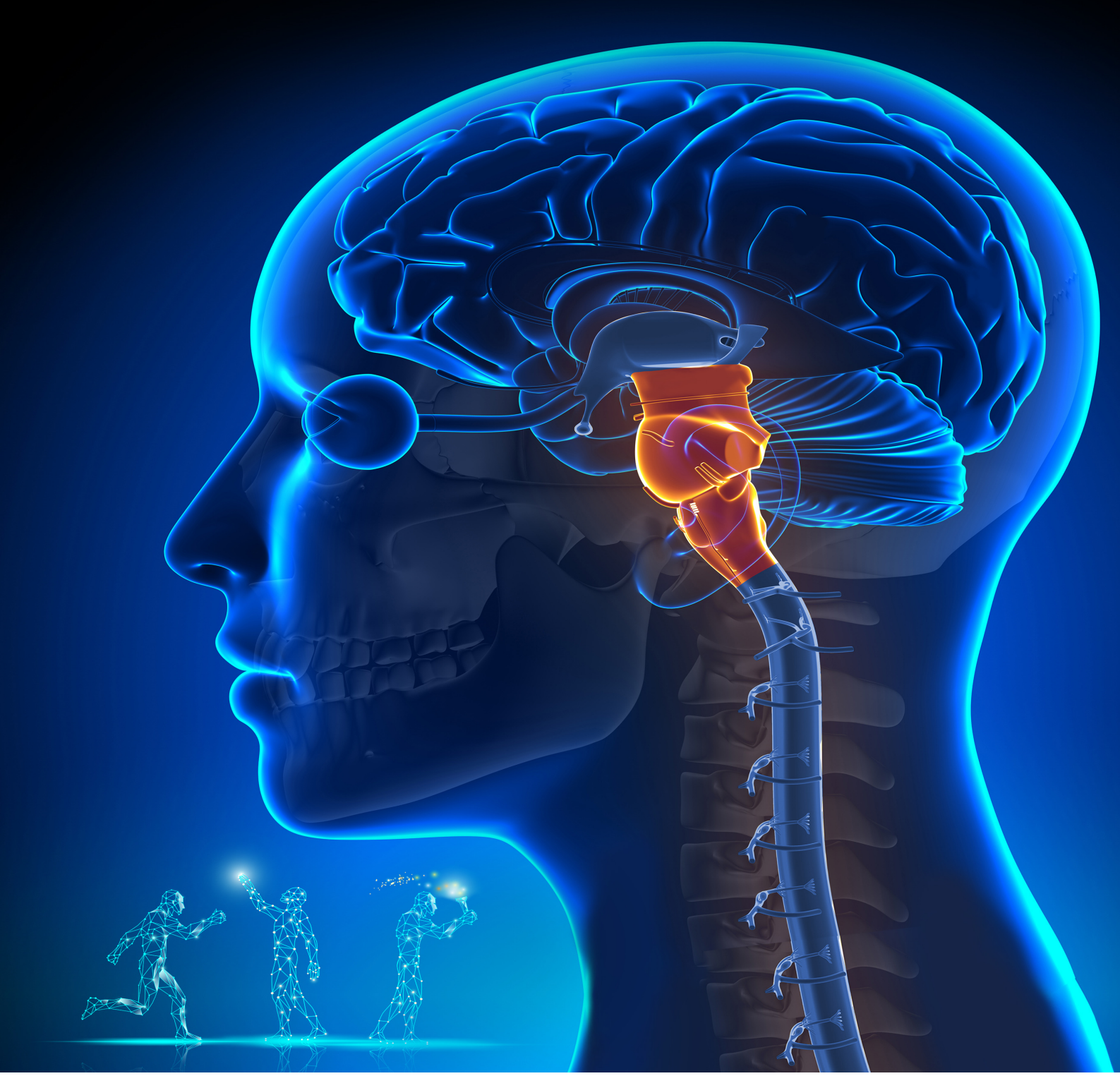

Section 2: Connecting circuits for supraspinal control of locomotion

Manuel J. Ferreira-Pinto[1], Ludwig Ruder[1], Paolo Capelli[1] and Silvia Arber

[1] These authors contributed equally

Neuron 2018

Summary

Locomotion is regulated by distributed circuits and it is achieved by the concerted activation of body musculature. While the basic properties of executive circuits in the spinal cord are fairly well understood, the precise mechanisms by which the brain impacts locomotion are much less clear. This review discusses recent work unraveling the cellular identity, connectivity and function of supraspinal circuits. We focus on their involvement in the regulation of the different phases of locomotion and their interaction with spinal circuits. Dedicated neuronal populations in the brainstem carry locomotor instructions including initiation, speed and termination. To align locomotion with behavioral needs, brainstem output structures are recruited by midbrain and forebrain circuits that compute and infer volitional, innate and context-dependent locomotor properties. We conclude that the emerging logic of supraspinal circuit organization helps to understand how locomotor programs from exploration to hunting and escape are regulated by the brain.

Introduction

Locomotion is the undoubtedly most universal and conserved form of movement of the virtually endless variety of behaviors that animal and human bodies perform. Understanding the mechanisms within the nervous system involved in controlling its planning and execution has been a longstanding scientific quest. Early studies have advanced the field by delineating regions in the nervous system linked to the control of locomotion through performing lesion experiments, pharmacological interventions, electrical stimulations and neuronal recordings. This body of work provided first important insights into how the nervous system controls locomotion, including the identification of key regions distributed throughout the nervous system, which will provide the organizational anchor points for this review.

Recent technological advances have revolutionized neuroscience and in parallel also strongly influenced research on the control of movement. These novel insights have transformed the way we think about the control of locomotion. It is now clear that defined neuronal cell types, characterized by various means including molecular, developmental and/or distinct synaptic input-output organization, are embedded into specifically wired neuronal circuits to implement many different aspects of locomotor function. Such work has been pioneered in the spinal cord and reviewed extensively (Alaynick et al., 2011; Arber, 2012; Goulding, 2009; Grillner and Jessell, 2009; Kiehn, 2016), allowing us to here only briefly summarize this work with an emphasis on some of the most recent relevant studies. On the other hand, the elucidation of specific supraspinal circuit architecture and organization using these emerging technologies has only just begun. We will highlight and synthesize predominantly a selection of this most recent literature on supraspinal control of locomotion. Our emphasis will be on circuit- and cell type-level insight and how

identified neuronal populations integrate into the complex locomotion-controlling circuitry of the nervous system. We refer readers to previously published review articles for historic coverage of this topic. To set the stage for this review, we will first briefly dissect the behavioral process of locomotion into temporal and regulatory categories. We will return to these definitions throughout the review with the goal to identify explanatory circuit level solutions for controlling and adjusting locomotion according to behavioral needs.

Dividing locomotion into temporal and regulatory behavioral categories

Three temporally separate behavioral phases accompany locomotion (Figure 1A). Initiation and termination are the two boundary events defining a locomotor episode. Transition from a stationary period or from another motor behavior to a locomotor episode can entail different circuit-level events to begin this full body action. It can be caused by a sensory stimulus such as a fearful encounter with a predator leading to an escape response, but also often occurs in the absence of obvious external triggers. Such initiations can be linked to internal needs, including hunger and thirst, but can also be caused by cognitive decisions or planning leading to exploration. In analogy, termination of locomotion can occur for a variety of reasons depending on the encountered behavioral context, ranging from immediate stopping with a freezing response to more gradual termination due to arrival at a food source or encountering an interesting object.

The time frames flanked by initiation and termination encompass the locomotor episode itself (Figure 1B). Each episode can be described by a set of behavioral attributes, patterns or categories. One important attribute during ongoing locomotion is speed. Locomotor behavior ranges from low-speed exploration to high-speed

escape running. Speed can also fluctuate within a given locomotor episode by virtue of acceleration and deceleration. Second, during locomotion, quadrupedal animals move their limbs in coordinated and stereotype patterns called gaits (Bellardita and Kiehn, 2015; Halbertsma, 1983; Lemieux et al., 2016). Behavioral studies in different species provide evidence that gait selection occurs linked to different speed ranges. Notably, during low-speed exploratory locomotion, many quadrupedal animals alternate paired fore- and hindlimbs respectively and exhibit synchrony in diagonal fore- and hindlimbs. In contrast, high-speed escape running goes hand in hand with bound gait selection. These observations suggest that a given gait likely represents the optimal biomechanical solution for the chosen speed range. Another behavioral attribute during locomotion is its directionality. Animals only rarely locomote along the shortest straight trajectory and they as well as humans also have the ability to locomote backwards, using the same muscles in different configurations, likely controlled and mediated by different networks (Choi and Bastian, 2007; Wang et al., 2011). This review will focus mainly on quadrupedal locomotion, although likely similar principles apply to bipedal locomotion, swimming, and flight.

Diversity and specificity in spinal circuits for execution of locomotion

The spinal cord harbors neuronal circuits required for the execution of locomotion. Skeletal muscles receive their commands for contraction from spinal motor neurons that are grouped into topographically arranged motor pools according to the innervated muscles (Romanes, 1951). Understanding the behavioral phenomenon of locomotion can therefore essentially be paraphrased into the question

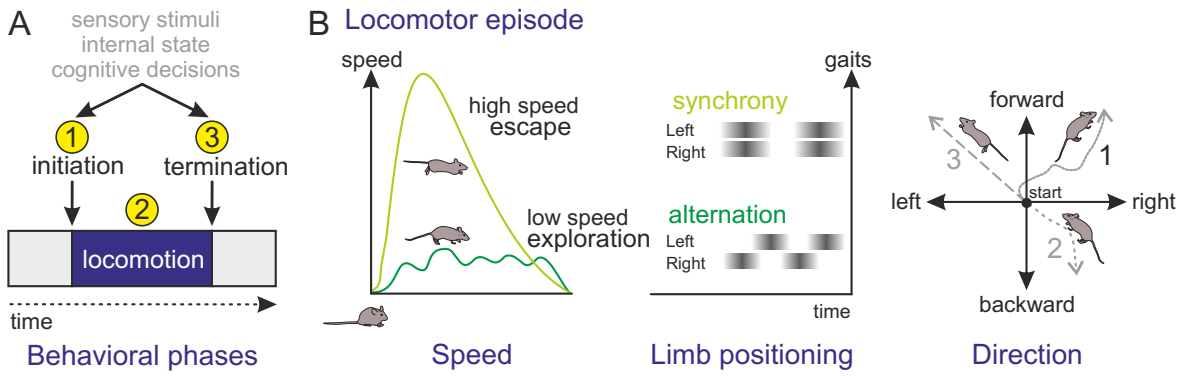

Figure 1. Temporal and regulatory categories of locomotion

(A) Division of the locomotor process in three behavioral phases (initiation, locomotion, and termination).

(B) A locomotor episode can range from low-speed exploration to high-speed escaping, during which different locomotor speeds align with alternating or synchronous gait patterns, and can have different directions of the chosen trajectory.

---

of how the temporally stereotypically patterned muscle activation inherent to locomotion is achieved through regulation of synaptic inputs to motor pools. Although many of these inputs arise from spinal neurons, the locomotor program requires supraspinal or sensory sources located outside the spinal cord for initiation, maintenance and adjustment. In fact, complete spinal transection in mammals leads to permanent paralysis of body parts innervated by segments below injury (Dietz, 2010; Shik and Orlovsky, 1976). In the absence of supraspinal input, spinal circuits can still be recruited for basic locomotion by either sensory feedback activation or application of neurochemical substances (Forssberg et al., 1980; Miller and van der Meché, 1976). These observations were extensively leveraged in reduced *in vitro* preparations, in which neonatal spinal cords are stimulated electrically or pharmacologically to delineate the function of broad spinal interneuron classes defined by genetics. It is now clear that the different spinal subpopulations are organized into specific circuit modules and contribute differentially to locomotion. These spinal networks that are also referred to as central pattern generators (CPGs) can generate locomotor pattern and rhythm upon extrinsic synaptic input, through microcircuits

encompassing interneuron subtypes and motor neurons (Alaynick et al., 2011; Arber, 2012; Goulding, 2009; Grillner and Jessell, 2009; Kiehn, 2016).

Spinal neurons are derived from different, transcriptionally-defined dorso-ventral progenitor domains during development, with several classes implicated in the regulation of important aspects of locomotion including interlimb coordination, speed and rhythmicity, work reviewed extensively elsewhere (Arber, 2012; Goulding, 2009; Jessell, 2000; Kiehn, 2016). While the existence of diversity beyond single progenitor domain origin was already apparent early on (Alaynick et al., 2011), a key open question has been the extent to which neurons diversify in the spinal cord to support generation of locomotor and other movement output of the body. It is also essential to resolve how a given population of spinal neurons defined by developmental and/or transcriptional entry points aligns to the functional attributes observed during *in vivo* locomotion. Recent work reviewed below has begun to shed light on these aspects of spinal neuron diversification, focusing on dorso-ventral and rostro-caudal axis, as well as the organization and connectivity of spinal neurons into circuits beyond local microcircuits (Figure 2A-D).

In adult zebrafish, motor neurons of the slow, intermediate and fast subtype are recruited progressively with increasing swimming speed (Ampatzis et al., 2013). Intriguingly, separate and speed-dependent modules also exist within the V2a spinal neuron population (Figure 2A). These V2a subpopulations exhibit preferential connectivity to corresponding motor neuron subtypes, and neurons within the same V2a submodule are interconnected but only rarely connect across submodules (Ampatzis et al., 2014). This study thus defines specific V2a neuron ensembles in the spinal cord aligned with locomotor speed to match behavioral need. In mice, execution of quadrupedal locomotion at higher speeds is accompanied by gait changes with limb

coordination changing from alternating to synchronous patterns (Bellardita and Kiehn, 2015; Lemieux et al., 2016), raising the question of how speed and gait phenomena are linked and whether they are mediated at least in part by spinal circuits. Developmental ablation of V2a neurons leads to deficits in hindlimb coordination exclusively at higher speeds in adult mice (Crone et al., 2009). These findings suggest that V2a neurons also exhibit speed-dependent roles in mice, but it is currently unclear whether functional subdivisions for V2a neurons similar to zebrafish exist. In addition, V0 spinal neurons subdivide into predominantly excitatory V0v (marked by Evx1) and mostly inhibitory V0d (marked by Pax7) subtypes, and these two classes exhibit distinct roles in maintenance of gait parameters adequately aligned with increasing speed during quadrupedal locomotion (Talpalar et al., 2013) (Figure 2A), phenotypes not discernable by studying V0 neurons as an entity. Locomotor parameters are also shaped by central processing of sensory feedback (Rossignol, 2006; Windhorst, 2007). Recent work identified an inhibitory spinal interneuron class characterized by the expression of RORβ orphan nuclear receptor (Koch et al., 2017) (Figure 2B). This population might gate proprioceptive information during the swing phase of the step cycle, acting by virtue of presynaptic inhibition of myelinated sensory and likely proprioceptive afferents. In the absence of these neurons, mice exhibit a peculiar duck-gait locomotor phenotype.

Gene expression analysis and computational methods are potent catalyzers to systematically unravel cellular diversity, also in the spinal cord (Bikoff et al., 2016; Hayashi et al., 2018; Sweeney et al., 2018). Focusing on V0-V2 spinal neuron distribution along the rostro-caudal axis, different patterns and gene expression profiles were observed comparing cervical, thoracic and lumbar levels (Francius et al., 2013). A more recent study dissected V2a neuron diversity in mice, demonstrating that

the expression of one of its canonical markers *Chx10* shows postnatal rostro-caudal expression differences (Hayashi et al., 2018) (Figure 2C). Notably, V2a type II neurons are characterized by low Chx10 expression, preferential residence at cervical segments and establishment of ascending axons to supraspinal targets. In contrast, the V2a type I cohort maintains Chx10 expression and is present at both lumbar and cervical levels (Figure 2C). What might be the mechanisms by which spinal neurons diversify along the rostro-caudal axis? It is well-established that rostro-caudal identity in motor neurons is driven by differential developmental expression of Hox transcription factors (Philippidou and Dasen, 2013). Evidence now supports the idea that this principle extends to other spinal neurons, where V1 spinal neuron diversification along the rostro-caudal axis can be regulated by Hox transcription factors independent of segmental motor neurons (Sweeney et al., 2018).

Most work aimed at understanding neuronal diversity in the spinal cord has focused on local circuit mechanisms. Yet, precise interactions of distributed spinal microcircuits along the length of the spinal cord is essential for locomotion, especially in quadrupedal animals where distant limbs must be coordinated to enable locomotion. While neuronal mechanisms involved in left-right coordination of hindlimbs are mostly driven by segmental spinal neurons and fairly well understood (Kiehn, 2016), much less is known about circuit mechanisms for fore- and hindlimb coordination. A recent study demonstrated that long projection neurons interconnecting the cervical and lumbar spinal cord are important in coordinating fore- and hindlimb patterns during high-speed locomotion as well as for maintenance of postural stability (Figure 2C) (Ruder et al., 2016), and silencing of lumbar spinal neurons projecting in ascending direction elicits similar phenotypes (Pocratsky et al., 2017). The characterized long projection neurons are composed of a major excitatory and a minor inhibitory

population derived from distinct developmental origin, each establishing specific projection patterns (Figure 2C). Furthermore, long descending projection neurons receive synaptic inputs from many centers in the brain engaged in the regulation of locomotion, and thus provide a neuronal substrate for integration and broadcasting of supraspinal information throughout the circuitry of spinal cord to coordinate locomotion.

Together, these findings demonstrate that important parameters of subtype identity for spinal neurons during early development arise by transcriptional programs intersecting along the dorso-ventral and rostro-caudal axis. These interactions as well as usage of emergent spinal networks likely dictate the ultimate connectivity of neurons into specific circuit modules as well as their function. Recent work demonstrates that the diversity of spinal neurons is higher than originally anticipated, foreshadowing the likely existence of microcircuits endowed with dedicated functions in the execution of locomotion. One big challenge is to unravel how such spinal microcircuits process input from descending pathways and sensory feedback circuits. Clearly, how long-range supraspinal inputs trigger the engagement of specific spinal microcircuit modules is instrumental for the execution of motor programs driving any form of body movement including locomotion (Figure 2D). We will now focus on supraspinal locomotion-regulatory signals in the brain and how they are conveyed to executive circuits in the spinal cord.

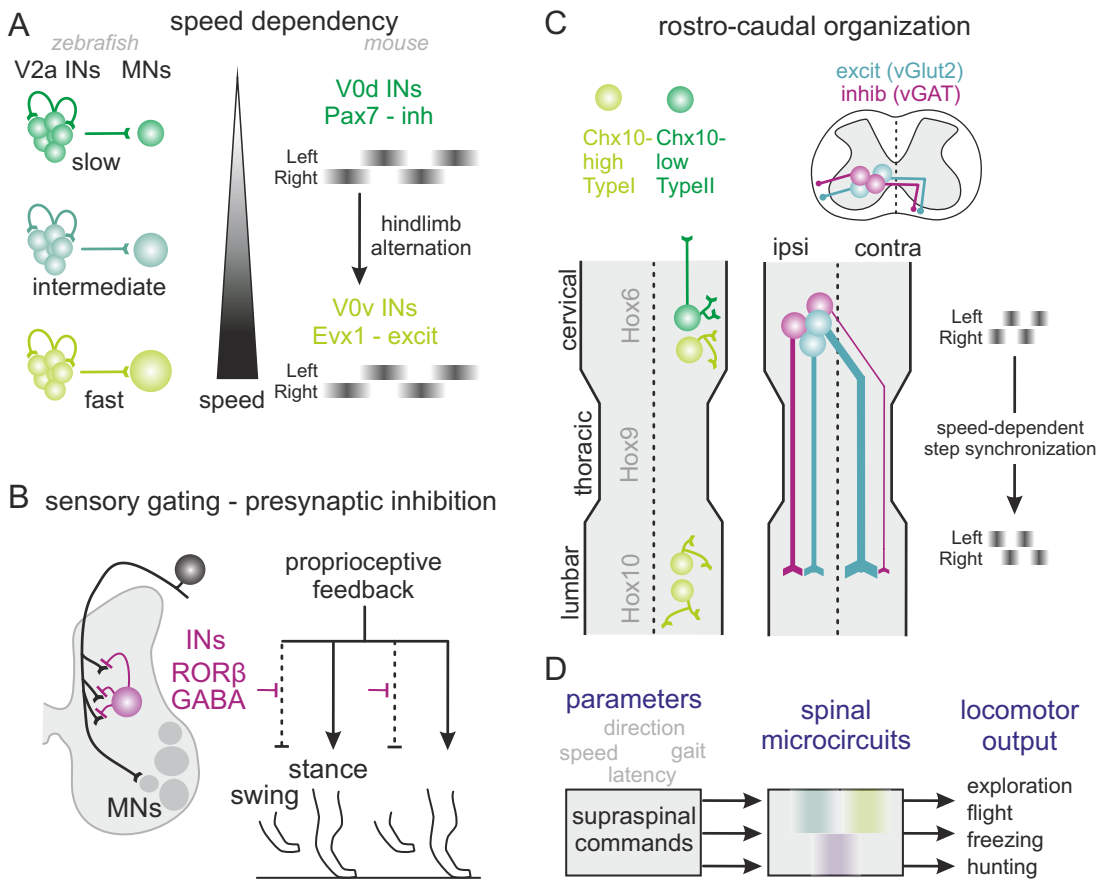

Figure 2. Diversity and specificity in spinal circuits for execution of locomotion

(A) Summary diagram of spinal circuits in zebrafish (left) and mice (right) implicated in speed control.

(B) Schematic summary of the role of ROR□-expressing spinal GABAergic neurons in sensory gating through presynaptic inhibition and influence on behavior.

(C) Rostro-caudal organization of spinal circuits based on Chx10-expression levels, Hox transcription factor expression (left), or the organization of descending projections from the cervical to the lumbar spinal cord and their influence on fore- and hindlimb coordination during locomotion (right).

(D) Proposed model of how supraspinal commands may signal locomotor parameters including speed, gait, latency or direction to spinal executive microcircuits that in turn regulate locomotor output.

Dissection of brainstem circuits regulating locomotor execution

Classical work performed in cats has mapped regions in the brain whose electrical stimulation elicits coordinated locomotion (Mori et al., 1989; Shik and Orlovsky, 1976; Shik et al., 1966). Several prominent regions were identified in the diencephalon, midbrain and ventral to the cerebellum. We will focus here on the mesencephalic locomotor region (MLR) in the midbrain due to recent progress in its characterization. Electrical stimulation of the MLR in cats elicits coordinated locomotion at a wide range of speeds and gaits scaling with applied stimulation frequency (Shik and Orlovsky, 1976). Still today, this functionally defined site is considered a key region in the supraspinal orchestration of locomotion. According to a unifying model based on many studies, the MLR integrates inputs from numerous brain regions and regulates locomotion in a context-adequate manner (Jordan, 1998; Ryczko and Dubuc, 2013) (Figure 3A). It accesses executive spinal circuits mostly by recruiting neurons residing in the reticular formation of the caudal brainstem acting as intermediaries to transmit locomotor signals to the spinal cord. Supporting such a model, MLR stimulation in conjunction with cooling the ventral medulla to attenuate synaptic transmission blunts transfer of the locomotor signal and its execution to the spinal cord (Shefchyk et al., 1984). This work suggests the existence of neurons in the reticular formation with a key role in the locomotor process. Homologous regions in the brainstem of several vertebrate species including humans have been identified (Grillner et al., 1997; Le Ray et al., 2011). These findings suggest that the concept of an MLR region and associated downstream structures in the brainstem are evolutionarily conserved throughout the vertebrate lineage, although some connectivity differences likely exist, perhaps also reflecting the adaptation of neuronal circuits to support bipedalism (Alam et al., 2011). We will now briefly summarize

historic entry points and debates in the field of how brainstem circuits between the MLR and the reticular formation impact locomotion and describe the most recent studies beginning to resolve the circuit mechanisms underlying these processes.

Historical perspective and open questions on MLR organization and function

Since the first description of the MLR following a functional definition, many studies have sought to pinpoint the exact location of the locomotion-promoting site and its neuronal identity in numerous animal models. Original studies in cats reported that the anatomical substrate of the MLR corresponds to the cuneiform nucleus (CNF) and its vicinity (Shik and Orlovsky, 1976). Interestingly, CNF stimulation in both rats and cats generates a type of locomotion that resembles aversive, escaping behavior with high-speed running at synchronous gaits and explosive jumps (Depoortere et al., 1990; Mori et al., 1989). Given the findings that the CNF also modulates nociception, cardiovascular and respiratory responses (Ryczko and Dubuc, 2013), it was proposed that the CNF supports defensive forms of locomotion (Jordan, 1998). Electrical mapping of the MLR in rats demonstrated that locomotion could be elicited by stimulation of both the CNF and the pedunculopontine nucleus (PPN) (Skinner and Garcia-Rill, 1984), but the region with the shortest latency was mapped to the caudal part of the PPN, coinciding with a distinct cholinergic cell cluster and its vicinity (Garcia-Rill et al., 1987). Given the absence of explosive behaviors elicited by PPN stimulation and the selective connectivity of the basal ganglia (BG) with the PPN (Martinez-Gonzalez et al., 2011), it was proposed that the PPN might mediate exploratory locomotor behaviors driven and actively selected by the BG, while the CNF mediates defensive locomotion for example in the context of an urgent need to escape from dangerous contexts (Jordan, 1998). Another layer of complexity emerges from

the fact that electrical stimulations along a dorso-ventral axis encompassing the CNF and PPN region can elicit variable responses ranging from opposing changes in muscle tone and posture to locomotion-promotion ones (Figure 3B) (Takakusaki et al., 2016).

Together, these experiments suggest that locomotion and posture controlling functional attributes in the MLR cannot be fully explained by neuronal position alone. While the literature consistently supports a role for the CNF as locomotion-promoting site, the PPN and adjacent regions might be composed of closely-located or even intermingled populations of locomotion-promoting and opposing posture-regulating neurons. In addition, PPN neurons also contact numerous rostral brain regions (Martinez-Gonzalez et al., 2011), making it challenging to dissociate direct effects on locomotion through descending pathways from indirect effects through ascending interactions. Thus, studies using electrical stimulation or pharmacology cannot disentangle the complexity of these circuits. Work described below and mostly carried out in mice makes use of viral and genetic tools to elucidate the cellular and functional identity within the MLR, with a focus on its descending circuits.

Neuronal and functional diversity in the mouse MLR

To consolidate results of experiments performed in other species in mice, electrical mapping of the mouse MLR revealed that the effective stimulation sites to elicit locomotion span over a rostro-caudally and dorso-ventrally broad region including the PPN, CNF, pre-CNF and the adjacent mesencephalic reticular formation (Roseberry et al., 2016). These regions contain intermingled glutamatergic, GABAergic and, exclusively in the case of the PPN, cholinergic neurons (Martinez-Gonzalez et al., 2011) (Figure 3C). The most advanced insight on control of

locomotion emerged from studying glutamatergic MLR neurons marked by the expression of the vesicular glutamate transporter vGlut2 (Caggiano et al., 2018; Josset et al., 2018; Lee et al., 2014; Roseberry et al., 2016), which will be the main focus here. All four studies demonstrate that optogenetic activation of glutamatergic neurons in the broad MLR region in mice recapitulates short latency initiation of locomotion with a stimulus intensity-to-speed correlation analogous to electrical stimulation experiments. Furthermore, optogenetic stimulation triggered during ongoing locomotion increases speed, by shortening the duration of hindlimb extensor muscle activation during stance and anticipating the next swing phase (Josset et al., 2018; Roseberry et al., 2016). Single unit neuronal recording experiments *in vivo* revealed that general vGlut2-MLR neurons correlate with locomotor state with a fraction of neurons also tracking locomotor speed (Caggiano et al., 2018; Roseberry et al., 2016). Optogenetic stimulation experiments were also carried out for other MLR populations. While the experimental outcome for stimulating cholinergic PPN neurons was somewhat contradictory across studies (Caggiano et al., 2018; Dautan et al., 2016; Josset et al., 2018; Roseberry et al., 2016; Xiao et al., 2016), it is nevertheless clear that they likely exhibit a modulatory rather than a driver role in locomotion. This seems to be at least partially mediated by direct regulation of dopaminergic neuronal activity in the SNc and the VTA (Dautan et al., 2016; Xiao et al., 2016), and possibly other ascending and descending targets (Mena-Segovia and Bolam, 2017; Moehle et al., 2017). In contrast, GABAergic neurons influence locomotion negatively through both local and distant circuit mechanisms (Caggiano et al., 2018; Roseberry et al., 2016). Taken together, these results demonstrate that glutamatergic MLR neurons constitute the neuroanatomical basis for the functionally-described short latency locomotion-promoting MLR site in the midbrain.

A long-lasting quest concerns the possible functional subdivision of regions residing within the MLR boundaries. While studies in mice consistently find that optogenetic stimulation of CNF-vGlut2 neurons can elicit locomotion, analogous evidence for PPN-vGlut2 neurons is variable (Caggiano et al., 2018; Josset et al., 2018). One study puts forward a model in which the PPN controls low-speed locomotion while the CNF regulates high-speed locomotion (Caggiano et al., 2018) (Figure 3C). In support, optogenetic activation of PPN-vGlut2 neurons induces low-speed, long-latency locomotion with alternating gaits, while CNF-vGlut2 neuron activation generates short-latency locomotion with speed scaling according to stimulation intensity and aligned with the selection of speed-appropriate gait types. Single unit recordings from PPN and CNF neurons during locomotion on a head-fixed treadmill also revealed differences in firing properties aligned with speed. Moreover, glutamatergic PPN neurons integrate inputs from a wide variety of brain structures contributing to action selection and voluntary movements including BG, while CNF neurons receive preferential input from structures implicated in escaping behavior, including the periaqueductal grey (PAG) and the inferior colliculus. The second study demonstrates that stimulation of either PPN or CNF glutamatergic neurons elicits short-latency EMG responses in both ankle flexor and extensor muscles, with the strongest responses in the ankle flexor (Josset et al., 2018). This study further compared the effects of stimulation at rest to during ongoing locomotion. Glutamatergic CNF neuron stimulation at rest increased postural muscle tone before eliciting locomotion, and shortened the extensor bursts to accelerate locomotion with transition to gaits typical for high-speed during ongoing locomotion. In contrast, stimulation of PPN-vGlut2 neurons at rest elicited phasic muscle activity but no locomotion, but surprisingly, either stimulation or silencing of these neurons during

locomotion slowed down locomotor rhythm rather than speeding it up. It is not straightforward to reconcile the results of these two studies on PPN-vGlut2 neurons, but one possibility is that subtle differences in neuronal targeting locations within the PPN area and/or currently unidentified cell type diversity provide explanations.

Overall, recent studies support the existence of at least two midbrain circuits, spatially segregated between the PPN and CNF regions, embedded within specific input-output matrices providing differential control over circuitry regulating the scale from low-speed to high-speed locomotion (Figure 3C). It is likely that these populations are recruited in a context-dependent manner, shaped by emotional valence, internal homeostatic needs and sensory perception, ultimately producing forms of locomotion with speed and gait needed for the respective context. These programs must include the full range of possible locomotor forms from quiet actively selected exploration to urgent, reflexive, escaping behavior from imminent dangers.

MLR-induced locomotion is preserved after precollicular transection, supporting a model in which locomotion-promoting effects are conveyed via caudal projections. Yet, an interesting additional aspect to consider in the equation of MLR function is that glutamatergic MLR neurons also provide input to rostral brain structures (Figure 3D). The PPN establishes connections with most BG nuclei as well as dopaminergic neurons in the ventral tegmental area (VTA) and substantia nigra compacta (SNc), the thalamus and the basal forebrain (Martinez-Gonzalez et al., 2011). These findings implicate the MLR not only in direct behavioral execution, but also put it in a position to influence rostral computations involved in motor program selection or reinforcement such as cortical processing. The role of rostral projections by glutamatergic MLR neurons remains mostly unexplored, with some notable exceptions. Stimulation of glutamatergic MLR projections to the basal forebrain

increases the gain of visual responses and generates gamma oscillations in the primary visual cortex (Lee et al., 2014), reproducing the previously described effects of spontaneous locomotion in cortical processing (Niell and Stryker, 2010). Interestingly, cortical effects were seen even at stimulation strengths below the threshold to induce locomotion by MLR neuron stimulation, demonstrating that the cortical changes and the production of the locomotor behavior are dissociable. Additionally, projections of PPN-vGlut2 neurons to the VTA target dopaminergic neurons and promote behavioral reinforcement (Yoo et al., 2017), presumably by promoting dopamine release in the nucleus accumbens and activating reward processing circuits. By demonstrating that MLR glutamatergic neurons not only convey descending signals for motor execution, but also send ascending projections to multiple brain regions that influence cortical processing and motivation/behavioral reinforcement, these studies suggest that the complexity of the MLR goes far beyond neurotransmitter identity and might also depend on target specificity, models to be explored in the future.

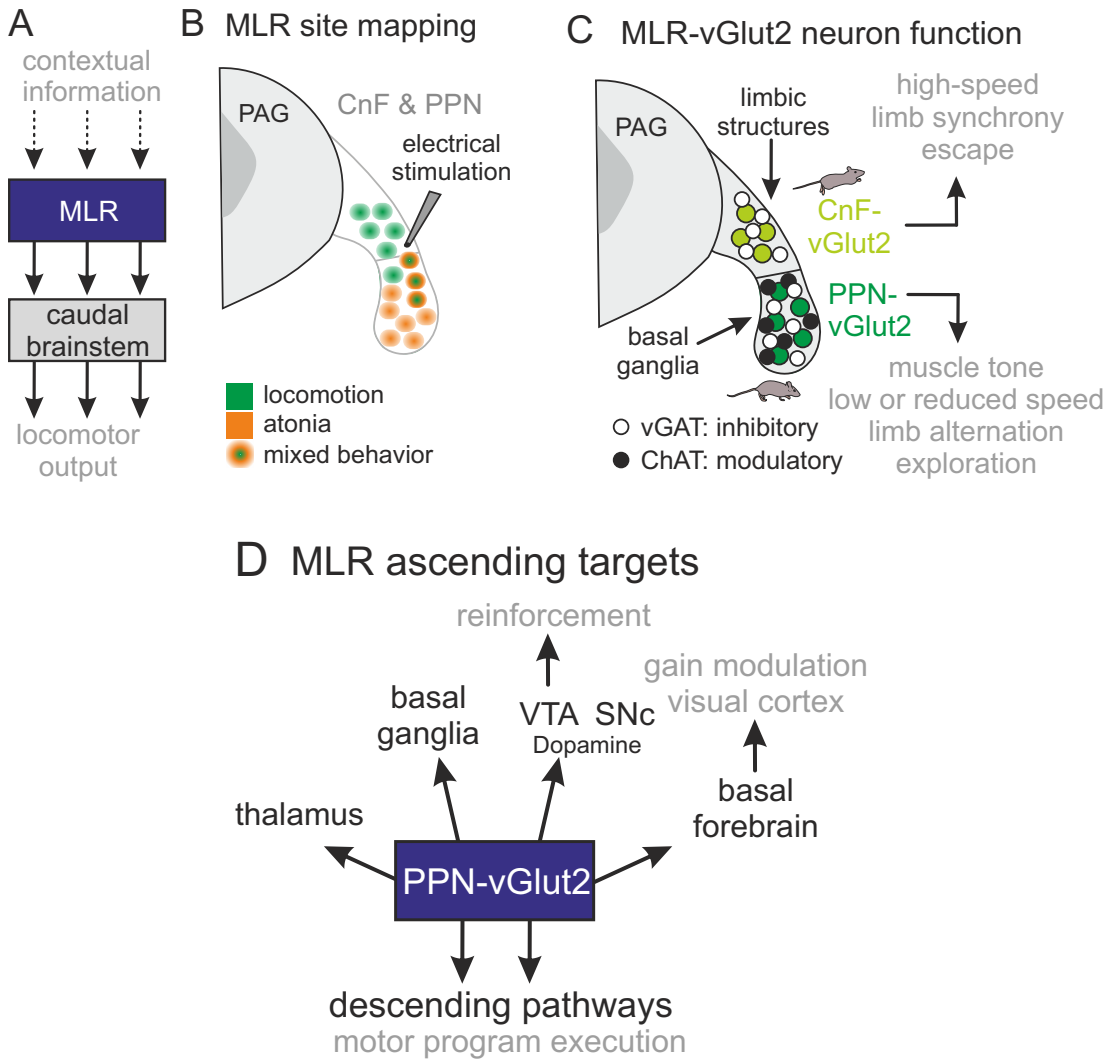

Figure 3. Functional and cellular diversity of mouse MLR

(A) MLR processes contextual information and its descending pathways signal to caudal brainstem neurons to influence locomotor output.

(B) Summary diagram of historical electrical site mapping experiments in the cat CNF and PPN to define locations influencing locomotion (see (Takakusaki et al., 2016) for review).

(C) Schematic diagram summarizing recent findings on the role of mouse MLR-vGlut2 neurons subdivided by location within CNF (cuneiform nucleus) and PPN (pedunculopontine nucleus). Both CNF and PPN also contain vGAT-neurons, but only PPN contains cholinergic neurons.

(D) Summary diagram of PPN-vGlut2 neuron projections to ascending targets and known implicated functions.

Identification of lower brainstem cell types conveying locomotor speed signals

The functional linkage between brain locomotor centers (most notably MLR) and executive circuits in the spinal cord has long been proposed to involve neurons in the lower brainstem reticular formation (Orlovsky et al., 1999). This model is based on experiments including regional injections of pharmacological substances and/or inactivation approaches using tissue cooling methods in conjunction with electrical microstimulation in several species including cats, rats and lampreys that have been extensively reviewed (Brownstone and Chopek, 2018; Mori, 1989; Orlovsky et al., 1999; Ryczko and Dubuc, 2013; Takakusaki et al., 2016). However, despite strong evidence supporting such a model, the precise identity of neurons in the reticular formation acting as intermediaries between MLR and the spinal cord was long unclear. Unlike in the midbrain, within the caudal brainstem reticular formation, electrical stimulation experiments produced variable results with no clear consensual sites able to elicit full body locomotion (Drew and Rossignol, 1990; Kinjo et al., 1990; Ross and Sinnamon, 1984), and it had been argued that neuronal cell type diversity might be the underlying reason for this failure of identification (Orlovsky et al., 1999).

Several studies in mice employing genetics and viruses intersectionally have addressed the identity of neurons in the caudal brainstem involved in regulation of locomotor speed (Bouvier et al., 2015; Capelli et al., 2017; Giber et al., 2015). These studies identify brainstem neurons with locomotion-promoting and/or locomotion-attenuating functional properties and jointly demonstrate that criteria other than simply location are often needed to unravel functional cellular identities in the brainstem.

Within the caudal medulla, the two broad regions magnocellular nucleus (Mc) and gigantocellular nucleus (Gi) have been shown to contain neurons with connections to both cervical and lumbar motor neurons (Esposito et al., 2014). These

neurons are thus in a position to influence spinal locomotor circuits throughout their rostro-caudal extent as might be expected for descending neurons targeting locomotor circuits. To map the precise location and neurotransmitter identity of these neurons in the adult, retrograde tracing from the spinal cord demonstrated that all three Mc subdomains (LPGi: lateral paragigantocellular nucleus; GiA: gigantocellular nucleus alpha; and GiV: gigantocellular nucleus ventral) and the more dorsally located Gi contain intermingled excitatory and inhibitory neurons (Capelli et al., 2017) (Figure 4A). Optogenetic activation of neurons confined to any of these four regions indiscriminate of neurotransmitter identity did not lead to changes in locomotor behavior (Figure 4A). Strikingly however, selective stimulation of vGlut2 neurons located in LPGi but not in any of the other three studied subdomains induced short latency locomotion from rest and increased speed of ongoing locomotion (Capelli et al., 2017). Elimination of LPGi-vGlut2 neurons selectively impaired high-speed locomotion but left exploratory low-speed locomotion unperturbed (Figure 4B). Given these functional studies on the role of LPGi-vGlut2 neurons in natural locomotion, and mapping experiments defining the descending synaptic outputs of CNF-vGlut2 neurons (Caggiano et al., 2018), it is likely that high-speed locomotor signals reach these caudal brainstem neurons from CNF-vGlut2 neurons. Indeed, locomotion-promoting signals from the MLR can be significantly attenuated by selective ablation of LPGi-vGlut2 neurons (Figure 4C), and optogenetic stimulation of MLR-vGlut2 axon terminals in the caudal medulla can also elicit locomotion (Capelli et al., 2017). Together, these findings demonstrate that at least in part, descending locomotion-promoting signals from the MLR reach spinal circuits by recruiting LPGi-vGlut2 neurons in the caudal brainstem. Yet, the findings also demonstrate the need to search for additional neuronal populations that transmit signals for low-speed exploratory

locomotion to the spinal cord. Such a network might be more distributed over several populations given its importance for survival, and/or perhaps an even finer dissection of cell types will be required to unravel identity of brainstem neurons involved in exploratory locomotion. Of note, some MLR neurons have been described to project directly to the spinal cord (Liang et al., 2012), but possible functional implications have not been tested.

The search for dissecting cell types according to a locomotion-attenuating activity in the lower brainstem has already provided more insight. Using developmental ontogeny as an entry point to stratify neurons, a study dissected the role of brainstem neurons expressing the transcription factor Chx10 in excitatory neurons (Bouvier et al., 2015). Optogenetic activation of Chx10 neurons in specific domains of the rostral medulla and caudal pons, but not the caudal medulla, attenuated ongoing locomotion (Figure 4D). Neuronal silencing by selective expression of a tetanus toxin variant led to behavioral hyperactivity with increased locomotion in an open field assay and a decreased ability to halt locomotion in a reward task. The study also demonstrates that the characterized excitatory Chx10 neurons connect to glycinergic spinal neurons that are likely mediators to execute behavioral arrest (Bouvier et al., 2015) (Figure 4D). There are also inhibitory brainstem neurons that can induce behavioral arrest (Capelli et al., 2017; Giber et al., 2015). Within the caudal medulla, separate optogenetic stimulation of each of 4 studied populations induced short-latency behavioral arrest during ongoing locomotion, ranging from simple stopping behavior to full body collapse reminiscent of atonia (Capelli et al., 2017) (Figure 4A), suggesting that different populations are involved in dissimilar forms of behavioral arrest. Interestingly, glycinergic LPGi neurons connect to motor neurons, whereas intermingled LPGi-vGlut2 neurons needed for high-speed locomotion target mostly

spinal neurons in intermediate lamina where rhythm- and pattern generating interneurons of the CPG reside, suggesting that functionally opposing brainstem populations act through different downstream circuits. Lastly, glycinergic neurons in the pontine reticular formation project to the intralaminar thalamic nucleus and optogenetic stimulation of their axon terminals induces behavioral arrest (Giber et al., 2015) (Figure 4E), indicating that also ascending brainstem pathways can have indirect impact on locomotion controlling pathways.

The concept of brainstem neurons in the reticular formation acting as intermediaries to coordinate spinal locomotion is evolutionarily conserved. Lamprey serves as a successful model organism to dissect circuitry regulating locomotion that recapitulates many of the organizational principles seen in mammals (Grillner, 2003; Ryczko and Dubuc, 2013). A recent calcium imaging study analyzed neurons in the reticular formation during MLR stimulation (Juvin et al., 2016), and identified three types of reticulospinal neurons based on their response properties (Figure 4F). One neuronal population maintained firing activity throughout the duration of MLR stimulation (i.e. maintain cells), a second exhibited a firing burst at the onset of MLR stimulation (i.e. start cells) and a third showed a two-phasic activity profile with a burst at the onset and another one at offset of MLR stimulation coinciding with the stop of swimming (i.e. stop cells). Because stop cells exhibited a spatially slightly segregated location from the other two cell types, the authors carried out local pharmacological gain- and loss-of-function experiments and found that while stop cell region activation terminated ongoing swimming, inactivation prolonged swimming (Juvin et al., 2016). Upstream drivers responsible for the different neuronal activity phases of the identified stop, maintain and start cells are currently unknown. Lower organisms also have highly developed circuits to mediate rapid escape behavior and one well-understood

brainstem cell type is the Mauthner cell extensively studied in fish and amphibia (Gahtan and Baier, 2004; Hale et al., 2016). The activation of a single Mauthner cell by mostly unilateral sensory information rapidly induces turning behavior away from dangerous stimuli. Thus, also studies in evolutionarily less developed species underscores the fact that functionally diverse cell types tuned to different locomotor parameters exist within the reticular formation and are embedded in specific circuits to process relevant inputs and transmit their output to spinal circuits for execution.

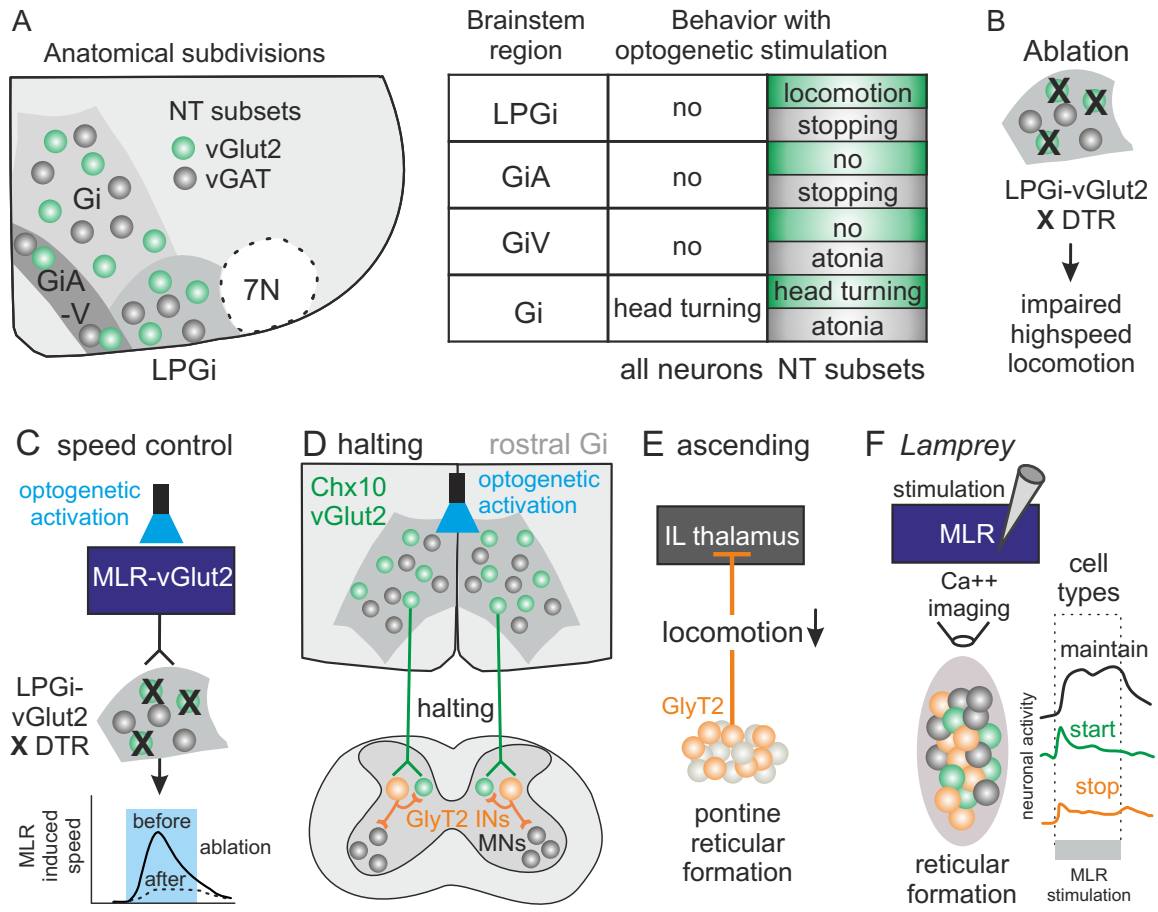

Figure 4. Brainstem cell types regulating locomotion

(A) Subdivision of ventral medulla into four regions (LPGi, lateral paragigantocellular nucleus; GiA, gigantocellular nucleus alpha; GiV, gigantocellular nucleus ventral; Gi, gigantocellular nucleus) all containing intermingled neurotransmitter (NT)-stratified (vGlut2/vGAT) neurons (7N demarcates facial motor nucleus). Table (right) summarizes behavioral findings from optogenetic activation experiments of different neuronal subpopulations.

(B and C) Ablation of LPGi-vGlut2 neurons impairs high-speed locomotion (B) and attenuates speed of locomotion induced by optogenetic stimulation of MLR-vGlut2 neurons (C).

(D) vGlut2 neurons expressing the transcription factor Chx10 in the rostral gigantocellular nucleus (Gi) implicated in halting by signalling through locomotion-inhibiting circuits in the spinal cord.

(E) Glycinergic neurons in the pontine reticular formation project ascendingly to the intralaminar nucleus of the thalamus (IL) to attenuate locomotion.

(F) Summary of firing properties of three populations of neurons in the lamprey reticular formation implicated in locomotor control.

Upstream circuitry supporting locomotor behavior from exploration to escape

One key question is how an animal selects the appropriate locomotor behavior, as well as its vigor, aligned with environmental constraints and needs. As summarized in work above, an important contributor to determine the vigor of a locomotor behavior in its execution phase from low-speed exploration to high-speed escape behavior is the recruitment of specific and distinct circuit elements within the broader MLR area. Conceptual division of locomotion into three categories has been proposed to be computed by different forebrain regions, reflecting the contexts in which locomotion is performed (Sinnamon, 1993). The described categories and structures would be exploratory locomotion (i.e. actively selected by volition and through the BG), primary appetitive locomotion (i.e. promoted by the lateral hypothalamus), and primary defensive locomotion (regulated by the medial hypothalamus and the PAG). These rostral regions would signal through selected MLR-reticulo-spinal networks to orchestrate behavioral execution (Jordan, 1998). Recent studies have addressed these concepts and dissected cell type identity of the more rostral brain structures involved in context-specific forms of locomotion. We will discuss the organization and function of these upstream structures with the goal to explain how appropriate locomotor vigor along a continuous scale can be implemented to regulate locomotion.

Supraspinal regulation of locomotion through basal ganglia circuits

The BG are interconnected brain structures that are involved in motor program selection (Albin et al., 1989; Chakravarthy et al., 2010; DeLong, 1990). The different components of the BG motor loop are connected in an interactive network that integrates and processes information from the cortex and thalamus. In such a model, the combined computations of these BG-thalamo-cortical circuits influence the activity

of brainstem motor circuits to select the movement to be executed in a volitional context (Hikosaka et al., 2000). BG activity is also modulated at several levels by dopaminergic neurons residing in the midbrain VTA and SNc providing crucial signals for motivation and movement initiation and vigor, respectively (Cohen et al., 2012; da Silva et al., 2018; Howe and Dombeck, 2016) (Figure 5A).

Despite its complex organization, the BG motor loop has been classically divided into two major pathways, diverging at the level of the striatum, the major BG input structure (Figure 5A). Two classes of GABAergic striatal spiny projection neurons (SPNs) stratify by distinct projection patterns and by differential expression of dopamine receptors D1 and D2 (Albin et al., 1989; Kreitzer and Malenka, 2008). D1-SPNs are the origin of the direct pathway and project to the main and inhibitory BG output structures, the internal globus pallidus (GPi, in rodents mostly referred to as entopeduncular nucleus) and the substantia nigra reticulata (SNr). D2-SPNs form the indirect pathway with the external globus pallidus (GPe) and the subthalamic nucleus (STN) as intermediate targets. However, the view of BG circuits being two parallel pathways independently influencing BG output structures is clearly too simplistic and many bridges exist that connect the two pathways at different levels (Cazorla et al., 2014; Mallet et al., 2012; Taverna et al., 2008).

Functionally, the classical model regarded the direct and indirect pathways as prokinetic and antikinetic, respectively (Albin et al., 1989; DeLong, 1990). This notion was supported by optogenetic experiments showing that D1-SPN activation throughout a broad striatal region enhances movement and D2-SPN activation produces bradykinesia (Kravitz et al., 2010). However, recent evidence monitoring neuronal activity of striatal subpopulations during natural behaviors points to a more complex involvement of BG circuitry in movement regulation. Endogenous neuronal

activity of the two striatal subpopulations demonstrated that both D1- and D2-SPNs are active during movement initiation and execution (Barbera et al., 2016; Cui et al., 2013; Jin et al., 2014; Klaus et al., 2017a; Parker et al., 2018; Tecuapetla et al., 2014). In addition, the activity of each neuronal population is necessary for the proper execution of an intended movement (Tecuapetla et al., 2016; Tecuapetla et al., 2014) and sufficient to bidirectionally modulate the speed of ongoing movement without affecting action selection (Yttri and Dudman, 2016). It is therefore likely that dedicated neuronal ensemble activity within the striatum, composed of D1- and D2-SPNs, is involved in movement orchestration. Such SPN ensembles could be viewed as the functional units of the striatum contributing to the selection of concrete forms of movement such as locomotion. In agreement with this model, D1 or D2 functional ensembles coherently active during locomotion are spatially closer and more correlated to each other than neurons engaged in other forms of movement (Figure 5B) (Barbera et al., 2016; Klaus et al., 2017a; Parker et al., 2018), suggesting that different actions likely recruit mostly distinct subpopulations of SPNs.

When focusing on descending motor pathway function, understanding how BG link to locomotor output circuitry is an important question. Optogenetic stimulation of D1- or D2-SPNs elicits opposing neuronal activity changes in glutamatergic MLR neurons (Figure 5C) (Roseberry et al., 2016). Furthermore, initiation of head-fixed treadmill locomotion upon bilateral stimulation of dorso-medial striatal D1-SPNs correlates with and depends on glutamatergic MLR neuron activity, whereas analogous experiments with D2-SPNs stop ongoing locomotion by decreasing the firing rate of glutamatergic MLR neurons (Roseberry et al., 2016). The involved anatomical link between D1 and D2 striatal neurons and glutamatergic MLR neurons has not been directly addressed but it is thought that the SNr, the most prominent BG

output structure in rodents (Alam et al., 2011; Hikosaka et al., 2000), provides tonic inhibitory control to MLR neurons (Garcia-Rill et al., 1985; Mori, 1987; Noda and Oka, 1984). Indeed, glutamatergic MLR neurons receive inhibitory input from GABAergic SNr neurons (Roseberry et al., 2016) that mostly target the PPN (Caggiano et al., 2018). In addition, individual SNr neurons are modulated by the activity of D1- and D2 SPNs (Figure 5D) (Freeze et al., 2013; Kravitz et al., 2010; Tecuapetla et al., 2016). Interestingly, optogenetic activation of either D1- or D2-SPNs produces heterogeneous responses in the SNr, with some neurons being excited and others inhibited by activation of each pathway. However, only SNr neurons suppressed by D1-SPN activation predict locomotion initiation, while D2-SPN-induced movement arrest was most strongly correlated with the activity of excited SNr neurons (Freeze et al., 2013). These activity changes in locomotion-related SNr neurons are probably transmitted downstream to glutamatergic MLR neurons, which influence locomotion. Although it is unknown whether locomotion-predictive SNr neurons are preferentially connected to locomotion-promoting neurons in the MLR, this is certainly an interesting possibility.

While these results support the idea that the BG output nucleus SNr constitutes a gate for movement, they also underscore the complexity of intrinsic SNr and BG organization, where likely neuronal subpopulations specialize in the regulation of different aspects of movement. In addition to the SNr, the MLR also receives input from other BG structures such as the GPi, the striatum and the STN (Caggiano et al., 2018; Roseberry et al., 2016), but the functional significance of SNr-bypassing circuits remains unaddressed.

BG circuits are also influenced by neuromodulators, most notably dopamine. The essential role of dopamine is most strikingly revealed in Parkinson's patients,

whose dopamine-depleted state is associated with akinesia and bradykinesia (Albin et al., 1989; Dauer and Przedborski, 2003; DeLong, 1990), and for whom dopamine replacement therapy provides the main intervention to alleviate symptoms. Early work suggested that dopamine might act as a modulator of striatal and cortical firing by activating striatal D1-SPNs and repressing D2-SPNs. However, augmenting or lowering dopamine signaling does not alter striatal and cortical firing rates similarly across the board, but rather influences individual neurons differentially (Costa et al., 2006). Following the same striatal neurons using calcium imaging across different dopaminergic states in a mouse model demonstrated that D1-SPNs and D2-SPNs respond differently to altered dopamine levels (Parker et al., 2018). Interestingly, movement-related activity of D2-SPNs in the dopamine-depleted state became less spatially biased and less correlated to movement on- and offset, whereas D1-SPNs showed analogous response pattern changes in the hyper-dopaminergic state (Parker et al., 2018). To more clearly resolve the temporal and behavioral role of SNc dopamine signaling in the regulation of locomotion and movement in general, several recent studies used high spatial precision at the level of single neurons or axons (da Silva et al., 2018; Dodson et al., 2016; Howe and Dombeck, 2016; Parker et al., 2018). Notably, movement-related dopaminergic SNc neurons do not only signal by slow tonic activity, but also display phasic bursting activity shortly before the onset of locomotion or other self-paced movements (Figure 5E). These observations suggest that locomotion-related dopamine signals can act at fast sub-second timescales, an activity pattern affected in a mouse model of Parkinson's disease (Dodson et al., 2016).

Calcium imaging of individual midbrain dopaminergic axons in the striatum revealed that locomotor- and reward-related signals were largely found in different

axons, suggesting spatial and functional segregation (Howe and Dombeck, 2016). Supporting a role of dopaminergic SNc neurons in movement initiation but not maintenance, their optogenetic stimulation increases the probability for movement initiation, whereas optogenetic inhibition only affects resting but not moving animals, by decreasing the probability of movement initiation (da Silva et al., 2018). Interestingly, the SNc dopamine signal is not specific for a certain type of movement such as locomotion, but rather represents a more general “go” signal and encodes the vigor of an upcoming movement (da Silva et al., 2018; Howe and Dombeck, 2016) (Figure 5E). Therefore, dopamine might provide a general motivational signal that modulates activity throughout the BG network, influencing the initiation of context-adequate movements with desired vigor. Such context-dependent modulation by dopamine could help to explain the heterogeneity of movement-related activity patterns observed in different SPN classes. Furthermore, in the specific case of locomotion, BG-imposed vigor needs to be translated into the desired speed of body translocation mediated by downstream brainstem centers, where speed-encoding neurons reside and receive input from BG output structures (Caggiano et al., 2018; Roseberry et al., 2016). It is also interesting to reflect on the fact that initiation of locomotion requires the simultaneous suppression of competing limb-dependent movements (such as grooming, scratching or reaching) through precise orchestration of activity between BG-thalamo-cortical circuits and brainstem centers. Although important questions remain to be addressed pertaining to how brainstem centers are regulated by dopaminergic signals influencing action initiation and vigor, these combined recent results call for an updated view on the role of dopaminergic SNc neurons and BG pathways in locomotion and movement in general.

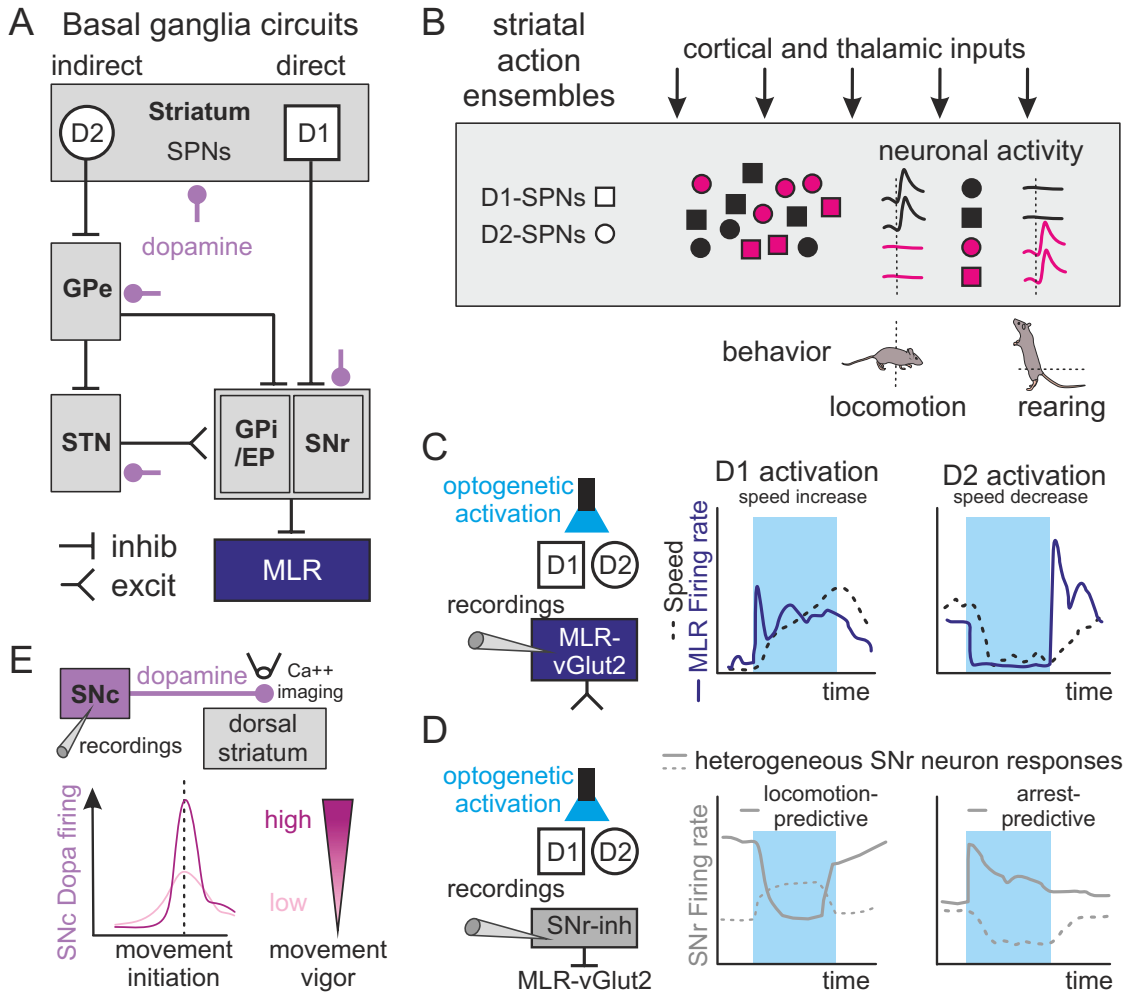

Figure 5. Basal Ganglia circuit control of locomotion

(A) Schematic diagram of the main feed-forward connectivity by indirect (D2) and direct (D1) striatal spiny projection neurons (SPNs) within the basal ganglia, as well as their dopaminergic inputs.

(B) D1- and D2-SPNs containing striatal functional ensembles exhibit a proximity-biased spatial distribution, according to different behaviors (e.g. locomotion or rearing). Summary of their neuronal activity patterns is depicted on the right.

(C, D) Recording of MLR-vGlut2 (C) or SNr-inhibitory (D) neurons upon optogenetic stimulation of D1- or D2-SPNs. Note that not all SNr neurons are predictive of locomotor behavior, likely a reflection of further neuronal diversity yet to be identified.

(E) SNc-derived dopamine signaling to the dorsal striatum before movement initiation (e.g. locomotion) determines the vigor of the future executed action.

How circuits for behavioral needs and contexts interface with action programs

While BG are essential for the smooth execution of planned movements including exploratory or goal-directed locomotion, locomotion can also be strongly shaped by emotional valance of a behavioral context as well as internal physiological needs. These internal and external cues can lead to abrupt changes of locomotor states, overriding ongoing plans and the complex information processing they entail. Escaping and hunting are examples of such behaviors classified as primary defensive and appetitive motivational locomotor forms (Sinnamon, 1993). We will discuss selected examples of circuits influencing defensive (escaping and freezing) and predatory (hunting) actions to illustrate this point, with a focus on their locomotor components. Brain structures implicated in these behaviors and mentioned here are hypothalamic nuclei, the central amygdala (CeA) and the superior colliculus. A frequent pattern of these upstream structures is the convergence of some of their outputs to the PAG, an intermediary midbrain structure between regions encoding internal and external states and locomotor executive centers in the brainstem (Figure 6A). It is important to note that the nervous system output accompanying innate responses goes well beyond the locomotion aspects discussed here, including other motor outputs (such as capture, biting, tail rattling, stretch posture, and actions related to internal needs including hunger, fear, social and sexual behavior) as well as autonomic responses (Fadok et al., 2018; Stuber and Wise, 2016).

Exposure to threatening situations such as predators induces a state of increased anxiety and fear. Two opposing reactive responses affecting locomotor states are flight, a high-speed form of locomotion intended to escape from a threat, and freezing, a sudden arrest of body movement intended to avoid detection. Freezing is produced by activation of glutamatergic lateral and ventrolateral PAG (l/vlPAG)

neurons with connections to medullary premotor neurons, while flight is mediated by activation of glutamatergic neurons in the dorso-lateral PAG (dlPAG) (Figure 6B) (Tovote et al., 2016). Also excitatory neurons in a more dorsal region of the PAG (dPAG) can control escape behavior and its vigor, by receiving processed visual information about looming stimuli from superior collicular neurons (Evans et al., 2018). The target regions that mediate escaping responses of d/dlPAG circuits have not yet been described, but glutamatergic CNF and/or LPGi neurons might be direct or indirect targets, since both receive input from more dorsal regions of the PAG, and control high-speed locomotion (Caggiano et al., 2018; Capelli et al., 2017). Lastly, defensive behavior can be elicited by neurons in the superior colliculus marked by parvalbumin, whose axons bypass PAG circuitry altogether, inducing escape followed by freezing through outputs to the parabigeminal nucleus and immediate freezing via the lateral posterior thalamic nucleus (LPTN) (Figure 6C) (Shang et al., 2018).

The situation is clearly more complex than simple PAG input-output transmission since intra-PAG circuitry is involved in guiding appropriate behavioral responses. Notably, GABAergic l/vlPAG interneurons locally inhibit freeze-neurons and can act as a switch to ensure that the execution of flight and freezing motor programs are mutually exclusive (Tovote et al., 2016). In support, freezing information is transmitted by long-range inhibitory projections from the central amygdala (CeA) that decrease the activity of GABAergic l/vlPAG interneurons with consequent disinhibition of l/vlPAG freeze-neurons. On the other hand, dlPAG flight-neurons contact and likely excite GABAergic l/vlPAG interneurons, thus silencing l/vlPAG freeze-neurons (Tovote et al., 2016). Additionally, glutamatergic lateral hypothalamus (LH) flight-neurons (Li et al., 2018) could also connect to the GABAergic l/vlPAG interneurons and silence the l/vlPAG freeze-neurons, similar to the excitatory dlPAG

flight-neurons. Lastly, neurons in the dorsomedial and central parts of the ventromedial hypothalamus (VMHdm/c) tailor their function according to environmental cues, with a population defined by the expression of Steroidogenic factor 1 (SF1) promoting the expression of either freezing or escaping responses depending on the magnitude of their activation and whether or not a shelter is present (Figure 6D) (Wang et al., 2015). Whereas flight responses are transmitted via projections to the AHN, freezing responses pass via descending projections to the dPAG, suggesting that SF1-expressing VMHdm/c neurons might even be further divisible.

The PAG is also a central player in the regulation of predatory hunting, for which prey pursuit requires suppression of glutamatergic l/vlPAG neurons (Figure 6D) (Han et al., 2017; Li et al., 2018). Individual GABAergic CeA neurons encode pursuit, capture and consumption during predatory hunting, and CeA pursuit-phase locomotor signals are conveyed to the l/vlPAG (Han et al., 2017). Predation-encoding GABAergic neurons projecting to l/vlPAG were also identified in the LH (Li et al., 2018). But whereas optogenetic stimulation of l/vlPAG projecting CeA neurons elicited only prey pursuit (Han et al., 2017), the analogous experiment with LH neurons additionally induced prey capture and consumption and even led to conspecific attacks (Li et al., 2018), suggesting only partially overlapping information coding for these two populations. Evidence is still insufficient to conclude whether the glutamatergic l/vlPAG neurons inhibited during predation are the same neurons active during freezing (Han et al., 2017; Li et al., 2018; Tovote et al., 2016), and what are the precise downstream targets receiving their output signals. Although data suggest that the predatory signal is conveyed to the MLR, it will be important to clarify which MLR subpopulations are targeted by these glutamatergic l/vlPAG neurons suppressed

during predatory hunting (Figure 6D). Glutamatergic MLR neurons seem unlikely candidates, as they are active during locomotion and receive most of their PAG input from dorsal domains (Caggiano et al., 2018; Roseberry et al., 2016). Instead, GABAergic MLR neurons might be candidates as they receive direct input from the PAG and exert local inhibitory effects on glutamatergic neurons (Roseberry et al., 2016).

In summary, innate forms of locomotion involve many neuronal subpopulations located in the mid- and forebrain (Figure 6B-D). The LH segregates neurons involved in predatory and escaping locomotion, while the CeA promotes both hunting and freezing. Several appetitive and defensive locomotion motives are also present in the PAG as a key intermediary structure. Revealing the detailed functional links between escape and predation-related PAG neurons and connected output brainstem neurons will contribute to understanding if these functionally distinct channels extend into downstream circuits or if they align with the described speed related populations distributed between PPN for exploration and CNF for fast locomotion.

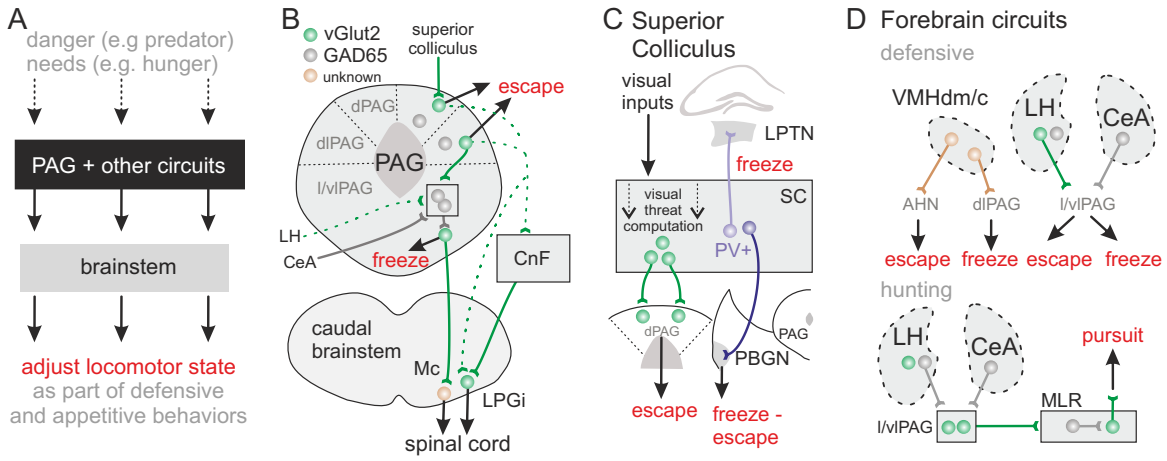

Figure 6. Circuits for behavioral need and context influencing locomotion

(A) Periaqueductal gray (PAG) and associated structures are central in processing information about danger and needs, to then signal through brainstem circuits to adjust locomotor state as part of numerous defensive and appetitive behaviors.

(B-D) Summary of functionally known (solid) and inferred (dashed) circuit organization for the PAG (B), superior colliculus (C) and forebrain circuits implicated in defensive and hunting behaviors (D). Neurons shown in boxes implies that there might be multiple neuronal subpopulations processing the shown inputs.

Outlook

Supraspinal circuits involved in the control of locomotion are distributed over many brain areas, making their comprehensive understanding a challenging task. Yet it has become clear that for many behavioral choices linked to locomotion, neuronal populations encoding and responsible for the implementation of specific functional attributes of locomotion are embedded in complex circuitry and can be recruited by different encountered contexts. The networks described in this review represent only a fraction of involved circuits, and as circuit dissection proceeds, connectivity matrices and functions will be understood better. Also other brain structures including the cerebellum and the cortex not described here contribute to shaping appropriate locomotor responses. Finally, another important question to consider will be how behavioral choice occurs at a more general level to select locomotion over the many other behaviors an animal can execute, for which supraspinal circuits are also responsible. Answers to all of these questions lie buried deep in the intricate circuitry of the brain.

Acknowledgements

The broad topical coverage in this review required a citation strategy mainly focusing on original recent literature described in more detail here. We would also like to apologize to authors of the many additional important original studies and older work for citing review articles instead. All authors were supported by an ERC Advanced Grant (No 692617), the Swiss National Science Foundation, the Kanton Basel-Stadt, the Novartis Research Foundation, and the Louis Jeantet Prize for Medicine.

Section 3: Functional diversity for body actions in the mesencephalic locomotor region

Manuel J. Ferreira-Pinto[1], Harsh Kanodia[1], Antonio Falasconi[1], Markus Sigrist, Maria S. Esposito and Silvia Arber

[1]These authors contributed equally

Cell 2021

Summary

The mesencephalic locomotor region (MLR) is a key midbrain center with roles in locomotion. Despite extensive studies and clinical trials aimed at therapy-resistant Parkinson's disease (PD), debate on its function remains. Here, we reveal the existence of functionally diverse neuronal populations with distinct roles in control of body movements. We identify two spatially intermingled glutamatergic populations separable by axonal projections, mouse genetics, neuronal activity profiles, and motor functions. Most spinally projecting MLR neurons encoded the full-body behavior rearing. Loss- and gain-of-function optogenetic perturbation experiments establish a function for these neurons in controlling body extension. In contrast, Rbp4-transgene-positive MLR neurons project in an ascending direction to basal ganglia, preferentially encode the forelimb behaviors handling and grooming, and exhibit a role in modulating movement. Thus, the MLR contains glutamatergic neuronal subpopulations stratified by projection target exhibiting roles in action control not restricted to locomotion.

Introduction

Locomotion is essential for survival across all species and is the terrestrial motor program translocating the entire body. It enables many forms of controlled interactions with the environment, including exploratory locomotion such as seeking food, as well as more urgent responses such as escaping from danger. Irrespective of the chosen locomotor form, its successful completion requires controlled postural adjustments of the entire body, the coordinated recruitment of limbs to translocate the body and the efficient suppression of other motor programs not compatible with locomotion. These behavioral observations raise the question of the underlying neuronal circuit mechanisms involved in the selection and regulation of locomotion and other forms of body movements.

The mesencephalic locomotor region (MLR) is a midbrain area that combines various attributes central to the regulation of locomotion by integrating many inputs and projecting to both descending and ascending targets. The historic definition of the MLR has been functional and based on the fact that its electrical stimulation can elicit full-body locomotion, with speed and gaits scaling with the stimulation intensity (Noga et al., 1988; Shik et al., 1966). Several questions related to MLR function arose following these observations, driven by attempts to define its precise location and the neuronal identities responsible for the observed effects. Anatomically, the confines of the MLR by its original functional definition include a midbrain area comprising the pedunculopontine nucleus (PPN), the rostro-caudally contiguous area of the pre-cuneiform and cuneiform nuclei (pCnF and CnF), and the adjacent mesencephalic reticular formation (mRT). These areas contain intermingled glutamatergic and GABAergic neurons, and the PPN also contains cholinergic neurons (Martinez-Gonzalez et al., 2011; Mena-Segovia and Bolam, 2017; Tubert et al., 2019; Wang and

Morales, 2009), necessitating a strategy to dissect and understand MLR function by location and neurotransmitter identity.

Mapping the broader MLR region by electrical stimulation and optogenetic techniques led to observations of functional diversity within the MLR. It is established that glutamatergic MLR (MLR-vGlut2) neurons constitute the neuroanatomical basis for the short-latency locomotion-promoting behavior observed upon MLR stimulation (Caggiano et al., 2018; Capelli et al., 2017; Josset et al., 2018; Lee et al., 2014; Roseberry et al., 2016). Using spatially more restricted dissection, studies agree that glutamatergic CnF (CnF-vGlut2) neurons elicit and control high-speed locomotion (Caggiano et al., 2018; Josset et al., 2018), resonating with other work (Jordan, 1998; Opris et al., 2019; Skinner and Garcia-Rill, 1984; Takakusaki et al., 2016). In contrast, evidence regarding the function of neurons in and around the PPN is more ambiguous. Electrical stimulation unraveled sites in the ventral PPN eliciting inhibition of muscle tone and sites in the dorsal PPN eliciting mixed responses (Takakusaki et al., 2016), while other studies identified locomotion-promoting sites in the PPN (Skinner and Garcia-Rill, 1984). Studies applying optogenetics to glutamatergic PPN (PPN-vGlut2) neurons did not provide definitive evidence on their function either, with reports supporting roles in low-speed exploratory locomotion (Caggiano et al., 2018), locomotion arrest (Josset et al., 2018), or both (Carvalho et al., 2020). Of note, recent studies were also mostly focused on limb dynamics during locomotion and did not take into account postural changes required for locomotion, as described before (Mori et al., 1992).

Studies on PPN are also of clinical importance. Application of PPN deep brain stimulation (DBS) (Lozano et al., 2017) to ameliorate parkinsonian gait and balance symptoms yields diverse findings (Nowacki et al., 2018; Thevathasan et al., 2018;

Tubert et al., 2019). A recent review article stresses the fact that functional diversity in the PPN area is likely the key reason for the lack of consensus on applied strategies to ameliorate Parkinson's disease (PD) symptoms, despite ongoing clinical work over many years (Garcia-Rill et al., 2019). Together, while it is clear that CnF-vGlut2 neurons can drive locomotion within an escape context, results on the function of the adjacent regions, including PPN, cannot be reconciled. These divergent observations underscore the need to better characterize the functional neuronal diversity within this midbrain region, also with respect to other motor behaviors, given that only a fraction of MLR neurons encode locomotion (Caggiano et al., 2018; Carvalho et al., 2020; Roseberry et al., 2016). Moreover, it is important to consider aspects other than speed regulation and limb coordination in locomotion, knowing that its successful execution also entails postural adjustments and suppression of other motor programs.

One still poorly explored dimension of the MLR is the diversity of output structures targeted by glutamatergic neurons in the PPN area. In addition to the descending projections to the medulla (Caggiano et al., 2018; Capelli et al., 2017; Noga et al., 1988), minor projections to the spinal cord (SC) also exist (Liang et al., 2012), which have not been studied functionally. PPN-vGlut2 neurons also have multiple ascending targets, including several basal ganglia components, basal forebrain, and thalamus (Martinez-Gonzalez et al., 2011). First reports begin to suggest that MLR-vGlut2 axons influence target structures differentially (Assous et al., 2019; Lee et al., 2014; Yoo et al., 2017). Yet, whether these effects represent differential responses of targets to a signal broadcasted by one population or reflect the action of distinct neuronal subpopulations remains unknown. The latter might explain the different findings in studies carrying out MLR neuron stimulations and DBS in PD patients.

Here, we identify and functionally dissect glutamatergic MLR subpopulations based on the premise that target connectivity might be linked to function. We found that MLR-vGlut2 neurons residing in spatial proximity segregate into separate neuronal populations based on axonal targets, transgenic marker expression, neuronal activity profiles, and roles in behavior. A spinally projecting population (MLR>SC) is distinct from an ascending population targeting basal ganglia output structures specifically marked by the $Rbp4^{Cre}$ transgene (MLR-Rbp4). While MLR>SC neurons are positively modulated during rearing, MLR-Rbp4 neurons are mostly recruited during the forelimb behaviors handling and grooming. Optogenetic perturbation experiments demonstrate a role for MLR>SC neurons in body extension while pointing to a function for MLR-Rbp4 neurons in modulation of various behaviors. We conclude that the proximity of functionally diverse MLR subpopulations likely explains the diverse results on glutamatergic MLR neurons and provides essential information for devising new strategies to ameliorate PD symptoms involving the PPN area.

Results

MLR-vGlut2 neurons divide into separate descending and ascending populations

We first determined the precise location of glutamatergic MLR neurons with descending and/or ascending projections. We injected adeno-associated viruses (AAVs) with Cre-dependent conditional expression and retrograde neuronal targeting potential (rAAV) (Tervo et al., 2016) into select descending and ascending MLR projection targets. We delivered rAAVs expressing different marker proteins targeted to nuclei (nTag) to allow for detection of cell body location. We restricted our analysis to glutamatergic MLR neurons by injecting variants of rAAV-flex-nTag into vGlut2^{Cre} mice (Figure 1A). To target MLR-vGlut2 neurons with descending projections, we injected rAAV-flex-nTag1 and -Tag2 into the medullary reticular formation (Med) and SC, respectively (see STAR Methods). As a major ascending target of MLR-vGlut2 neurons, we injected rAAV-flex-nTag3 centered into the substantia nigra (SN) reticulata (SNr), the main basal ganglia output structure in rodents (Oorschot, 1996; Smith et al., 1998), implicated in movement control (Figure 1A).

We assessed the location of MLR>Med, MLR>SC and MLR>SN neurons. To get a measure of distributions for retrogradely labeled MLR-vGlut2 neurons, we reconstructed cell body position based on nTag labeling. We restricted our analysis to the rostro-caudal levels of the PPN, the perimeter of which is defined by the presence of cholinergic neurons (Martinez-Gonzalez et al., 2011; Mena-Segovia and Bolam, 2017), the rostrocaudally contiguous pCnF/CnF and the adjacent mRT (Franklin and Paxinos, 2007). We found that MLR>Med neurons were most numerous and widely distributed (Figures 1B–1E and S1), in agreement with previous work demonstrating that glutamatergic neurons in both PPN and pCnF/CnF subregions project to the

caudal medulla (Caggiano et al., 2018; Capelli et al., 2017). In contrast, we observed a more restricted localization for MLR>SC and MLR>SN neurons (Figures 1B–1E and S1).

Analysis of neuronal positioning revealed that MLR>Med neurons are scattered throughout the four MLR subdomains and along the rostro-caudal axis (Figures 1D, 1E, and S1). In contrast, MLR>SC and MLR>SN neurons were preferentially located within the PPN and mRT, with only rare residence in the pCnF/ CnF domains (Figures 1D, 1E, and S1). In addition, MLR>SN neurons were more frequently located within the mRT immediately adjacent to PPN particularly in the caudal part, while MLR>SC neurons exhibited a slightly laterally shifted and more PPN-biased residence (Figures 1C, 1D, and S1). In summary, glutamatergic neurons within the PPN and immediately adjacent mRT subregion projecting to the three studied target sites Med, SC and SN are located in close spatial proximity and intermingled. The remainder of the MLR subregions, including the pCnF/CnF and large parts of the mRT, contained mostly neurons projecting to the Med.

Given the close spacing of glutamatergic neurons within the PPN and adjacent mRT with respect to different projection targets, we determined whether single neurons project to multiple targets. We found that most MLR>SC neurons (81.3% ± 2.7%) also project to the Med, indicating that the majority of spinally projecting neurons collateralize to medullary targets (Figures 1F and S1). In contrast, only few MLR-vGlut2 neurons with descending projections to the medulla (2.7% ± 0.8%) or SC (3.1% ± 0.8%) elaborate bifurcating axons projecting to the SN (Figures 1F and S1). We conclude that the assessed descending and ascending MLRvGlut2 populations are largely separate entities. Due to the proximity of these neurons in and close to the PPN region, possibly divergent functions cannot be assessed purely by location.

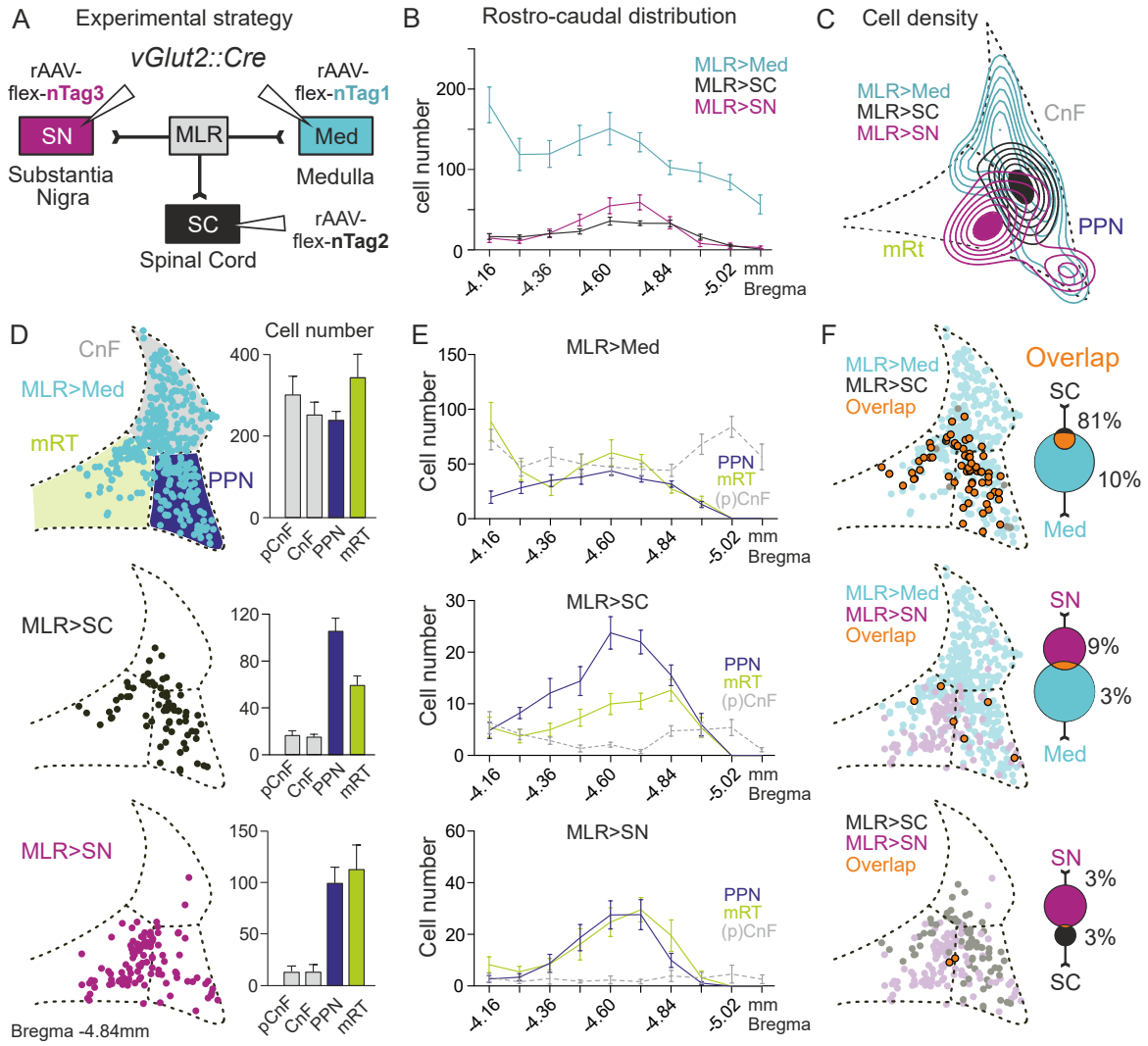

Figure 1. Glutamatergic MLR neurons segregate by projection target

(A) Strategy for retrograde labeling of glutamatergic MLR neurons from substantia nigra (SN), spinal cord (SC), and medulla (Med).

(B) Average number (±SEM) of labeled cells along the rostro-caudal axis (n = 9).

(C) Cell density from an example animal at bregma -4.84 mm containing PPN, mRT, and CnF subdivisions.

(D) Left: two-dimensional reconstruction of MLR neurons projecting to Med, SC, or SN at bregma -4.84mm(n = 3). Right: quantification of labeled cell number in MLR subregions for each subpopulation (n = 9). Error bars represent SEM.

(E) Average number (±SEM) of labeled cells for the three retrograde injections in PPN, mRT, and (p)CnF along its rostro-caudal axis (n = 9).

(F) Pairwise comparison of the cellular overlap between MLR subpopulations. Two-dimensional distribution of single or double (orange) labeled cells at bregma -4.84mm (left) and total percentage of overlapping cells for each subpopulation pair shown in Venn diagrams (right; n = 6 per pair). Percentage of double-labeled neurons (mean ± SEM) were Med+SC/SC, 81.3% ± 2.7%; Med+SC/Med, 10.1% ± 1.1%; Med+SN/SN, 8.8% ± 2.4%; Med+SN/Med, 2.7% ± 0.8%; SN+SC/SN, 2.8% ± 0.9%; SN+SC/SC, 3.1% ± 0.8%.

See also Figure S1.

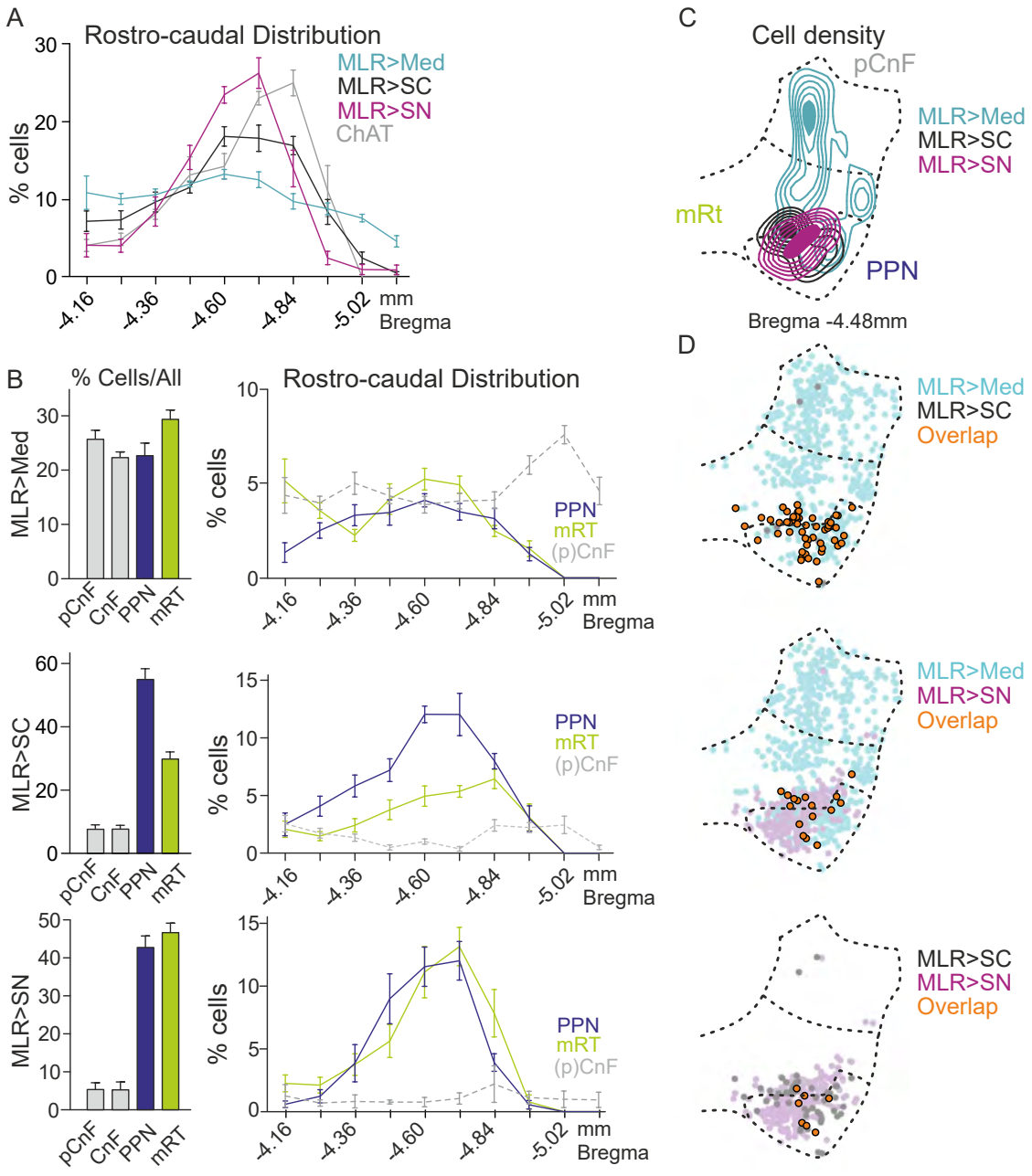

Figure S1. Distribution of glutamatergic MLR neuron subpopulations, related to Figure 1

(A) Percentage of labeled cells (mean ± SEM) for each of the three MLR subpopulations (n = 9) or ChAT positive cells along the rostro-caudal axis (n = 5).

(B) Left, percentage of labeled cells for the 3 retrogradely labeled populations in each MLR subregion (n = 9; pCnF, CnF, PPN and mRT). Right, mean percentage of labeled cells in each MLR subregion along its rostro-caudal axis (n = 9; mean ± SEM; pCnF and CnF pooled for this analysis).

(C) Cell density from one example animal at Bregma -4.48 mm in a studied MLR section containing PPN, mRT and CnF subdivisions at this level.

(D) Pairwise comparison of the cellular overlap between MLR subpopulations by projection target in two-dimensional distribution of single or double (orange) labeled cells at Bregma -4.48 mm (n = 3).

Rbp4^{Cre} transgene marks glutamatergic MLR neurons with SN projections

The cluster of glutamatergic SN-projecting neurons immediately adjacent to cholinergic PPN neurons prompted us to determine whether we can find genetic means to access these neurons. We used systemic injections of AAV-PHP.eB-flex-nTag viruses, an AAV variant efficiently transducing the central nervous system (Chan et al., 2017), into existing mouse lines expressing Cre recombinase. We found that the transgenic mouse line Rbp4^{Cre}, widely used to target layer 5 pyramidal tract (PT) neurons in the cerebral cortex (Gerfen et al., 2013), also exhibits selective expression in a cluster of neurons immediately adjacent and partially intermingled with cholinergic PPN neurons (Figure 2A). Quantification of MLR-Rbp4 neurons revealed distribution profiles with more prominent occupancy of mRT and PPN subdivisions than pCnF and CnF, and the rostro-caudal distribution profile aligned with the one for glutamatergic MLR>SN neurons (Figure 2A).

To visualize the synaptic targets of MLR-Rbp4 neurons, we injected a virus expressing a protein tag fused to synaptophysin (AAV2.9-flex-SynTag) into the MLR of Rbp4^{Cre} mice (Figure 2B). We compared the synaptic distribution patterns to straight injections of the same tracer into vGlut2^{Cre} mice and to injections targeting specifically glutamatergic MLR>SN neurons (Figure 2B) (Fenno et al., 2014). AAV2.9-flex-SynTag injections into vGlut2^{Cre} mice revealed dense synaptic terminations in the Med and the SN (Figure 2B), other basal ganglia output structures (Figure S2), as well as thalamus and basal forebrain (data not shown). Much in contrast, the synaptic output of either MLR-Rbp4 or MLR>SNvGlut2 neurons was strong in the ascending direction to the SN and other basal ganglia structures but minimal in the descending direction, with only sparse synapses in the Med (Figures 2B and S2).

To quantify these findings at the neuronal level, we injected rAAV-flex-nTags into the SN and Med of Rbp4^{Cre} mice (Figure 2C). We found that injection of rAAV-flex-nTag1 into the SN of Rbp4^{Cre} mice marked a selective MLR neuron cluster, while injections of rAAV-flex-nTag2 into the Med led only to very sparse labeling (Figure 2C). We next analyzed the distribution of all MLR-Rbp4 neurons marked by the dual-injection experiment. We found that the large majority of marked neurons projects to the SN, while Med-projecting neurons were dominant for the analogous experiment carried out in vGlut2^{Cre} mice (Figure 2C). We conclude that the Rbp4^{Cre} transgene is expressed in MLR neurons with ascending projections to the SN and other basal ganglia structures but fails to express in MLR neurons with descending projections to the Med.

Although MLR-Rbp4 neurons occupy the same MLR subregion as MLR>SN glutamatergic neurons and have similar synaptic projection patterns, it is still possible that MLR-Rbp4 neurons are inhibitory or cholinergic, since these three neuronal subtypes are intermingled within the PPN (Martinez-Gonzalez et al., 2011; Mena-Segovia and Bolam, 2017; Wang and Morales, 2009). We found negligible overlap between MLR-Rbp4 neurons and the cholinergic marker choline acetyltransferase ChAT (0.36% ± 0.17%; n = 3; Figure 2D). Moreover, additionally using vGAT^{FLP} mice as tool to mark inhibitory neurons, we only found small overlap between MLR-vGAT and MLR-Rbp4 neurons (1.9% ± 0.72%; n = 3; Figure 2D). By exclusion, the predominant neurotransmitter used by MLR-Rbp4 neurons is most likely glutamate (Figure 2D). Together, our findings reveal the existence of two anatomically and genetically separable but intermingled glutamatergic PPN/mRT populations.

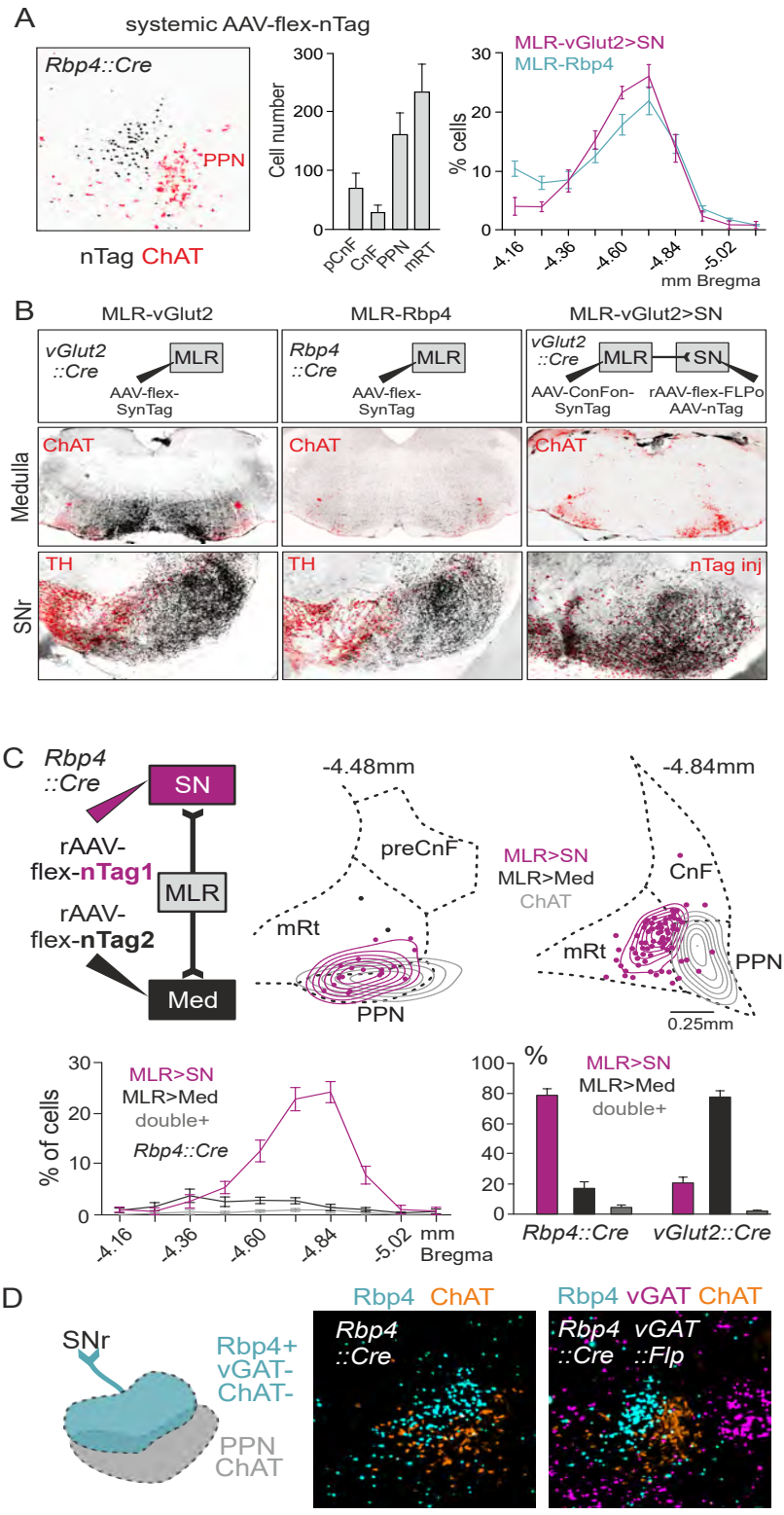

Figure 2. Rbp4 transgene marks basal ganglia output projecting MLR neurons

(A) Picture showing localization of MLR Rbp4-transgene-positive neurons (black) adjacent to cholinergic PPN neurons (red) (left). Average number of Rbp4-transgene-positive cells in each subregion (n = 5; middle; Error bars represent SEM).

Comparison between the rostro-caudal distribution of Rbp4-transgenepositive neurons (n = 5) and glutamatergic neurons projecting to SN (n = 9; right; ± SEM).

(B) Scheme and images showing the distribution of descending (Med) versus ascending (SN) synaptic terminals arising from glutamatergic (vGlut2) (left), Rbp4 transgene positive (middle), or MLR>SN projecting glutamatergic (right) MLR neurons. Med sections are counterstained for ChAT, and SNr sections are counterstained for Tyrosine Hydroxylase (TH; left, middle) or AAV-nTag co-injected for injection specificity (right).

(C) Distribution of Rbp4-transgene-positive MLR neurons revealed by retrograde labeling in Rbp4::Cre mice. (top) Experimental scheme, cell density (lines), and distribution (dots) of MLR>SN and MLR>Med Rbp4 neurons compared to ChAT PPN neurons from one example mouse at bregma -4.48 and -4.84mm. (bottom) Rostro-caudal distribution of Rbp4-transgene-positive MLR subpopulations (n = 5) and percentage of glutamatergic (n = 6) or Rbp4-transgene-positive (n = 5) MLR>SN, MLR>Med, or MLR>SN/Med (double-positive) neurons (Error bars represent SEM).

(D) Neurotransmitter phenotype of MLR-Rbp4 neurons. Left: summary diagram of findings demonstrating that MLR-Rbp4 neurons do not express vesicular GABA transporter (vGAT) or ChAT (n = 3).

See also Figure S2.

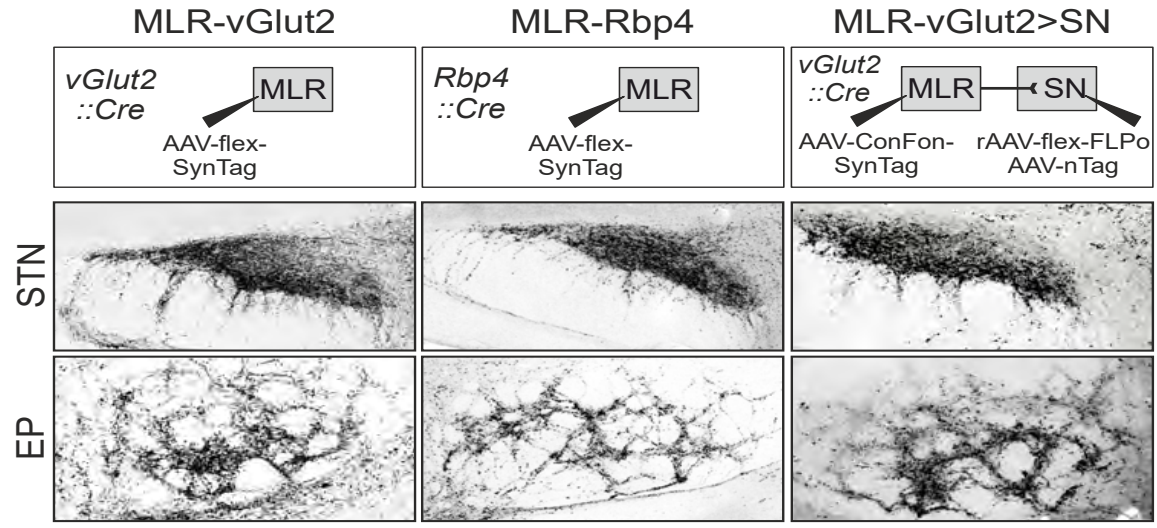

Figure S2. Ascending connectivity of MLR-vGlut2 neurons, related to Figure 2

Visualization of synaptic terminations in subthalamic nucleus (STN; top row) or entopeduncular nucleus (EP; bottom row) derived from glutamatergic (vGlut2) MLR neurons (left), Rbp4-transgene expressing MLR neurons (middle) or SN-projecting glutamatergic MLR neurons (right).

Differential action tuning of glutamatergic MLR subpopulations

The possibility to target descending and ascending excitatory MLR neuronal populations allowed us to next determine recruitment profiles during self-motivated behavior in the open field by monitoring their activity through a gradient index (GRIN) lens coupled to a miniaturized fluorescent microscope (Figure 3A). Since previous work demonstrated that the activity of a fraction of MLR-vGlut2 neurons tracks locomotor state (Caggiano et al., 2018; Carvalho et al., 2020; Roseberry et al., 2016), we first assessed whether we also detect neurons preferentially active during locomotor bouts. To determine neuronal activity changes during behavior, we computed the mean fluorescence during the studied behavior and subtracted the mean fluorescence during frames for which no behavior was detected, resulting in a modulation index assigned to every neuron for a behavior compared to still episodes. We found that only a fraction of neurons is positively modulated during locomotion, a property more prominently associated with MLR>SC than MLR-Rbp4 neurons (MLR>SC: 39.3%; MLR-Rbp4: 19.9%; Figures S3A–S3E).

These findings raised the question of whether MLR>SC and MLR-Rbp4 neurons are recruited during other behaviors. Therefore, we tracked the occurrence of the other frequent spontaneous behaviors rearing, grooming, and handling of available food in the open field (Figure 3B). Behavioral episodes were identified using a supervised learning algorithm employing highspeed video and inertial sensor data (Figure 3C). Analyzing the responses of MLR>SC neurons (Figures 3D–3H), we found a prominent population increase in fluorescence associated with the onset of rearing (Figure 3E). In contrast, onsets of locomotion or the forelimb behaviors handling and grooming did not result in increased recruitment of the overall MLR>SC population (Figure 3E). We next determined the modulation indices of individual MLR>SC

neurons and their distribution for the four analyzed behaviors. We found most striking recruitment of MLR>SC neurons during rearing, while only few neurons were strongly positively modulated during any of the other three behaviors (Figures 3F and 3G). Thus, also at the single neuron level, positive modulation during rearing was the most prominent effect, while the impact of modulation during other behaviors can be detected in some neurons but is much smaller (Figures 3E–3G). We also investigated the relationship between neuronal activity and rearing episodes by single-neuron and single-trial analysis (Figures 3D, S4A, and S4B). Individual MLR>SC neurons exhibited differential dynamics in timing and magnitude, as can be particularly well discerned in analyzing several MLR>SC neurons imaged in one mouse over the same behavioral time frames (Figures 3D, S4A, and S4B). Together, these findings demonstrate that MLR>SC neurons are preferentially tuned to rearing.

MLR-Rbp4 neurons exhibited a very distinct recruitment profile from the one observed for MLR>SC neurons (Figures 3I–3M). Population analysis of all MLR-Rbp4 neurons showed strong recruitment at the onset of the forelimb behaviors handling and grooming but no overall recruitment during rearing and locomotion (Figure 3J). These findings were corroborated by analysis of modulation indices for individual neurons, for which we found that many MLR-Rbp4 neurons were strongly modulated during handling and/or grooming, while only few were modulated weakly during rearing and locomotion (Figures 4K and 4L). Determining the number of positively tuned neurons to the four different behaviors also confirmed the strong overrepresentation of tuning toward forelimb behaviors compared to full-body behaviors and revealed abundant overlap between the grooming and handling population (Figure 3M). The temporal structure of the observed neuronal activity patterns was complex, differed between grooming and handling, and did not simply

reflect the general behavioral state of the mouse (Figures 3I, S4A, and S4C). While neuronal recruitment clearly occurred during the behavioral time windows, neurons were not constantly active but instead exhibited peaks within the behavioral time window. Furthermore, different neurons in one mouse tracked over the same behavioral time windows exhibited distinct dynamics (Figures 3I and S4C), suggesting the existence of fine neuronal differences with respect to precise behavioral engagement. Together, these findings demonstrate that MLR-Rbp4 neurons exhibit rich temporal coding for different aspects of forelimb movements.

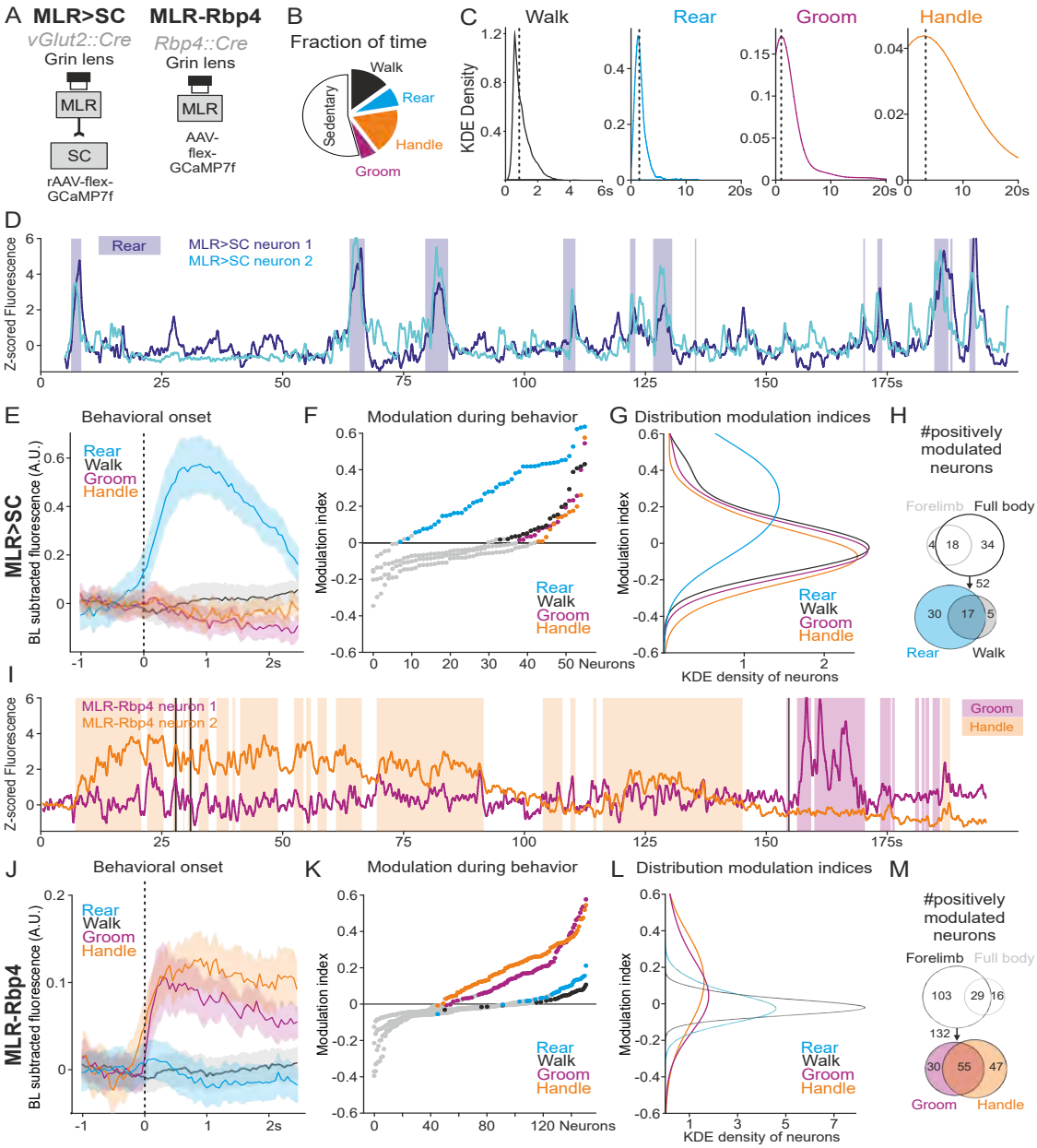

Figure 3. Differential recruitment of MLR subpopulations during behavior

(A) Approach for in vivo calcium imaging of MLR>SC and MLR-Rbp4 neurons.

(B) Fraction of time mice spend sedentary, walking, rearing, handling or grooming in the open field (n = 11).

(C) Distribution for lengths of locomotor, rearing, grooming, handling episodes observed in open field (kernel density estimate [KDE] density; dashed lines: median of distribution).

(D) Z-scored fluorescence with overlaid rearing episodes from two rearing-tuned example neurons.

(E) Baseline (BL) subtracted average fluorescence (±SEM) of all MLR>SC neurons aligned to behavioral onset (56 neurons, n = 7 mice).

(F) Graphs depicting mean evoked fluorescence during rearing, walking, grooming, and handling of all MLR>SC neurons in rising order (colored dots, positively modulated neurons; gray dots, all others).

(G) KDE density of neurons from graphs shown in (F).

(H) Number of positively modulated MLR>SC neurons across behaviors (Venn diagrams). Comparison between forelimb and full-body behaviors (top) and between the full-body behaviors rear and walk (bottom).

(I) Z-scored fluorescence with overlaid grooming and handling episodes from two MLR-Rbp4 example neurons.

(J) Baseline (BL) subtracted average fluorescence (±SEM) of all MLR-Rbp4 neurons aligned to behavioral onset (152 neurons, n = 4 mice).

(K) Graphs depicting mean evoked fluorescence during rearing, walking, grooming, and handling of MLR-Rbp4 neurons in rising order (colored dots, positively modulated neurons; gray dots, all others).

(L) KDE density of neurons from the graphs shown in (K). (M) Number of positively modulated MLR-Rbp4 neurons across different behaviors (Venn diagrams). Comparison between forelimb and full-body behaviors (top) and the forelimb behaviors groom and handle (bottom).

See also Figures S3 and S4.

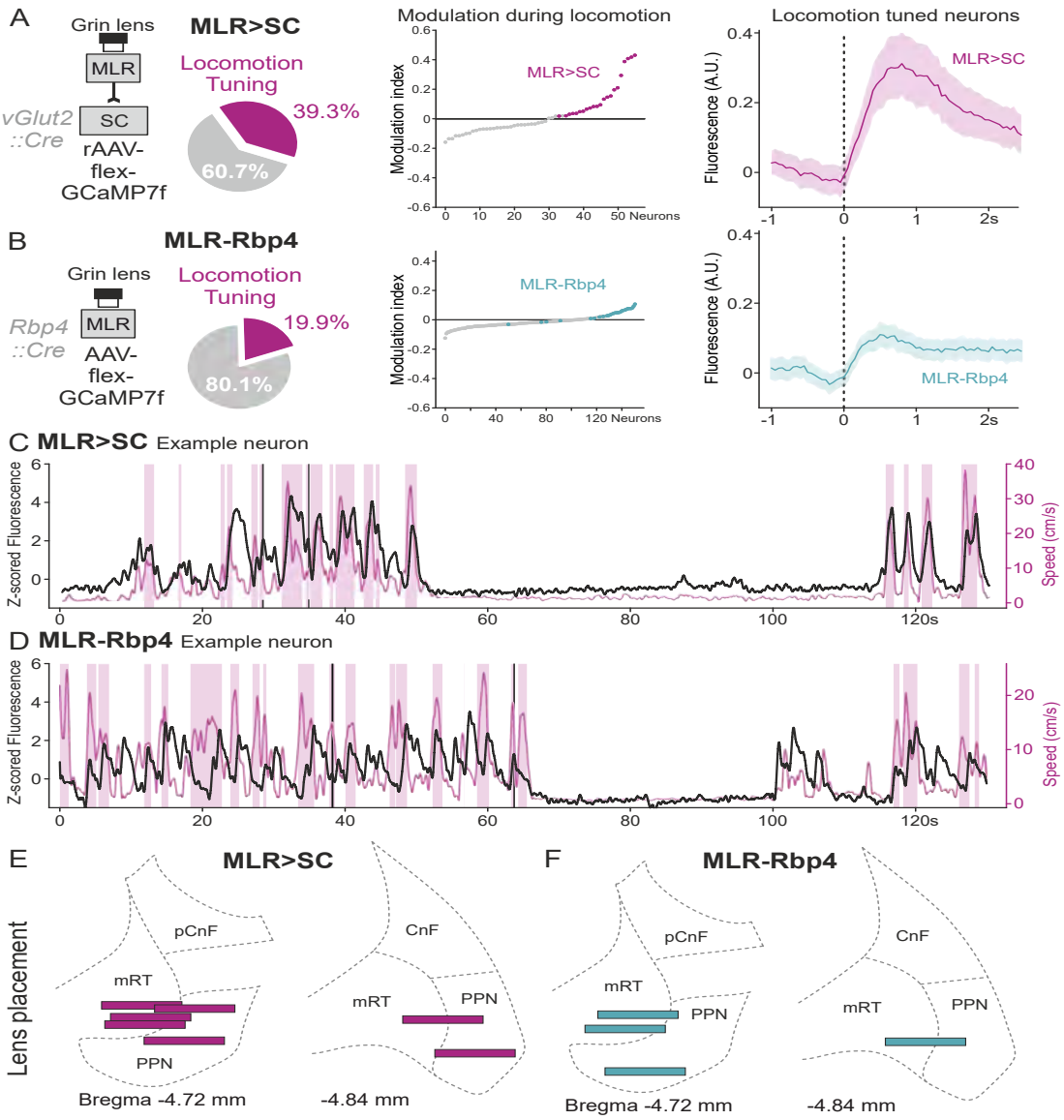

Figure S3. Subpopulation of MLR neurons recruited during locomotion, related to Figure 3

(A) Left: Experimental approach used for calcium imaging of spinally-projecting glutamatergic MLR neurons and fraction of MLR>SC neurons positively modulated by locomotion (39.3%; 56 neurons, n = 7 mice). Middle: Graphs depicting modulation indices during open field locomotion of MLR>SC neurons in rising order (neurons positively modulated by locomotion in magenta dots; all other neurons shown as gray dots). Right: Baseline subtracted average fluorescence (± SEM) of locomotion-tuned MLR>SC neurons, aligned to locomotion onset.

(B) Left: Experimental approach used for calcium imaging of Rbp4 transgene positive MLR neurons and fraction of MLR-Rbp4 neurons positively modulated by locomotion (19.9%; 152 neurons, n = 4 mice). Middle: Graphs depicting modulation indices during open field locomotion of MLR-Rbp4 neurons in rising order (positively modulated neurons are depicted in cyan; all other neurons shown as gray dots). Right: Baseline subtracted average fluorescence (± SEM) of locomotion-tuned MLR-Rbp4 neurons, aligned to locomotion onset.

(C, D) Two representative locomotion-tuned example neurons (C: MLR>SC; D: MLR-Rbp4) from our experimental dataset. Speed traces (magenta), locomotor bout time windows (transparent magenta boxes) and Z-scored fluorescence (black) are depicted. Note low fluorescence for both neurons in non-locomotion time windows in the center.

(E) Anatomical reconstruction of GRIN lens placements for MLR>SC (left) and MLR-Rbp4 (right) experiments shown on corresponding atlas sections (Bregma level indicated).

See also Figure S4.

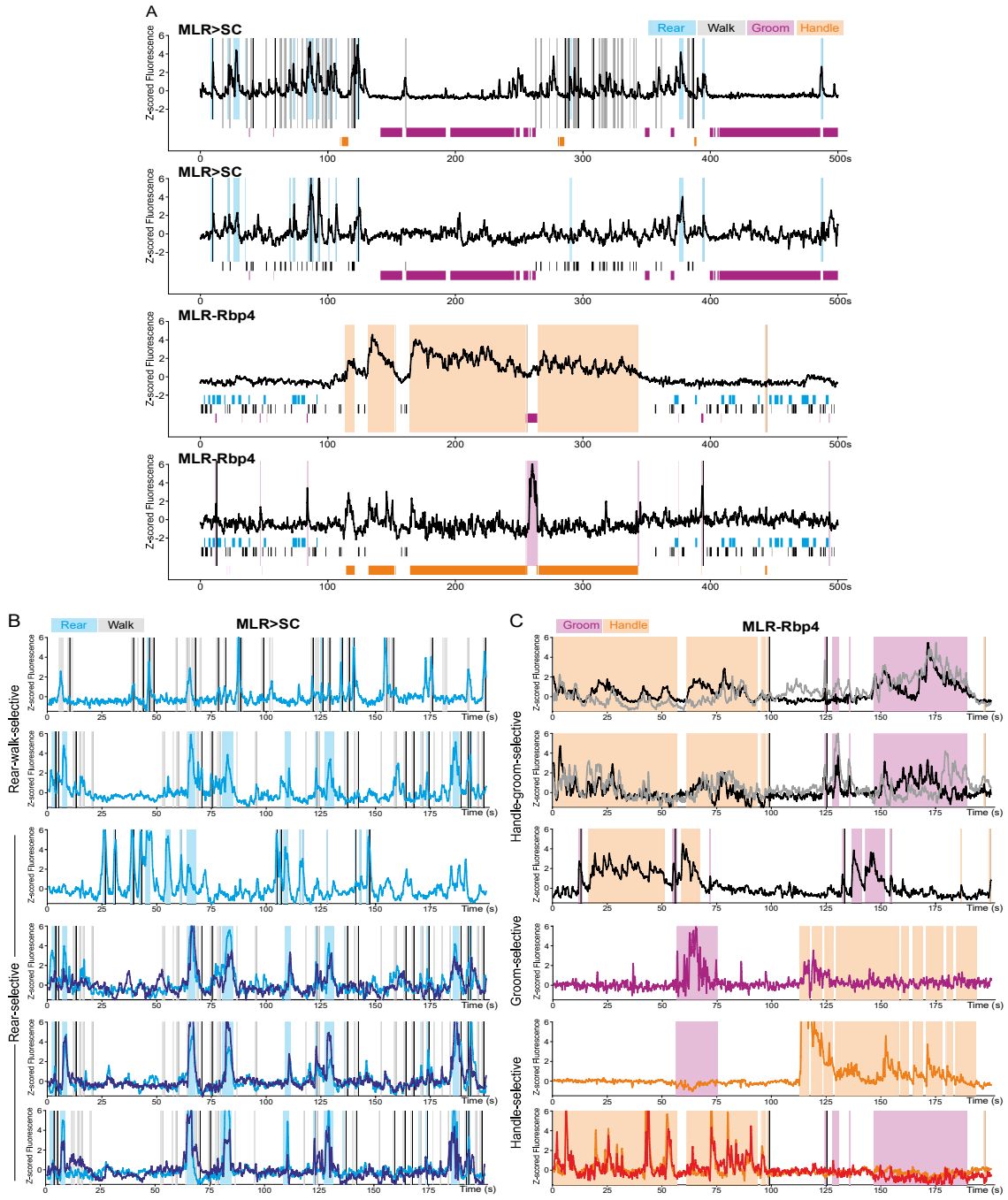

Figure S4. Representative example neurons for MLR>SC and MLR-Rbp4, related to Figure 3

Representative MLR>SC and MLR-Rbp4 example neurons (A: as indicated; B: MLR>SC; C: MLR-Rbp4) from our experimental dataset with Z-scored fluorescence and behavioral time (transparent boxes overlaid to traces or shown as boxes below traces to indicate identity of behavior carried out; colors indicate different behaviors as depicted). Note that for some examples, two fluorescent traces in different colors are shown for space reasons. Examples illustrate differential dynamics of neurons at the single cell and single trial level.

Differential decoding of behaviors from MLR neuron populations

To further explore the relationship between neuronal activity profiles and the different behaviors, we took a reverse approach. We extracted the highest peaks of neuronal activity for all analyzed neurons and computed the probability of each behavior occurring at the time of peak (Figure 4A) or in a -2.5s to +5s time window for single neurons (Figure 4B). We found that MLR>SC neurons exhibited the highest probability of being strongly recruited during rearing, followed by walking, but the highest peaks were rarely found during handling and grooming (Figures 4A and 4B). In contrast, the highest activity peaks for MLR-Rbp4 neurons were most prominently associated with handling, followed by grooming, while walking and rearing were only poorly represented (Figures 4A and 4B). Together, these findings support the observation that the majority of MLR>SC neurons are recruited during full-body behaviors, and MLR-Rbp4 neurons exhibit the most striking recruitment during the forelimb behaviors handling and grooming.

To characterize the population-level representation of full-body and forelimb movements in MLR>SC and MLR-Rbp4 neurons, we performed a correlation analysis of modulation indices across the four different behaviors (Figures 4C and 4D). Analysis of MLR>SC neurons revealed no correlation between rearing and locomotion tuning, suggesting dissimilar overall recruitment profiles of MLR>SC ensembles during these two full-body behaviors. In contrast, modulation indices for the few handling- or grooming-tuned MLR>SC neurons were very small and exhibited a strong positive correlation to each other (Figures 4C and 4D). Correlation analysis of MLR-Rbp4 neurons across different behaviors revealed no significant correlation between grooming and handling modulation indices. In contrast, rearing and walking modulation indices were very small but highly correlated (Figures 4C and 4D).

Together, these findings suggest that MLR>SC neuron activity may have low decoding accuracy to distinguish handling from grooming, while MLR-Rbp4 neurons may be poor predictors to distinguish rearing from walking. On the other hand, one may expect MLR>SC neurons to be good predictors of rearing and walking, while MLR-Rbp4 neurons may distinctly encode grooming and handling.

To test this hypothesis, we applied a generalized linear model. We used 80% of the recording time to train the models and 20% to test the accuracy of differentiating each pair of behaviors studied based on neuronal recording data (Figures 4E and S5A; with 100-fold cross validation). We found that MLR>SC neurons performed worse at distinguishing between forelimb behaviors compared to all other behavioral pairs, while MLR-Rbp4 neurons were worse at distinguishing the two full-body behaviors compared to all other behavioral pairs (Figures 4E and S5A). This statement was true not only for neurons tuned to a single behavior (i.e., handle or groom; rear or walk) but also for neurons tuned to two behaviors (i.e., handle and groom; rear and walk) (Figure S5B), suggesting that the fine details of behavioral recruitment at the neuronal level determine the neuronal fingerprint allowing decoding of behavior also for populations recruited during multiple behaviors. Together, these findings suggest that within the MLR>SC population, neuronal encoding is sufficiently rich to distinguish the full-body behaviors rearing and walking or distinguish these from forelimb behaviors. In contrast, MLR-Rbp4 neurons provide rich information about the forelimb behaviors of grooming and handling but do not carry information to differentiate the full-body behaviors rearing and walking.

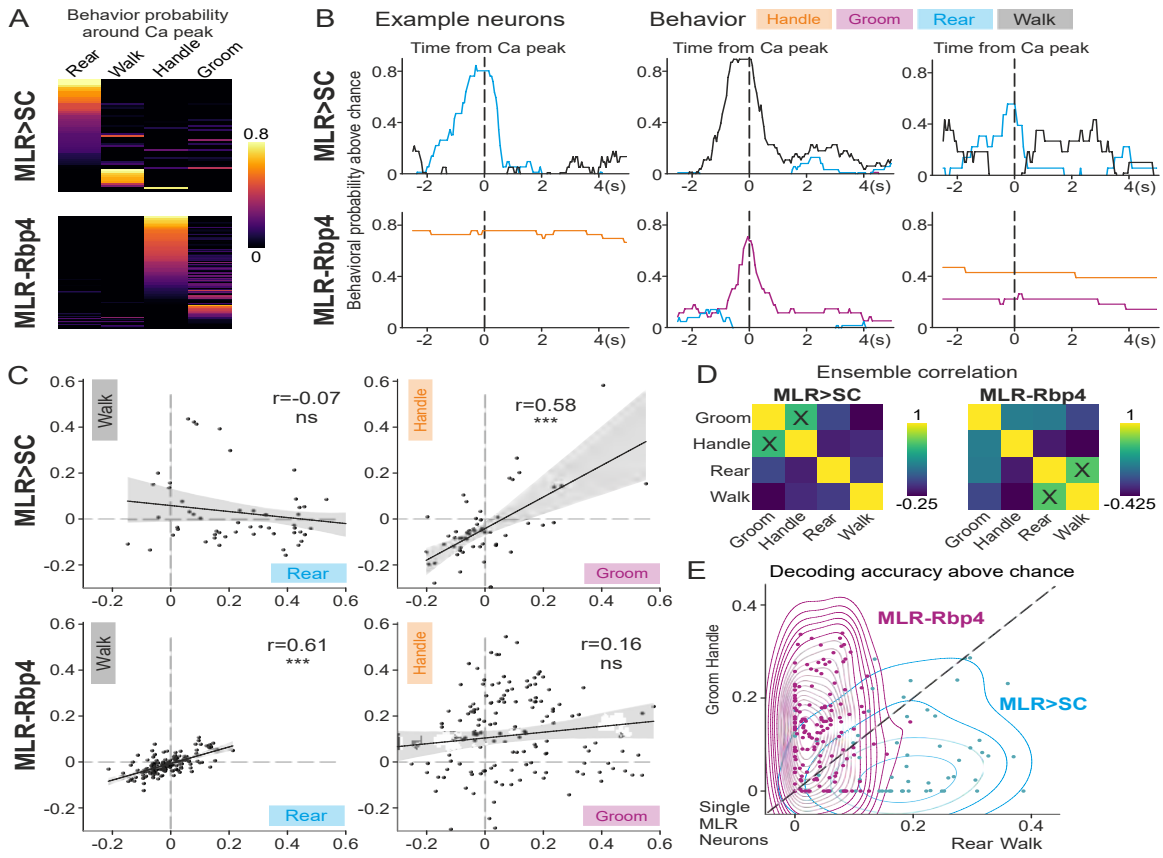

Figure 4. Differential behavioral decoding from MLR>SC and MLR-Rbp4 neuron activity

(A) Behavioral probability above chance around peak calcium activity of all recorded MLR>SC and MLR-Rbp4 neurons for four behaviors (MLR>SC: 56 neurons from n = 7 mice; MLR-Rbp4: 152 neurons from n = 4 mice).

(B) Behavioral probability above chance of handle, groom, rear, and walk for six example neurons around time from calcium peak (T = 0; top: three MLR>SC neurons; bottom: three MLR-Rbp4 neurons).

*(C) Correlation plots for behavioral modulation indices with respect to different behaviors for all studied MLR>SC (top) and MLR-Rbp4 (bottom) neurons and relative Spearman correlation coefficients (r). Shaded region represents 95% confidence intervals. ***p ≤ 0.001; ns, not significant.*

(D) Spearman correlation of neuronal modulation indices for all neurons for MLR>SC (left) and MLR-Rbp4 (right) neurons.

(E) Decoding accuracy of each neuron above chance for all MLR-Rbp4 and MLR>SC neurons (single neurons: dots, overlaid by KDE density isolines).

See also Figure S5.

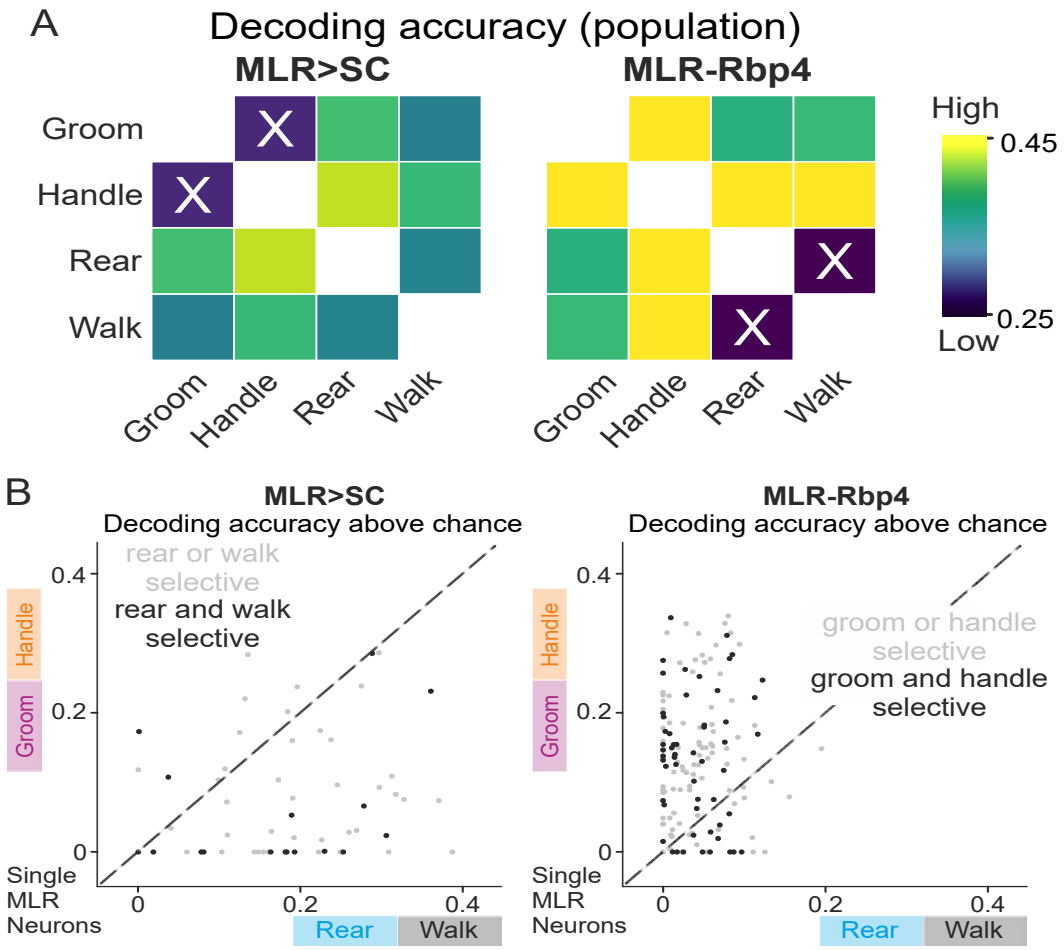

Figure S5. Differential behavioral decoding from MLR>SC and MLR-Rbp4 neuronal activity, related to Figure 4

(A) Average population decoding accuracy above chance across all mice analyzed for MLR>SC (n = 7) and MLR-Rbp4 (n = 4) populations. Note low decoding ability for MLR-Rbp4 neurons with respect to differentiating rearing from walking, and low decoding accuracy for MLR>SC neurons to distinguish handling from grooming consistent with results for single neurons as well.

(B) Same plot as shown in Figure 4E but differentiating neurons with bi-selective behavioral tuning (black) from neurons with tuning to a single behavior (gray). Note random distribution of the bi-selective neurons in their ability to distinguish distinct behaviors.

MLR>SC neurons regulate body extension

We next studied the role of MLR>SC and MLR-Rbp4 neurons in behavior through complementary loss- and gain-of-function experiments. Considering the observation that both MLR>SC and MLR-Rbp4 populations exhibit sophisticated tuning properties related to multiple behaviors, optogenetic perturbation of each entire population is predicted to test the impact that joint down or upregulation of neuronal activity exhibits on behavioral output.

For loss-of-function experiments, we expressed the soma-targeted anion-conducting channelrhodopsin stGtACR2 (Mahn et al., 2018) in glutamatergic MLR>SC neurons (Figures 5A and S6A). Since many MLR>SC neurons exhibit modulation during rearing, we first performed bilateral optogenetic activation of stGtACR2 in MLR>SC neurons during rearing (Figures 5B and S6B). We observed that shortly after onset of optogenetic inhibition, mice terminated rearing, shortening their body to reach a stable position on the ground (Figure 5B; Video S1). We used the markerless pose estimation approach DeepLabCut (Mathis et al., 2018) to track the nose of mice during optogenetic inhibition and found that the termination of rearing was highly reproducible across trials and mice (Figures 5B–5D). Notably, within 200ms after stimulation onset, the body of the mice shortened considerably, interrupting the ongoing rearing episode, an effect not observed in control mice (Figures 5D and S6B). Stimulation applied during ongoing locomotion resulted in reduced locomotor speed (Figures 5EandS6B; Video S1), which we interpret as interference with locomotion through the induced postural changes.

We next performed gain-of-function experiments by targeting the optogenetic activator Red-activatable channelrhodopsin (ReaChR;(Lin et al., 2013) to MLR>SC neurons (Figures 5F and S6C). Bilateral stimulation of stationary mice resulted in

consistent body stretching shortly after onset of optogenetic stimulation irrespective of body position (Figure 5G; Video S1). Using DeepLabCut (Mathis et al., 2018), we found that both hindlimbs remain essentially stable on the ground throughout the stimulation period, but optogenetically induced body extension had a striking impact on frontal body parts, resulting in a joint forward movement of head and forelimbs (Figures 5H, 5J, and S6D). Quantification of many trials over mice confirmed this finding and demonstrates that optogenetic activation of MLR>SC neurons elicits body stretching (Figures 5I and 5J). In contrast, optogenetic stimulation of vGlut2-expressing MLR neurons with projections to the medulla (MLR>Med neurons) elicited reliable locomotion (Figures S6E–S6I), in agreement with previous work showing that MLR-vGlut2 projections to the caudal medulla convey a descending locomotor signal (Capelli et al., 2017). Interestingly, when conditions favored transition to locomotion, i.e., with the mouse facing away from walls with all feet on the ground, optogenetic activation of MLR>SC neurons induced body stretching transitioning into at least one full stepping cycle in a fraction of trials (Figure 5K), suggesting that body stretching may facilitate the transition to locomotion. Notably, a fraction of rearing-tuned MLR>SC neurons are also recruited during locomotion (Figures 3H, S3A, and S3C). Neither body extension nor stepping could be elicited by light application in the sole presence of the fluorophore (Figures 5I–5K and S6D). Together, our findings support a model in which spinally projecting MLR neurons are required for postural body adjustments needed for full-body exploratory behaviors, while reliable locomotion-promoting effects of excitatory MLR neuron stimulation rely on interaction with caudal medullary circuits.

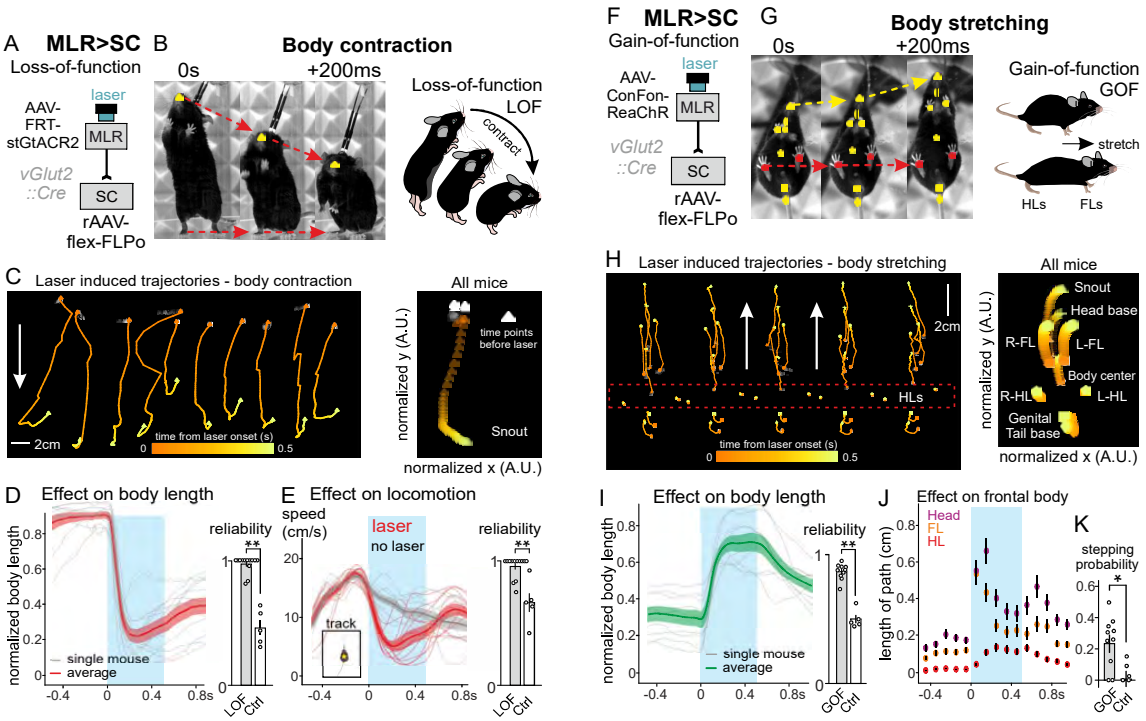

Figure 5. MLR neurons with spinal projections regulate body extension

(A) Approach to target the optogenetic inhibitor stGtACR2 into MLR>SC neurons for loss-of-function (LOF) experiments (n = 13).

(B) Left: snapshots from video analysis of rearing mouse just before laser onset (0 s) to +200 ms after laser onset, with one intermediate frame (snout: yellow). Right: Cartoon representation of body contraction effect induced by optogenetic LOF of MLR>SC neurons during rearing.

(C) DeepLabCut tracking of snout position upon optogenetic inhibition of MLR>SC neurons (white points before stimulation; orange to yellow points from 0 to 500 ms of laser stimulation), showing single trials (left) and normalized snout trajectory over all trials and mice (right) (n = 13).

(D) Average (±SEM) of normalized body length (red) of rearing mice and single mouse averages (gray) upon optogenetic inhibition (blue window) of MLR>SC neurons and reliability of laser-induced decrease in average body length (0.5 being chance level) in mice expressing stGtACR2 (LOF, n = 13) or GFP (Ctrl, n = 5) in MLR>SC neurons.

(E) Average (±SEM) of locomotor speed upon closed loop optogenetic inhibition (blue window, red line) of MLR>SC neurons during locomotion and control trials with no laser stimulation (black line) with single-mouse averages of the two conditions and reliability of locomotor speed decrease (n = 13), compared to the reliability of occurrence of the same phenotype in control mice upon light application (n = 5).

(F) Approach used to target the optogenetic activator ReaChR into MLR>SC neurons for gain-of-function (GOF) experiments (n = 10 mice).

(G) Left: snapshots from video analysis of stationary mouse just before laser onset (0 s) to +200 ms after laser onset, with one intermediate frame. Snout, head base, forelimbs, hindlimbs, body center, genital, and tail base are marked through DeepLabCut analysis. Right: cartoon representation of the body extension effect induced by optogenetic GOF of MLR>SC neurons in stationary mice.

(H) DeepLabCut tracking of body part position upon optogenetic activation of MLR>SC neurons through laser application (white points before stimulation; orange to yellow points from 0 to 500 ms of laser stimulation), showing single trials (left) and normalized body part trajectories over all trials and mice (right) (n = 10; compared to n = 5 control mice).

(I) Average (±SEM) of normalized body length (green) of stationary mice and single-mouse averages (gray) upon optogenetic activation (blue window) of MLR>SC neurons and reliability of laser induced increase in body length (n = 10) compared to the probability of observing an increase in body length in control mice upon light application (n = 5).

(J) Binned average path length (±SEM) for head (average of snout and head base), forelimbs (FL; average of left and right forelimb), and hindlimbs (HL; average of left and right hindlimb) for stationary mice upon laser application (blue window) to MLR>SC neurons for optogenetic activation (n = 10).

(K) Graph depicting probability above baseline levels (baseline: application of a 0-mW laser with same closed-loop protocol) to initiate at least one cycle of four limb stepping after body stretching upon optogenetic activation of MLR>SC neurons (n = 10) and light application in control mice (n = 5). Stimulations were performed when mice were sedentary with all four paws on ground in an unrestrained open field environment.

See also Figure S6.

**p ≤ 0.05 **p ≤ 0.01.*

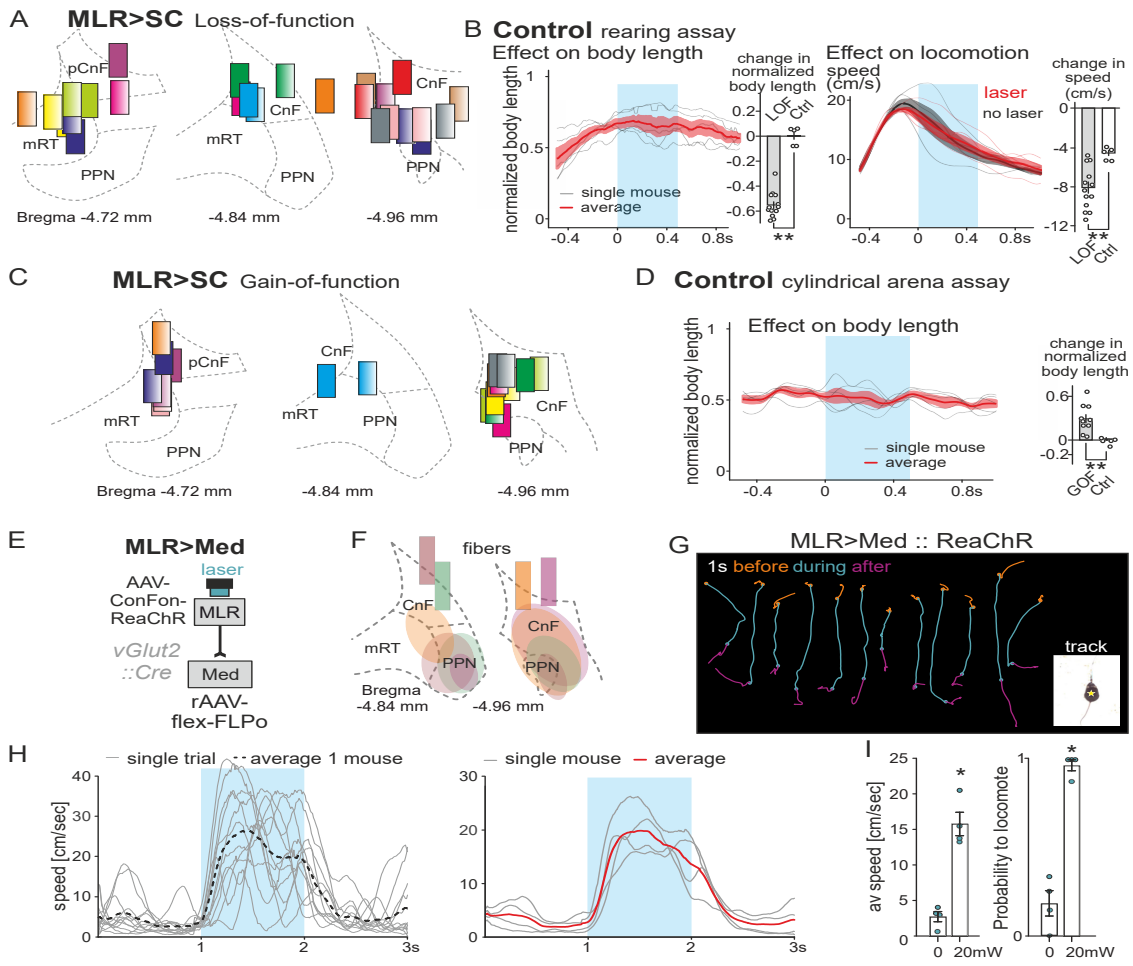

Figure S6. Optogenetic stimulation of medulla-projecting MLR neurons elicits locomotion, related to Figure 5

(A) Anatomical confirmation of fiber placements for MLR>SC loss-of-function (LOF) mice at corresponding rostro-caudal levels (distance from Bregma indicated).

(B) (left) Average (±SEM in red; single mouse averages in gray) of normalized body length upon light application (blue window) in control mice during rearing and bar plot comparing light-evoked change in normalized body length in MLR>SC LOF (n = 13) and control mice (n = 5) (right). Average (±SEM; single mouse averages) of locomotor speed upon light application (red) and in no laser trials (black) in control mice and bar plot comparing light-evoked change in speed in MLR>SC LOF (n = 13) and control mice (n = 5).

(C) Anatomical confirmation of fiber placements for MLR>SC gain-of-function (GOF) mice at corresponding rostro-caudal levels (distance from Bregma indicated).

(D) Average (±SEM in red; single mouse averages in gray) of normalized body length upon light application (blue window) in stationary control mice and bar plot comparing light-evoked change in normalized body length in MLR>SC GOF (n = 10) and control mice (n = 5).

(E) Experimental approach for optogenetic activation of medulla-projecting glutamatergic MLR neurons (MLR>Med).

(F) Anatomical confirmation of fiber placement and expression of optogenetic activator for MLR>Med GOF mice at corresponding rostro-caudal levels (distance from Bregma indicated).

(G) Single trajectories of center of body mass for 1 s before (orange), during (cyan) and after (magenta) laser application, visualizing induction of locomotion by stimulation of MLR>Med neurons (multiple trials from example mouse).

(H) Analysis of locomotor speed based on tracked center of body mass over time for single trials and average thereof (left) as well as single mice (n = 4) and average thereof (right), for optogenetic activation (blue window) of MLR>Med neurons.

(I) Quantification of average speed during the laser ON period and probability to locomote for optogenetic activation of MLR>Med neurons. (n = 4 mice; $p < 0.05$ calculated with the Mann-Whitney U test).

**$p \leq 0.05$ **$p \leq 0.01$.*

MLR-Rbp4 neurons modulate behavior through impacting basal ganglia

To determine the role of MLR-Rbp4 neurons in behavior, we performed loss-of-function experiments by expressing stGtACR2 in Rbp4 neurons (Figure 6A). We reasoned that acutely reducing neuronal activity in MLR-Rbp4 neurons might lead to generalized disinhibition of behaviors due to reduced excitatory drive onto behavioral inhibition-promoting basal ganglia output structures (Figures 2 and S2). Bilateral optogenetic inhibition of MLRRbp4 neurons indeed led to uncoordinated body movements (Figure 6B; Video S2). Optogenetically induced movements entailed all body parts with highly variable movement sequences across trials (Figures 6B, S7A, and S7B; Video S2), independent of the particular movement a mouse was engaged with at the time of stimulation (data not shown). We found that the aberrant optogenetically induced movements came to a halt while optogenetic stimulation was still ongoing, and no additional excessive movement was observed at or after laser offset (Figures 6C, S7A, and S7B; Video S2). Light application in control mice did not elicit speed changes of tracked body parts (Figure S7A). Together, these findings demonstrate that optogenetic inhibition of MLR-Rbp4 neurons leads to rapid misbalancing of motor output across all body parts, likely due to perturbation of the physiologically fine-tuned signaling between MLR-Rbp4 neurons and basal ganglia output structures.

Based on these findings, one may predict that optogenetic activation of MLR-Rbp4 neurons has the opposite effect, i.e., would lead to stalling of body movements. To address this question, we targeted MLR-Rbp4 neurons with the optogenetic activator ReaChR (Figure 6D). We found that bilateral optogenetic activation of MLR-Rbp4 neurons during movement leads to rapid stalling of the body (Video S2). Body parts rapidly stopped moving shortly after laser onset as observed in analysis of single stimulation trials (Figure 6E). We found that stimulation during ongoing locomotion led to reliable stopping of locomotion compared to no laser trials or control mice (Figures 6F and S7D; Video S2). Locomotion stops were accompanied by cessation of regular limb muscle contractions during rhythmic stepping determined by electromyographic recordings (Figure S7C). Also the other three behaviors (rear, groom, and handle) were efficiently halted by application of optogenetic stimulation to MLR-Rbp4 neurons, exhibiting rapid speed decreases for moving body parts, not observed in control mice (Figures 6G–6I and S7E). Lastly, to determine whether the observed behavioral effects are not due to genetic targeting through a transgenic line, we applied optogenetic stimulation on excitatory MLR neurons retrogradely targeted from the SN or stimulated axons from MLR-vGlut2 neurons expressing an optogenetic activator (Rajasethupathy et al., 2015) in the SN during locomotion (Figure S7F). We found that all three approaches induced termination of locomotion during the period of laser application (Figure S7F). These findings demonstrate that loss- and gain-of-function perturbations have opposite impacts, and together suggest that excitatory MLR inputs to basal ganglia structures play a more holistic modulatory role to orchestrate body movements.

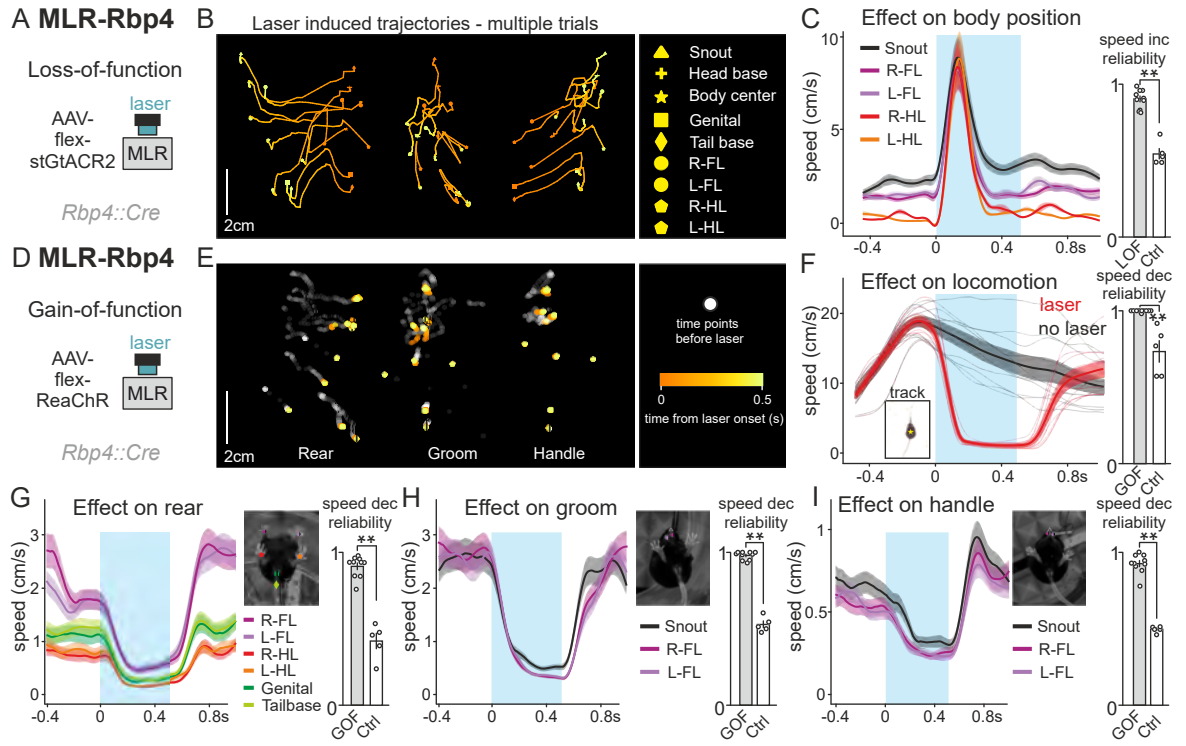

Figure 6. Opposite perturbation of MLR-Rbp4 neurons elicits pro- and antikinetic modulation of behavior

(A) Approach to target the optogenetic inhibitor stGtACR2 into MLR-Rbp4 neurons for LOF experiments (n = 10).

(B) DeepLabCut tracking of body part position (list shown to the right) upon optogenetic inhibition of MLR-Rbp4 neurons through laser application (white points before stimulation; orange to yellow points from 0 to 500 ms of laser stimulation), showing three single trials from one mouse.

(C) Average speed of body parts (±SEM) upon optogenetic inhibition (blue window) of MLR-Rbp4 neurons and reliability of laser induced speed increase (n = 10) compared to the probability of increase in speed in control mice upon light application (n = 5).

(D) Approach to target the optogenetic activator ReaChR into MLR-Rbp4 neurons for GOF experiments (n = 10).

(E) DeepLabCut tracking of body part position (list shown in B) upon optogenetic activation of MLR-Rbp4 neurons through laser application (white points before stimulation; orange to yellow points from 0 to 500 ms of laser stimulation), showing three single trials during rearing, grooming, or handling.

(F) Average (±SEM) of center-of-body-mass speed upon closed loop optogenetic activation (blue window) of MLR-Rbp4 neurons during locomotion and control no laser trials (black) with single-mouse averages of the two conditions (n = 10). Graph to the right shows reliability in speed decrease upon optogenetic activation of MLR-Rbp4 neurons compared to the probability of observing a locomotor speed decrease in control mice expressing GFP upon light application (n = 5).

*(G–I) Average (±SEM) of speed of body parts (as indicated: forelimbs, hindlimbs, genitals, tail base, and snout) for rearing (left), grooming (middle), and handling (right) trials (n = 10). Graphs to the right show reliability in speed decrease upon optogenetic activation of MLR-Rbp4 neurons compared to the probability of observing a decrease in speed in control mice upon light application (n = 5). See also Figure S7. **p ≤ 0.01.*

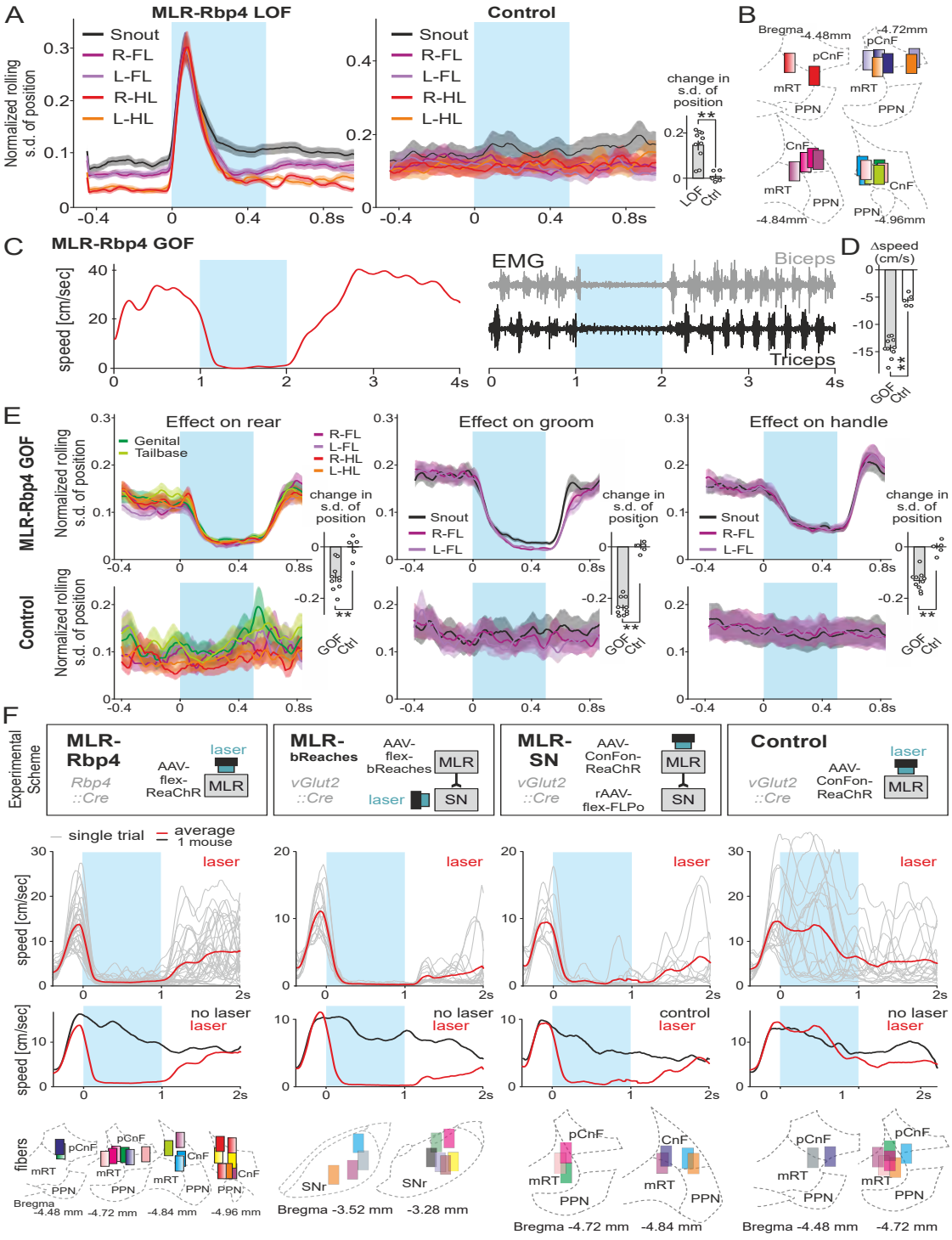

Figure S7. Optogenetic perturbation of SN-projecting MLR neurons, related to Figure 6

(A) Effect of laser stimulation on normalized rolling s.d. of position (mean ± SEM) of body parts (forelimbs, hindlimbs, snout) upon laser application in MLR-Rbp4 loss-of-function (LOF) (n = 10; left) and control mice (n = 5, right) and bar plot comparing light-induced change in the normalized s.d. of position (mean ± SEM) in MLR-Rbp4 LOF (n = 10) and control mice (n = 5).

(B) Anatomical confirmation of fiber placements for MLR-Rbp4 LOF mice at corresponding rostro-caudal levels (Bregma indicated).

(C) Electromyography in the forelimb muscles biceps and triceps during ongoing locomotion and upon optogenetic stimulation of MLR-Rbp4 neurons in an example mouse (blue window: laser application; red line: speed trace). Note that behavioral arrest is accompanied by cessation of biceps and triceps alternating muscle contraction.

(D) Comparison of the change in speed (mean ± SEM) between the MLR-Rbp4 gain-of-function (GOF; n = 10) and control mice (n = 5) upon light application.

(E) Effect of light application on normalized rolling s.d. of position (mean ± SEM) for different body parts (as indicated: forelimbs, hindlimbs, genitals, tail base, snout) for rearing (left), grooming (middle) and handling (right) trials upon laser application in MLR-Rbp4 GOF (n = 10) and control mice (n = 5). The bar plots indicate the comparison of the light induced change in the normalized rolling s.d. of position (mean ± SEM) for each behavior between MLR-Rbp4 GOF (n = 10) and control mice (n = 5).

(F) Top: Experimental strategy for optogenetic activation of MLR-Rbp4 neurons (n = 10), axonal terminals of vGlut2-MLR neurons over SN (n = 10), vGlut2-MLR neurons with projections to SN (n = 7), compared to control mice (n = 8) not expressing optogenetic activators. Middle: Graphs from example mice showing speed versus time plots and depict single trials (in gray) and their averages for closed loop laser application (red), no laser application (black), as well as an overlay of these two experimental conditions. Bottom: Anatomical confirmation of fiber placements for analyzed mice at corresponding rostro-caudal levels (Bregma indicated; one fiber of one animal not shown due to unilateral dorsal fiber placement).

***p ≤ 0.01.*

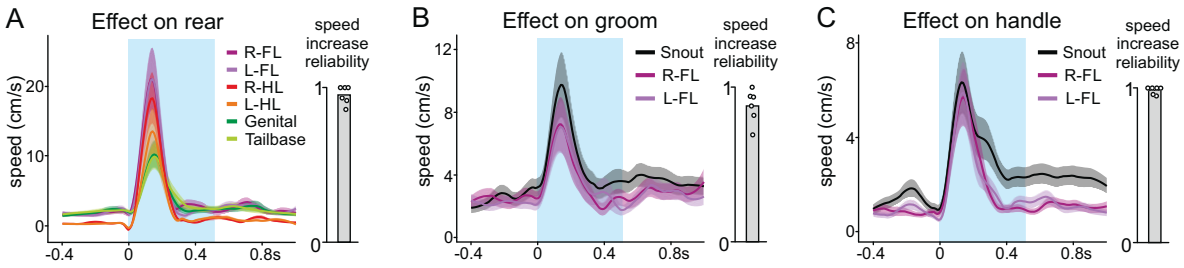

Figure S8. Effect of optogenetic silencing of MLR-Rbp4 neurons on specific behaviors.

(A-C) Average (± SEM) of speed of body parts (as indicated: forelimbs, hindlimbs, genitals, tail base, snout) for rearing (left), grooming (middle) and handling (right) trials, illustrating a rapid increase in speed of body parts upon laser application (blue window) to MLR-Rbp4 neurons to induce optogenetic inhibition (n = 10). Graphs to the right show reliability in speed increase upon optogenetic inhibition of MLR-Rbp4 neurons compared to the probability of observing the same phenotype in control mice upon light application (n = 5).

Discussion

Locomotion is a universal animal behavior engaging distributed neuronal circuits. Cumulative work on the MLR has elicited discussion with respect to understanding its function in natural locomotor behavior (Caggiano et al., 2018; Ferreira-Pinto et al., 2018; Josset et al., 2018), but it is also unclear with respect to application of DBS to treat therapy-resistant PD symptoms (Garcia-Rill et al., 2019). Here, we show that dedicated neuronal populations are recruited during different forms of body movement, notably not restricted to locomotion. We believe that these findings shed light on both ongoing debates and call for a radically updated view of neuronal function in this midbrain region. We will discuss the implications of our work for motor system function and design of future DBS interventions.

Functional separation of glutamatergic MLR neurons by projection target

Recent studies on the control of locomotion by the midbrain began to functionally dissect the broader MLR area. Studies agree on important roles of specifically glutamatergic MLR neurons in the regulation of locomotion. Most recordings from glutamatergic MLR neurons were focused on correlating their activity with positive locomotion attributes, yet many neurons remain uncharacterized (Caggiano et al., 2018; Carvalho et al., 2020; Roseberry et al., 2016). Our work reveals that anatomically identified subpopulations of excitatory MLR neurons are recruited during different body movements and that locomotion is but one type of movement involving excitatory MLR neurons. We describe two cleanly divided populations of ascending and descending glutamatergic neurons in the PPN region characterized by essentially opposite behavioral recruitment profiles. An ascending population with terminations in the basal ganglia structures SNr, entopeduncular nucleus, and

subthalamic nucleus (STN) is positively modulated during the forelimb movements grooming and handling. In contrast, neurons with descending projections to the SC are recruited mostly during rearing. To what extent inhibitory and cholinergic PPN neurons share this organizational principle remains to be determined, but single-cell reconstructions of cholinergic PPN neurons revealed a high degree of collateralization, distinct from non-cholinergic PPN neurons (Mena-Segovia et al., 2008). Nevertheless, cholinergic PPN neurons are organized along the rostro-caudal axis according to preferential projection targets (Mena-Segovia and Bolam, 2017). In lamprey, medullary cholinergic projections were implicated in locomotion control via fast ionotropic mechanisms (Le Ray et al., 2003), and in cat, MLR neurons also recruit spinally projecting monoaminergic neurons to modulate locomotion (Noga et al., 2017).

What are possible functional implications for the regulation of motor behavior that might follow from our observations? MLRRbp4 neurons are glutamatergic and project to generally behavior-inhibitory basal ganglia structures, the recruitment of which by excitatory inputs is predicted to increase inhibitory drive to their output structures (Hikosaka, 2007). Through this connectivity loop, joint recruitment of MLR-Rbp4 neurons provides strong inhibition to neurons in the brainstem motor output pathways and motor thalamus. In agreement, optogenetic activation of MLR-Rbp4 neurons stalls all forms of body movements, likely due to the indirect negative impact on overall motor output pathways. In contrast, optogenetic inhibition of MLR-Rbp4 neurons leads to rapid, explosive body movements, which we interpret as a misbalancing of excitatory drive at the level of basal ganglia output structures, thereby leading to disinhibition of many body behaviors.

In light of the up-to-now studied function of MLR in locomotion, our findings on the prominent modulation of MLR-Rbp4 neurons during forelimb movements might be interpreted as keeping command pathways promoting locomotion repressed whenever forelimb movements are executed. An alternative possibility is that the MLR region might also actively contribute to non-locomotor behaviors. In such a model, the activity of MLR-Rbp4 neurons through their indirect action on SNr might help to modulate the choice or dynamics of specific forelimb and orofacial actions. Since different forelimb actions can be decoded from MLR-Rbp4 neurons, their impact on SNr neurons might contribute to the selection of appropriate downstream neurons. Their role might thus not be restricted to limiting recruitment of locomotion-promoting brainstem circuits. Testing these alternative models awaits the identification of entry points to separately target ascending projection neurons active selectively during specific forms or phases of body movement but leaving other subpopulations unaffected by the applied manipulation.

MLR>SC neurons control body extension

We also address the role of spinally projecting MLR neurons, which up to now have been neglected as a minor population with unknown function. Our loss- and gain-of-function experiments support a role for MLR>SC neurons in regulation of body extension. Our work agrees with models in which locomotion- promoting neurons, as opposed to body extension-controlling neurons, within the MLR area act on spinal circuits primarily indirectly through descending projections to intermediary neurons located in the caudal brainstem (Capelli et al., 2017; Garcia-Rill and Skinner, 1987; Shefchyk et al., 1984). We found that medulla-projecting glutamatergic neurons distribute broadly within all MLR subdivisions, whereas spinally projecting

counterparts are largely intermingled with cholinergic PPN neurons and reside in the neighboring mRT. In rodents, glutamatergic MLR neurons implicated in the regulation of high-speed locomotion were recently demonstrated to reside within the pCnF/CnF (Caggiano et al., 2018), but these do not project to the SC. Moreover, high-speed locomotion depends on glutamatergic neurons within the medulla subdivision lateral paragigantocellular nucleus (LPGi) and ablation of these neurons attenuates the locomotor drive provided by glutamatergic MLR neurons (Capelli et al., 2017). Furthermore, in other species including the lamprey and the cat, normal or MLR-induced locomotion can modulate the activity of medullary reticulospinal neurons in nuanced ways (Brocard and Dubuc, 2003; Deliagina et al., 2000; Matsuyama and Drew, 2000; Perreault et al., 1993). Together, these data lend support to the idea that neurons in the midbrain charged with roles in complex regulatory parameters of limbed locomotion, including instructions on how to move limbs and at what speed, do not communicate with spinal circuits directly but engage at least the medulla as an intermediate processing step. This is conceptually similar to recent findings on neuronal circuits controlling the construction of forelimb movements (Ruder et al., 2021). In this work, neurons with direct spinal projections from the rostral lateral medulla can induce unilateral forelimb reaching movements, while digit involving forelimb movements can only be elicited by stimulation of neurons with targets in the caudal medulla (Ruder et al., 2021). In an analogous model, MLR>SC neurons may carry signals for postural adjustments to aid the body to engage in exploratory activities, including locomotion.

Implications of distinct MLR subpopulations for DBS interventions in PD patients

Our findings on functionally distinct excitatory MLR populations is also of value to the DBS field, where the PPN has been hotly discussed (Garcia-Rill et al., 2019; Nowacki et al., 2018; Tubert et al., 2019). Some PD patients exhibit postural instability and gait impairment that are resistant to dopamine replacement therapy or STN-DBS. PPN-DBS was tried as a possible intervention to ameliorate these resistant symptoms. Yet, results are not convincing, with patients reporting minimal benefits and many side effects. Decades of discussing about the best possible location within the PPN for stimulation did not lead to a solution.

Reviewing clinical and basic literature, it has been proposed that the PPN might be too complex a brain region for reliable direct DBS interventions (Tubert et al., 2019). Our results agree with this assessment. Even if DBS were to target primarily neuronal cell bodies, the intermingling of neurons within the PPN/mRT with distinct functions would make it impossible to reliably target one or the other separately to assess possible outcomes in patients cleanly. Our findings also reconcile the apparently conflicting published results in the field of basic research (Caggiano et al., 2018; Carvalho et al., 2020; Josset et al., 2018), since direct virus injections into the PPN/mRT area, inherently leads to co-infection of functionally mixed neurons. Only disentanglement of glutamatergic PPN/mRT neurons by projection target can reveal the behavioral output that stimulation of these neurons produces.

We conclude that while targeting the adequate neurons within the PPN/mRT region might indeed be beneficial for patients, current technology fails to produce reproducible benefits. Our work suggests that targeting spinally projecting MLR neurons might be beneficial for postural stabilization, whereas promoting limb stepping

might need targeting of medulla-projecting populations. In contrast, targeting SN-projecting MLR population is likely going to be of limited value, since it encodes many behavioral parameters and its perturbation likely leads to noncontrolled behavioral effects. Interestingly, the stalling of ongoing movements induced by stimulation of SNr-projecting MLR neurons resembles the freezing episodes of PD patients. This observation raises the question of how this population is affected in the parkinsonian state, opening new entry points into PD symptom research. At a clinical level, only once technologies for accessing functionally more uniform neuronal populations become available in humans can we expect to produce the needed better outcomes for PD patients.

Limitations of the study

Individual MLR-Rbp4 neurons change their firing profiles in highly varied and nuanced patterns during natural behavior and are never modulated as an entire population, like we artificially impose during optogenetic experiments. Therefore, the natural impact of MLR-Rbp4 neurons during behavior on SNr and other basal ganglia structures cannot be deduced from whole-population loss- or gain-of-function experiments. It most likely depends on the precise connectivity patterns between different populations of MLR neurons and basal ganglia recipient neurons, as well as their recruitment profiles during natural behavior regulated through their inputs. In line with this idea, different behaviors are encoded by specific neuronal ensembles in the striatum (Klaus et al., 2017b), and SNr neurons divide into at least seven populations based on their projection targets (McElvain et al., 2021). Movement therefore entails the orchestrated activation and inhibition of these ensembles in adequate sequence and vigor. It is conceivable that the functionally diverse MLR-Rbp4 ensembles we

describe here are part of a broader network, including the basal ganglia, and responsible for the selection of desired and the inhibition of nonselected motor programs. Further tool development for perturbation of neuronal circuits may help in reinforcing the results of our and related studies.

Acknowledgements

We are grateful to M. Mielich, C. Pivetta, K. Fidelin for experimental help, J. Hinz for precious advice and sharing his pipeline for extracting calcium imaging data, N. Whittle and G. Martins for help setting up miniscope calcium imaging experiments, P. Argast and P. Buchmann from the FMI mechanical workshop for building devices for behavioral experiments, R. Thierry for support on scripting for data analysis, K. Yamauchi for help with setting up high-speed video recording system, and to P. Caroni for discussions and comments on the manuscript. M.J.F.P. was supported by a PhD student fellowship from the Portuguese Foundation for Science and Technology (PD/BD/105867/2014), H.K. by a Biozentrum PhD Fellowship, and M.S.E. by funding from Synapsis Foundation Grant, NARSAD Young Investigator Grant by the Brain and Behavior Foundation, Career Development Award from HFSP, CONICET and PICT 2018-00607. All authors were supported by funding from the European Research Council (ERC) under the European Union's Horizon 2020 research and innovation programme (Descent, grant agreement No 692617), the Swiss National Science Foundation, the Kanton Basel-Stadt, the Novartis Research Foundation, and the Louis Jeantet Prize for Medicine.

Author Contributions

All authors were involved in the design of experiments and data analysis. M.J.F.P. and M.S.E. carried out most anatomical characterization of neuronal

subpopulations. M.J.F.P., H.K. and A.F. carried out neuronal recording experiments. H.K. and A.F. analyzed neuronal recording experiments. M.J.F.P., H.K. and A.F. performed and analyzed gain-of-function experiments. H.K. and A.F. performed and analyzed loss-of-function experiments. M.S. processed most tissues for post-experimental validation. S.A. initiated the project and wrote the manuscript. All authors discussed the experiments and commented on the manuscript.

Declaration of interests

The authors declare no competing interests.

STAR METHODS

KEY RESOURCES TABLE

REAGENT or RESOURCE	SOURCE	IDENTIFIER
Antibodies		
chicken anti-GFP	Invitrogen	Cat# A10262; RRID: AB_2534023
chicken anti-Myc	Invitrogen	Cat# A21281; RRID: AB_2535826
chicken anti-TH	Neuromics	Cat# CH23006; RRID: AB_2201403
goat anti-ChAT	Millipore	Cat# AB144P; RRID: AB_2079751
mouse anti-Myc	ATCC	Cat CRL-1729; RRID: CVCL_G671
mouse anti-NeuN	Millipore	Cat# MAB377; RRID: AB_2298772
mouse anti-V5	Invitrogen	Cat# R960CUS; RRID: AB_2792973
rabbit anti-RFP	Rockland	Cat# 600-401-379; RRID: AB_2209751
Donkey anti-rabbit Cy3	Jackson ImmunoResearch	Cat#711-165-152; RRID: AB_2307443
Donkey anti-goat Cy5	Invitrogen	Cat# A-21447; RRID: AB_2535864
Donkey anti-chicken 488	Jackson ImmunoResearch	Cat#703-545-155; RRID: AB_2340375
Donkey anti-chicken Cy5	Jackson ImmunoResearch	Cat#703-605-155; RRID: AB_2340379
Donkey anti-goat 488	Invitrogen	Cat# A-11055; RRID: AB_2534102
Donkey anti-mouse 647	Invitrogen	Cat# A-31571; RRID: AB_162542
Donkey anti-mouse Cy3	Invitrogen	Cat# A-31570; RRID: AB_2536180
Donkey anti-mouse DyL405	Jackson ImmunoResearch	Cat# 715-475-150; RRID: AB_2340839
Donkey anti-goat DyL405	Jackson ImmunoResearch	Cat# 705-475-147; RRID: AB_2340427
Virus Strains		
AAV-flex-SynGFP	Pivetta et al., 2014	N/A
AAV-ConFon-SynGFP	This study	N/A
AAV-flex-ReaChR-YFP	Capelli et al., 2017	N/A
AAV-flex-Flp-H2B-V5	Capelli et al., 2017	N/A
AAV-H2B-10xMyc	Capelli et al., 2017	N/A
AAV-flex-TdTomato	Capelli et al., 2017	N/A
AAV-flex-Flp-H2B-V5	Ruder et al., 2021	N/A
AAV-flex-H2B-GFP	Ruder et al., 2021	N/A
AAV-flex-H2B-TdTomato	Ruder et al., 2021	N/A
AAV-flex-H2B-V5	Ruder et al., 2021	N/A
AAV-Con-Fon-ReaChR-Citrine-YFP	Ruder et al., 2021	N/A
AAV-frt-H2B-TdTomato	This study	N/A
AAV-flex-GCaMP7f	Dana et al., 2019	N/A

AAV-flex-stGtACR2-FusionRed	Mahn et al., 2018	N/A
AAV-frt-stGtACR2-FusionRed	This study	N/A
AAV-flex-bReaChEs	Rajasethupathy et al., 2015	N/A
Deposited Data		
CNMF-E	Pnevmatikakis et al., 2016; Zhou et al., 2017	https://github.com/zhoupc/CNMF_E
Experimental Models: Organisms/Strains		
Mouse: vGlut2^{Cre}: Slc17a6$^{tm2(cre)Lowl}$	Jackson Laboratory	JAX:028863
Mouse: Rbp4^{Cre}: Tg(Rbp4-cre)KL100Gsat/Mmucd	MMRRC	MMRRC_031125-UCD
Mouse: vGAT^{FLP}: Slc32a1$^{tm1.1(flpo)Hze}$	Jackson Laboratory	JAX:029591
Software and Algorithms		
MATLAB (v2017b)	Mathworks	https://www.mathworks.com/ *RRID*:SCR_001622
GraphPad PRISM (v7.0)	GraphPad PRISM	http://www.graphpad.com/ *RRID*:SCR_002798
Python (v3.7)	Python	https://www.python.org/ RRID:SCR_008394
Knime (v3.3.1)	Knime	https://www.knime.com/ RRID:SCR_006164
CorelDraw (vX6 to X9)	Corel	https://www.coreldraw.com/ RRID:SCR_014235
Inscopix Data Acquisition Software (v1.2.1 and 1.4.1)	Inscopix	https://www.inscopix.com
Bonsai (v2.3)	NeuroGEARS Ltd.	https://bonsai-rx.org
CinePlexStudio (v3.7.1)	Plexon Inc.	https://plexon.com
DeepLabCut	Mathis Lab (Mathis et al., 2018)	http://www.mousemotorlab.org/deeplabcut
Other		
200mm: MFC_200/230-0.48_3.5mm_ZF1.25_FLT Mono Fiberoptic Cannula	Doric	http://doriclenses.com/life-sciences/
200mm: MFC_200/230-0.48_6mm_ZF1.25_FLT Mono Fiberoptic Cannula	Doric	http://doriclenses.com/life-sciences/
ProView™ Lens Probe 0.6 mm diameter, ~7.3 mm length	Inscopix	https://www.inscopix.com
Microendoscope (Inscopix nVista 3.0)	Inscopix	https://www.inscopix.com
Wired 9-axis motion sensor	Champalimaud Foundation's Scientific Hardware Platform	https://www.cf-hw.org
Harp WEAR basestation	Champalimaud Foundation's Scientific Hardware Platform	https://www.cf-hw.org
Clock synchronizer	Champalimaud Foundation's Scientific Hardware Platform	https://www.cf-hw.org
PlexBright Optogenetic Stimulation System	Plexon Inc.	https://plexon.com
OmniPlex Neural Recording Data Acquisition System	Plexon Inc.	https://plexon.com

FV1000 confocal microscope	Olympus	http://www.olympusconfocal.com/products/fv1000/index.html
ZEISS Axio Imager 2	Zeiss	https://www.zeiss.com/microscopy/int/products/light-microscopes/axio-imager-2-for-biology.html
CSU-W1 Confocal Scanner Unit	Yokogawa	https://www.yokogawa.com/solutions/products-platforms/life-science/spinning-disk-confocal/csu-w1-confocal-scanner-unit/
OxyletPro System - Treadmill	Panlab	https://www.harvardapparatus.com/catalog/product/view/id/9001/s/oxyletpro-system-treadmill-with-indirect-calorimetry/category/448/
Ace 2 Area Scan Cameras	Basler AG	a2A1920-160umBAS
Pike Cameras	Allied Vision Inc.	https://www.alliedvision.com/en/support/technical-documentation/pike-documentation.html
Cobolt 06-MLD; 473nm; 100mW	HÜBNER Photonics	https://hubner-photonics.com/products/lasers/diode-lasers/06-01-series/
Model 2650 Micropositioner	Kopf	https://kopfinstruments.com/product/model-2650-micropositioner/
Mouse schemes	Zenodo, scidraw.io	doi.org/10.5281/zenodo.3925993 doi.org/10.5281/zenodo.3925913

RESOURCE AVAILABILITY

Lead Contact

Further information or requests for reagents and resources should be addressed to the Lead Contact, Silvia Arber (silvia.arber@unibas.ch).

Materials Availability

All custom-made scripts and codes for analysis, as well as newly made constructs for AAV production described in this manuscript are available upon request by contacting the lead author.

EXPERIMENTAL MODEL AND SUBJECT DETAILS

Animals

We used adult male and female *vGlut2*^{Cre} (RRID: IMSR_JAX:028863), *Rbp4*^{Cre} (RRID: MMRRC_031125-UCD) and *vGAT*^{FLP} (RRID: IMSR_JAX:029591) mice, maintained on a mixed genetic background (129/C57B16). Experimental animals were 2-4-month-old heterozygous, backcrossed to C57Bl6. They originated from different litters, were randomly allocated to experimental groups and identified by earmarks. All procedures pertaining to housing, surgery, behavioral experiments and euthanasia were performed in compliance with the Swiss Veterinary Law guidelines.

METHOD DETAILS

Virus production, injections and implantations

Most adeno-associated viruses (AAV) used in this work are based on a backbone derived from Allen Brain (AAV-CAG-flex-tdTomato-WPRE-bGH). Previously described viruses include: AAV-flex-SynGFP (Pivetta et al., 2014), referred to as AAV-flex-SynTag, as well as AAV-flex-ReaChR-eYFP, AAV-flex-Flp-H2B-V5, AAV-H2B-10xMyc, AAV-flex-TdTomato (Capelli et al., 2017), AAV-flex-Flp-H2B-V5, AAV-flex-H2B-GFP, AAV-flex-H2B-TdTomato, AAV-flex-H2B-V5 (last three referred to as AAV-flex-nTagX), AAV-Con-Fon-ReaChR-Citrine-YFP (Ruder et al., 2021). Not previously reported viral constructs were designed in analogy to above constructs: AAV-frt-H2B-TdTomato (referred to as AAV-frt-nTagX), AAV-flex-GCaMP7f (Dana et al., 2019), AAV-flex-stGtACR2-FusionRed and AAV-frt-stGtACR2-FusionRed (Mahn et al., 2018). The AAV-Con-Fon-SynGFP construct was designed following a published strategy (Fenno et al., 2014). The AAV-flex-bReaChEs construct (Rajasethupathy et al., 2015) was created using previously described strategies with

an Ef1alpha promoter. To infect neuronal soma, a 2.9 serotype plasmid was used for production as in previous studies (Basaldella et al., 2015; Esposito et al., 2014; Pivetta et al., 2014; Ruder et al., 2021). For retrograde labelling of neurons by means of axonal infection, a rAAV2-retro capsid plasmid (Tervo et al., 2016) was used for coating as described previously (Capelli et al., 2017; Ruder et al., 2021). For systemic labelling of the central nervous system, a PHP.eB serotype was used (Chan et al., 2017) to produce AAV-PHP.eB-flex-nTag and AAV-PHP.eB-frt-nTag viruses. Genomic titers for AAVs used in this study were between 1-5x10e13 and produced following standard protocols. Viruses were delivered to the target brain regions via stereotaxic injection with high precision stereotaxic instruments (Kopf Instruments, Model 1900) under isoflurane anesthesia as previously described (Capelli et al., 2017; Esposito et al., 2014; Ruder et al., 2021). Viral injections in the spinal cord were targeted to the cervical spinal segments C1-C8. Injections in the medulla spanned the rostro-caudal extent of the gigantocellular reticular formation and its subdivisions (Gi, GiA, GiV) and the lateral paragigantocellular nucleus (LPGi), in agreement with anterograde tracing experiments, revealing that the most abundant synaptic output of glutamatergic MLR neurons is directed to this brainstem region (Figure 2B) (Caggiano et al., 2018; Capelli et al., 2017). The stereotaxic coordinates for brain injections are defined as antero-posterior (AP), medio-lateral (ML) and dorso-ventral (DV) (AP; ML; DV) in mm, taking lambda as a reference for the AP and ML axis for MLR and Med injections, while bregma was used as a reference point for the AP and ML axis for SNr; the reference for the DV axis was the dura mater surface at the site of the respective burr hole: MLR (-0.2; -1.19; -3,1); Med (-1.95; -0.7; -5,4); SNr (-3.1; -1.65; -4,6). For synaptic tracing experiments, we injected AAV-flex-SynTag and waited at least two weeks for expression before analysis. Triple rAAV injections in *vGlut2*^{Cre}

mice were performed for the combinations of spinal cord, Med and SNr. Before injection, the different rAAVs were diluted with saline solution to obtain the same titer for all viruses. For most injections, we used the combination of AAV-flex-H2B-GFP, AAV-flex-H2B-TdTomato, AAV-flex-H2B-V5 for triple injections, but AAV-flex-TdTomato was used for some spinal cord injections. We added AAV2.9-H2B-10xMyc to the mix to label the injection site. Viruses were allowed to express for at least two weeks before analysis. Double rAAV injections in the Med and SNr of *Rbp4*^{Cre} mice were performed using an analogous approach. Systemic labelling of the central nervous system was achieved with intravenous delivery of AAV-PHP.eB via retro-orbital injections under anesthesia (Challis et al., 2019), followed by tissue processing at least 4 weeks later. For optogenetic manipulation of projection-specific glutamatergic MLR subpopulations, we used the optogenetic activator ReaChR or inhibitor stGtACR2. ReaChR has been previously demonstrated to activate neurons in the brainstem and elicit behavior (Capelli et al., 2017; Lin et al., 2013; Ruder et al., 2021), and stGtACR2 has been used successfully to silence neurons, including excitatory glutamatergic neurons in subcortical structures (Karigo et al., 2021; Pamukcu et al., 2020). For targeting, rAAV-flex-Flp-H2B-V5 was injected in the cervical spinal cord, Med or SNr of *vGlut2*^{Cre} mice, with AAV2.9-H2B-10xMyc added to the mix to visualize the injection site. AAV-Con-Fon-ReaChR-Citrine-YFP (for activation) or AAV-frt-stGtACR2-FusionRed (for inhibition) was subsequently injected in the MLR. To target the Rbp4-transgene expressing neurons in the MLR, AAV-flex-ReaChR-Citrine-YFP (for activation) and AAV-flex-stGtACR2-FusionRed (for inhibition) were injected in the MLR of *Rbp4*^{Cre} *mice.* This strategy allowed us to restrict the expression of opsins to the identified MLR neuron subpopulations. To control for the effect of light application during optogenetic manipulations, AAV-flex-H2B-GFP

was injected in the MLR of *vGlut2*^{Cre} mice. After injections were completed, optic fibers were implanted bilaterally 200mm above the injection site in the MLR (diameter: 200mm: MFC_200/230-0.48_Xmm_ZF1.25_FLT Mono Fiberoptic Cannula; X refers to fiber length according to the stereotaxic coordinates; Doric lenses). For experiments concerning optogenetic stimulation of glutamatergic MLR terminals over SNr, AAV2.9-flex-bReaChEs was injected in the MLR bilaterally and an optic fiber was implanted in the SNr (-3.1; -1.65; -4,6) of *vGlut2*^{Cre} mice. All optogenetic stimulation experiments were performed >2 weeks after injection, to allow for adequate viral expression. For microendoscope calcium imaging experiments, the fluorescent calcium sensor flex-GCaMP7f was expressed in MLR neurons either by retrograde infection from the cervical spinal cord in *vGlut2*^{Cre} mice (MLR>SC) using a rAAV construct, or direct injection of an AAV2.9 construct into the MLR in *Rbp4*^{Cre} mice (MLR-Rbp4). After injection, a 0.7mm diameter needle was slowly lowered through the burr hole until a depth of 100mm above the injection site, in order to create a path for the lens. Through this procedure, brain damage was kept minimal due to lateral pushing of tissue rather than removal. After the needle was retracted, a 0.6mm-diameter gradient index (GRIN) lens (ProView™ Lens Probe 0.6 mm diameter, ~7.3mm length, Inscopix; smallest possible diameter to keep brain damage minimal) was implanted directly above the injection site. A Micropositioner (Kopf) was used to descend into the tissue with the needle first and GRIN lens after, at a speed of 10 µm per second to minimize tissue damage. Mice were closely monitored after implantation and throughout the entire experimental period and no obvious behavioral consequences from lens implantation were observed. At least 4 weeks after virus injection and lens implantation, the microendoscope was connected and the field of view was inspected to determine the best focal plane. Subsequently, we mounted the baseplate.

After termination of experiments, injection sites were assessed by using choline acetyltransferase (ChAT) or tyrosine hydroxylase (TH) immunohistochemistry (see immunohistochemistry and microscopy section) to visualize the cholinergic clusters of the PPN, the motor nuclei in the brainstem and the dopaminergic neurons of the substantia nigra compacta (SNc) and VTA. For optogenetic and microendoscope imaging experiments, we also visualized the tip of the artifact left by the implant on the parenchyma to confirm correct placement. We employed a widely used mouse brain atlas as reference to assess the specificity of our injections and implantations (Franklin and Paxinos, 2007). Only mice with confirmed anatomical accuracy were included in the subsequent analysis (number of mice passing anatomical exclusion criteria: anatomical retrograde tracing experiments: n = 9 of 16 *vGlut2*^{Cre} mice and n = 5 of 7 *Rbp4*^{Cre} mice; systemic labeling of Rbp4-positive neurons in *Rbp4*^{Cre} mice: n = 5 of 5; systemic labeling of Rbp4-positive and vGAT-positive neurons in *Rbp4*^{Cre}-*vGAT*^{FLP} mice: n = 3 of 3; MLR>SC calcium imaging experiments: n = 7 of 12; Rbp4 calcium imaging experiments: n = 4 of 8; MLR>SC ReaChR experiments n = 10 of 10, MLR>SC stGtACR2 experiments n = 13 of 14, MLR-Rbp4 ReaChR n = 10 of 10, MLR-Rbp4 stGtACR2 n = 10 of 10; MLR>Med ReaChR experiments: n = 4 of 7; MLR>SN ReaChR experiments: n = 7 of 10; stimulation of MLR-vGlut2 axonal terminals over SN: n = 10 of 10).

Immunohistochemistry and microscopy

After termination of all experiments, mice were euthanized and brains and spinal cords were collected for processing, as previously described (Capelli et al., 2017). Briefly, animals were anaesthetized with a ketamine–xylazine solution and transcardially perfused with PBS, followed by a solution containing 4%

paraformaldehyde (PFA) in PBS. The brain and spinal cord were dissected, post-fixed overnight in 4% PFA, and incubated in 30% sucrose (w/v) in PBS for at least two days before cryopreservation. Brain and spinal cord tissue were cut on a cryostat at 80 µm thickness (coronal sections for brain tissue and transverse sections for spinal cord tissue), with the exception of all the MLR spanning sections from triple or double rAAV injection experiments, which were cut at 40 µm thickness. Floating sections were collected in sequential order into individual wells and incubated for 1 hour in blocking solution (1% BSA, 0.2% Triton X-100, PBS). Primary antibodies were then applied in blocking solution and incubated for 1–3 days at 4°C. Fluorophore-coupled secondary antibodies (Jackson or Invitrogen) were applied to floating sections after extensive washing and incubated for 1 day at 4°C. Sections were then washed and mounted with anti-bleach preservative medium on slides in sequential rostro-caudal order. Primary antibodies used in this study were: chicken anti-GFP (Invitrogen), chicken anti-Myc (Invitrogen), chicken anti-TH (Neuromics), goat anti-ChAT (Millipore), mouse anti-Myc (ATCC), mouse anti-NeuN (Millipore), mouse anti-V5 (Invitrogen), rabbit anti-RFP (Rockland). For low-resolution overview imaging, slides were scanned with an Axioscan light microscope (Zeiss). For higher resolution imaging, we used a FV1000 confocal microscope (Olympus) or an Axio Imager M2 microscope (Zeiss) with a Yokogawa CSU W1 Dual camera T2 spinning disk confocal scanning unit.

Microendoscopic calcium imaging of MLR subpopulations

One-photon calcium imaging of MLR-Rbp4 and glutamatergic MLR>SC neurons was recorded in freely moving animals in a 35x35 cm open field arena, using a microendoscope (Inscopix nVista 3.0) controlled with the Inscopix Data Acquisition Software (versions 1.2.1 and 1.4.1). The recording sessions started at least one week

after baseplate implantation (see behavioral experiments). In the first imaging session, the focal setting was adjusted to select the focal distance that allowed for optimal visualization of the field of view. Data was acquired continuously at 20 Hz. Animal behavior during microendoscopy experiments was monitored with 2 video cameras (Pike, Allied Vision Inc.) acquiring at 100fps, controlled by the software Bonsai version 2.3 (NeuroGEARS Ltd.). Additionally, an Inertial Measurement Unit (IMU) (Wired 9-axis motion sensor, Champalimaud Foundation's Scientific Hardware Platform) mounted on the microendoscope was used to measure the accelerometer, gyroscope and magnetometer data of the animal, sampled at 100Hz. All recording equipment was connected to a harp wear device and clock synchronizer (Champalimaud Foundation's Scientific Hardware Platform) to synchronize the video, IMU measurements and calcium imaging time stamps. All behavioral movies and data synchronization information were saved with Bonsai.

Optogenetic Perturbation Experiments

Optogenetic stimulation was performed using a PlexBright Optogenetic Stimulation System (Plexon Inc.) in combination with a laser (Cobolt 06-MLD; 473nm; 100mW). Light was delivered via a patch cord (Doric Lenses), connected to the animal's implant. Laser intensity was measured at the beginning of every session with an optical power meter (Thorlabs Inc.) on the tip of an optic fiber of the same length as the one implanted to ensure accurate stimulation strengths. Locomotion perturbation experiments were carried out in a 35x35cm open field arena and recorded with one camera (Pike, Allied Vision Inc.) from above at 100 fps. Laser timestamps and camera exposure timestamps were collected using Plexon Inc. software. We tracked center-of-body mass online using the CinePlexStudio tracking function

(CinePlexStudio v3.7.1. Plexon Inc.) in order to be able to trigger the laser in a closed loop fashion (Figure 5, 6 and S7). For stimulation during locomotion, the laser was triggered when the speed crossed a threshold value for a given duration of time (either 12.5cm/s for 100ms or 5cm/s for 200ms). For stimulation during rest in the open field arena for the MLR>SC ReaChR mice, the laser was triggered when the speed of the animal was below 3cm/s for 500ms. Additionally, for both of the above, a set of control trials were collected with the same thresholds but with the laser power set to 0mW to enable comparison of the perturbation with natural locomotion (no laser controls). All other optogenetic perturbation experiments were carried out in a 20 cm diameter arena and recorded from below and side for pose estimation with Basler cameras (Ace 2 series). A minimum of 10 trials was used for each mouse for each experimental condition. Laser and camera exposure timestamps were collected using the Inscopix DAQ system (software version 1.4.1). Continuous laser stimulation was used for optogenetic experiments at laser powers as described below. For MLR>SC stGtACR2 experiments, we used bilateral stimulation powers of 5mW for 500ms. In the cylindrical arena, we encouraged rearing by attaching spaghetti to the walls of the cylinder, adjusted to the size of the mouse to allow it to rear comfortably and reach the spaghetti. The laser was triggered manually in a randomized fashion during rearing trials. For MLR>SC ReaChR experiments, we used powers of 5-10mW for 500ms, with trials from all powers pooled. Mice were bilaterally stimulated manually when they were stationary in the circular arena or in a closed-loop fashion in the open field arena (speed < 3cm/s for 500ms). For MLR-Rbp4 stGtACR2 experiments, we used powers of 1mW for 500ms. Mice were bilaterally stimulated manually when they were stationary or during spontaneous rearing, grooming or handling of spaghetti. For MLR-Rbp4 ReaChR experiments, we used 0.1mW laser power for 500ms. Mice were

bilaterally stimulated manually during spontaneous rearing, grooming or handling of spaghetti. For optogenetic stimulation of MLR>Med neurons, SNr-projecting glutamatergic MLR neurons or glutamatergic MLR terminals over SNr, we used 1s unilateral stimulation at 20mW laser power. To control for the effect of light, we performed the application of light under identical conditions in the control mice expressing GFP instead of the opsins for each of the above experiments, as described in the 'Virus production, injections and implantations' section.

Electromyography

For electromyographic (EMG) recordings during stimulation of MLR-Rbp4 neurons, injection and fiber implantation were conducted as described above (see virus production, injections and implantations). Cable preparation and EMG implantation of the biceps and triceps muscle of the forelimb were conducted as previously reported (Miri et al., 2017). Acquisition was carried out together with optogenetic stimulation (1 s continuous light, 20mW), during locomotion on a treadmill, set to 10 cm/s to encourage continuous locomotion. The signal was amplified and bandpass filtered (A-M systems 1700, gain 100, bandpass 100-1000 Hz) and acquired using a plexon recording system (Omniplex, Plexon Inc.) at 5000 Hz. Mean subtraction was applied to correct for the DC offset. Movies were recorded from the side with a video camera (Pike, Allied Vision Inc.) acquiring at 100 fps, controlled by the Cineplex Studio software (Plexon Inc.).

Quantification and statistical analysis

All data are presented as mean ± SEM unless otherwise stated, and significance levels are indicated as: *$p < 0.05$, **$p < 0.01$, ***$p < 0.001$. No statistical

methods were used to predetermine sample size. All plots, scripts and analysis were generated or performed in MATLAB v2017b (The Mathworks Inc.), GraphPadPrism7 (GraphPad Inc.), Python 3.7 or KNIME (v3.3.1). Figures were assembled using CorelDraw (versions X6 to X9; Corel Inc). All statistical tests used in this study and exact number of mice used in each experiment are spelled out in the corresponding Figure legends.

Anatomical reconstructions

To map the local distribution and cellular overlap between MLR subpopulations stratified by projections, viral injections and tissue processing were performed as described above. Images from 40 µm thick sections encompassing the full MLR area along its rostro-caudal axis were acquired using a FV1000 confocal microscope (Olympus) with a 20X objective (*z*-steps of 1 µm) and stitched offline. We used every third MLR image along the rostro-caudal axis for further analysis to best fit the anatomical properties depicted in the atlas (Franklin and Paxinos, 2007). Maximal projection intensity of z-stack mosaics was used to detect MLR neurons using a custom-built workflow in KNIME (Dietz and Berthold, 2016). Virally expressed markers were detected automatically using KNIME cell segmentation nodes, or assigned manually in experiments where AAV-flex-TdTomato was used for injection. Cell segmentation parameters were adjusted to fit the results obtained by manual detection of one example image for each set of confocal acquisitions (sigma range used:4-5, threshold range used: 15-25, watershed threshold range used: 56000-65500). Automatic spot detection was visually validated on every section for all experiments. Detection of td-Tomato- and ChAT-expressing neurons was done manually in the same KNIME workflow. MLR subregions were drawn manually following the atlas

(Franklin and Paxinos, 2007) using KNIME interactive annotator. The coordinates from the annotated MLR subregions were then used to split detected MLR neurons according to their location. Colocalizing neurons were detected using the feature calculator node from KNIME. We then extracted the number and x-y position of detected overlapping and single-positive neurons in each MLR subregion. Extracted x-y coordinates were used to plot the distribution of labeled neurons using custom-built MATLAB scripts. Density plots were generated using 2d-kernel density estimate, plotting 6 density lines of highest density using the MATLAB function kde2d.

Behavioral classification in the open field arena

Top-down view open field videos to track the locomotor state of the mouse were saved in .avi format and subsequently cropped to regions of interest and split into multiple shorter files using a MATLAB script. The machine learning software Ilastik (version 1.1.5) was used to track the position of mice in the open field. For every acquisition, a training session with refinement via machine learning was used to instruct the software to detect the mouse body and distinguish it from the background. The features used for this purpose were color/intensity (Gaussian smoothing), edge (Gaussian gradient magnitude, difference of Gaussians) and texture (structure tensor eigenvalues, hessian of Gaussian eigenvalues). For each of the features, the probability was calculated using a sigma of 0.3, 1, 3.5 and 10 pixels. With this training, a probability map with the positional information of the mouse for each video was created. From this, we obtained the center of body mass (COBM) of the mouse by extracting the centroid of the filled area corresponding to the animal tracking, with a custom-made MATLAB script. For open field video analysis, we used the x-y position of the COBM in each frame to calculate the instantaneous animal speed as pixel

displacement per frame, which was converted into cm/s by incorporating the knowledge of the pixel size in cm and the frame rate (in fps) of each video.

Locomotion bouts were then excluded from the data for behavioral classification purposes. The rest of the video data was split in a training set and tracking set. The training set was manually annotated to identify grooming, handling and rearing during the open field session. Training data was used to train a one-dimensional convolutional neural network implemented in a custom-script in Python 3.7 to recognize behavior from IMU data. The IMU data was median filtered. The accelerometer data from the three axes was high pass filtered with a Butterworth filter (0.5Hz critical frequency). Sensor data was then z-scored. Briefly the network architecture consisted of two 1D convolutional layers (rectifier or “relu” activation) followed by a max pooling layer. This was followed by two more 1D convolutional layers (rectifier or “relu” activation), one global average pooling layer and a dropout layer before the output of the network composed of a dense layer composed of three softmax units (Groom, Handle and Rear). The trained network was used to predict the behavior for the training set and the output prediction was then manually curated to reach perfect annotation of behavioral episodes in the open field arena. To directly relate the behavior to the calcium imaging data, it was down sampled to 20Hz to match the microendoscopic image acquisition frequency. For each behavior, the distribution of the duration of behavioral episodes was studied by computing KDE density through Seaborn, a Python data visualization.

Detection and analysis of locomotor speed during optogenetic perturbation

To study the effects of perturbation on locomotion (Figures 6, 7, S6 and S7), mice were studied in the open field arena as described above. The speed was obtained using the Ilastik tracking. The speed is first median filtered and then a Savitzky–Golay filter was applied. We then temporally aligned the instantaneous speed information with laser onset time stamps, recorded by the Plexon system. The average speed for all trials for each mouse in laser on and control trials was plotted along with the s.e.m. and average across mice in a window of -0.5 s before laser stimulation onset and 1.0 s after stimulation onset. The probability of speed reduction of locomotion for MLR>SC stGtACR2 and MLR-Rbp4 ReaChR experiments was calculated as the proportion of trials in which the average speed in the laser stimulation window was below the average speed in the 500ms preceding the stimulation. For MLR>Med perturbation experiments, the probability to initiate a locomotor bout during the 1 s period of laser stimulation was quantified to compute reliability of the observed stimulation effect. To visualize the trajectory of the animals before, during and after laser-induced locomotion, we displayed the 2D trajectories of the COBM before, during and after the one-second laser-ON period (1 s each time window). For MLR-SC ReaChR experiments in the open field arena, we estimated the probability of the laser stimulation being followed by at least one full four limb stepping cycle in the trials where the animal was on all four limbs and not facing the walls of the arena. The trials which led to at least one complete step cycle in the laser on window were used to estimate the probability. In the same way, the probability was estimated for the control trials where the power was set to 0mW using the same parameters to trigger stimulation. This probability in the control trials was subtracted from the one with the laser on to obtain the control subtracted probability of stepping in Figure 5K.

Pose estimation and analysis for optogenetic perturbation experiments

The machine learning algorithm DeepLabCut (Mathis et al., 2018) was used in combination with high-speed videography (100fps, Basler Ace 2 cameras) to characterize behavioral phenotypes in optogenetic experiments. Video frames were synchronized with the laser pulses using the Inscopix DAQ system. The network for the MLR>SC ReaChR, MLR-Rbp4 stGtACR2 and MLR-Rbp4 ReaChR experiments was trained using at least 300 frames distributed equally over all the videos obtained from recording the mice from below. The training frames were annotated with the following body parts: nose, head base, forepaws, wrists, hands, body center, forelimb hands, hindlimb balls, genitals and tail base. For MLR>SC stGtACR2 experiments, the network was trained on at least 200 frames of videos of the mice recorded from the side distributed equally over all the corresponding videos. Here, the snout was annotated for quantification of the height of the mouse during rearing episodes. To ensure reliable tracking of all body parts, for all videos, trials in which any of the body parts in analysis were not tracked reliably ($p < 0.4$) for a period of over 200ms were excluded. For the others, in case of p falling below the threshold of 0.4, we linearly interpolated the trajectories. For MLR-Rbp4 stGtACR2 experiments, snout, forelimb hands and hindlimb balls were used for analysis because of their reliable tracking. For MLR-Rbp4 ReaChR experiments during grooming and handling, snout, forelimb hands and hindlimb balls were used for analysis because of their reliable tracking; for tracking during rearing, forelimb hands, hindlimb balls, genitals and tail base were used for analysis because of their reliable tracking.

For body length analysis in MLR>SC ReaChR experiments, the obtained trajectories were centered at the tail base position (onset of laser on time window) and rotated to have the snout vertically align with the origin. Trajectories were normalized

between 0 and 1 for averaging across mice in order to account for differences in dimensions between animals. Body length was calculated as the sum of the distances of the nose to head base, head base to body center, body center to genital and genital to tail base. For body length analysis in MLR>SC stGtACR2 experiments, the body length was calculated as the height of the snout from a side camera. The obtained body length was then median filtered and Savitzky-Golay filtered for both MLR>SC ReaChR and MLR>SC stGtACR2 experiments. Each trial was normalized between 0 and 1 to account for different starting positions of the subjects and correct for differences in body size between mice. For path length analysis for MLR>SC ReaChR experiments, the absolute path traveled by each plotted body part was computed in 100ms time bins. For MLR-Rbp4 perturbation experiments, speed of all body parts was calculated from a differential of the coordinates. Rolling standard deviation of two-dimensional position (Figure S7A, E) was computed with a 100ms centered moving window for each coordinate axis and then averaged across them. All standard deviation measurements were then normalized on a trial by trial basis between 0 and 1.

For MLR>SC ReaChR experiments, the reliability of the stimulation inducing the behavioral phenotype was measured as the fraction of trials in which the maximum body length during the laser-on window was higher than the maximum body length during the 500ms window preceding the laser stimulation. For MLR>SC stGtACR2 experiments, the reliability was calculated as the fraction of trials in which the average body length during laser-on window was lower than the average body length during the window of 500ms preceding laser stimulation. For MLR-Rbp4 stGtACR2 experiments, reliability of the stimulation in inducing behavioral phenotypes was measured as the fraction of trials in which the max speed during the laser-on window

was higher than the max speed during the 500ms before laser stimulation for all studied body parts. For MLR-Rbp4 ReaChR experiments, reliability was computed as the fraction of trials in which the average speed during laser application was lower than the average speed during the 500ms preceding laser stimulation for all studied body parts. All reliability computations were also done for the relative controls expressing GFP instead of the opsin. Note that for all light controls expressing GFP, the reliability of observing behavioral phenotypes is distributed around 0.5 as is expected by chance, indicating no effect of light application in the absence of optogenetic tools. Reliability of speed decrease is instead higher for locomotor speed even in control mice due to the natural tendency to slow down after a certain speed threshold is crossed (note the overlap between laser and no laser conditions in control mice (Figure S6B, right)). The reliability of the optogenetic experiments was compared to the controls using the Wilcoxon ranked sum test (MLR>SC stGtACR2, body length: $p = 0.001$; MLR>SC stGtACR2, locomotion: $p = 0.003$; MLR>SC ReaChR: $p = 0.002$; MLR-Rbp4 stGtACR2: $p = 0.002$; MLR-Rbp4 ReaChR, Grooming: $p = 0.002$; MLR-Rbp4 ReaChR, Handling: $p = 0.002$; MLR-Rbp4 ReaChR, Rearing: $p = 0.002$; MLR-Rbp4 ReaChR, Locomotion: $p = 0.002$).

To compare the effects of optogenetic manipulations and light application in control mice expressing GFP in MLR-vGlut2 neurons, for each variable considered, we calculated the light induced change as the difference between the mean of the variable during light application and the mean of the variable in the preceding 50ms. Specifically, for MLR>SC stGtacr2 experiments, we performed this computation on normalized body length for the rearing assay and locomotor speed for the stimulation during ongoing locomotion (Figure S6B); for MLR>SC ReaChR experiments, we performed this computation on normalized body length (Figure S6D); for MLR-Rbp4

stGtacr2 experiments, on normalized s.d. of pose for all body parts recorded (Figure S7A); for MLR-Rbp4 ReaChR experiments, we performed this computation on normalized s.d. of pose for all body parts recorded in each behavior (Figure S7E) and locomotor speed for the stimulation during ongoing locomotion (Figure S7D). The same was performed on the relative controls to allow for statistical comparison. The Wilcoxon ranked sum test was used to compare the effects of optogenetic perturbation and light application (MLR>SC stGtACR2, body length: $p = 0.001$; MLR>SC stGtACR2, locomotion speed: $p = 0.007$; MLR>SC ReaChR body length: $p = 0.002$; MLR-SC ReaChR no-laser subtracted probability of stepping: $p = 0.028$; MLR-Rbp4 stGtACR2, $p = 0.007$; MLR-Rbp4 ReaChR, Grooming: $p = 0.002$; MLR-Rbp4 ReaChR, Handling: $p = 0.003$; MLR-Rbp4 ReaChR, Rearing: $p = 0.005$; MLR-Rbp4 ReaChR, Locomotion speed: $p = 0.002$).

EMG data plotting

For EMG plotting, biceps and triceps signal was temporally aligned to animal speed of locomotion on the treadmill, tracked as described above (see behavioral tracking). For plotting, we used EMG data processed as described above and as published (Ruder et al., 2021) and the speed trace was smoothened using a moving average window (150ms).

Calcium image processing and analysis

All fluorescence movies were processed using a custom-made script. First, all frames were spatially binned by a factor of 4. To correct the movie for translational movements and rotations, motion correction was performed. Then, neuronal signals were extracted using the ‘constrained non-negative matrix factorization for endoscopic

data' (CNMF-E) framework (Pnevmatikakis et al., 2016; Zhou et al., 2018). 'C_raw' obtained from the CNMF-E was used for all further analysis of the fluorescent signal of the neurons. Calcium traces for each neuron were normalized through division by the 99th percentile for all analyses or z-scored for single-neuron examples plotting and peak detection analysis. The average fluorescence for all neurons of the MLR>SC or MLR-Rbp4 subpopulation was calculated centered around the onset for each behavior in a window from -1 s to 2.5 s. From this, we subtracted the average fluorescence during the baseline period defined from -1 s to -0.05 s with respect to behavioral onset, to obtain the baseline subtracted mean fluorescence as shown in Figures 3 and 4. For example neurons obtained from the same mouse, the traces in the same time window of a behavioral session were overlaid. In the case of correlation of neuronal activity with speed, speed obtained from COBM tracking with Ilastik was median filtered and then a Savitzky-Golay filter was applied. To quantitatively assess neuronal tuning to each of the behavioral categories, we computed a modulation index: the activity of a single neuron during each behavior was averaged and subtracted by the average activity of that neuron during frames not detected by any of the four behaviors. To assess the statistical significance of the obtained modulation index, we shuffled each neuronal time series 1000 times and computed the 99.9 percentile ($p < 0.001$) of the distribution of modulation indices for that neuron. Any value higher than the 99.9 percentile was considered significant. To study the general distribution of modulation indices for different behaviors in MLR neuronal populations, we plotted all neuron modulation indices and sorted them with ascending order for each behavior. We also performed a KDE analysis to display the distribution of modulation indices in each behavioral category using the Python library Seaborn. The baseline subtracted average fluorescence of the MLR>SC and MLR-Rbp4 neurons significantly tuned to

locomotion was calculated as described above. Venn diagrams were plotted to compare the number of neurons positively modulated to each behavior. The “full-body” class comprised locomotion and rearing and “forelimb” class comprised grooming and handling. A linear regression analysis was performed between the modulation indices in the behaviors of Rear versus Walk and Groom versus Handle respectively for each of MLR>SC and MLR-Rbp4 (Figures 5 C, D). The modulation indices in these behaviors were plotted along with the linear fit and the 95% confidence interval for that regression indicated by the shaded region along the line. The Spearman’s correlation coefficient and p value were calculated for each of the pairs. For MLR>SC neurons, there was a significant positive correlation between the modulation indices for Groom and Handle with a Spearman’s $r = 0.58$ and $p < 0.001$ and a no significant correlation between the modulation indices for Rear versus Walk ($r = -0.07$, $p = 0.606$). For MLR-Rbp4 neurons, there was no significant correlation between the modulation indices of Groom versus Handle ($r = 0.16$, $p = 0.053$), while there was a significant positive correlation between the modulation indices for Rear versus Walk ($r = 0.61$, $p < 0.001$). The results for the Spearman’s correlation coefficient for the modulation indices for all pairs of behaviors are summarized in Figure 4D.

To identify peaks in neuronal calcium activity we used SciPy, a Python library for scientific computing. Specifically, we applied the “find_peaks” function using as parameters a height of 3 and a distance of 100. We computed the probability of each behavior occurring at the time of peak for each neuron. This probability was then corrected to be above chance, accounting for differences in time spent during each behavior during the imaging session (Figure 4A). Precisely, we computed the fraction of frames in each session assigned to each behavioral category and subtracted it from the obtained peak triggered probabilities for each neuron on a single mouse basis.

The full dataset for each subpopulation was then plotted as a heatmap and sorted according to Handle, Groom, Rear, Walk for MLR-Rbp4 neurons and to Rear, Walk, Handle, Groom for MLR>SC neurons. For Figure 4B, the probability of behaviors above chance was plotted in time from -2.5 s to +5 s from time of Calcium peak for single representative example neurons.

For decoding analyses, we used scikit-learn, a Python library for statistical learning and glmnet (version 2.2.1), a Python wrapper for the fortran library used in the homonymous R package. Specifically, all decoding analyses were performed through the use of a Regularized Logistic Regression, LogitNet, with an elastic net penalty (alpha = 0.5, 0 for ridge, 1 for lasso) with 100-fold cross-validation and averaging of decoding accuracy. For each model fit, a shuffled version of the time series was used to evaluate chance decoding accuracy (for single neuron decoding, at the single neuron level; for population decoding, at the single mouse level). Final results were obtained by subtracting mean decoding accuracy with chance decoding accuracy and every negative value was set to 0. For population decoding in Figure S5A, the decoding accuracies obtained from each mouse were averaged and plotted. We applied models trained to distinguish between each behavioral pair separately.

Section 4:
Discussion

Implications for the field of MLR and Basal Ganglia in Motor Control

The present work provides evidence that the role of MLR in motor control goes beyond locomotion. On the one hand, the direct output to the spinal cord signals postural changes that control body length independently of locomotion state. On the other hand, the rostrally-projecting population interconnects with the basal ganglia circuitry, including the SNr, the STN and the GPi, and is in a privileged position to shape the output of basal ganglia computations; in fact, our functional manipulation experiments clearly demonstrate that optogenetic activation of MLR-Rbp4 neurons halts ongoing movement, irrespective of the specific behavior the mouse is engaged with at the time of stimulation, while optogenetic silencing of this population triggers uncoordinated movements from all tracked body parts. Although these manipulations are certainly non-physiological, the produced phenotypes correspond to the predicted effects of providing or subtracting an indiscriminate, strong excitatory input to the SNr (and the STN and GPi) whose inhibitory neurotransmitter identity is generally behavioral-suppressive. The fact that we are able to interfere with all body parts likely results from mass activation of the MLR-Rbp4 population, which, as our calcium imaging experiments demonstrate, further subdivides into neurons encoding different behaviors, which could, predictively, connect to different target cells within the basal ganglia, concerned with the control of different movements. On this note, a recent study mapping the organization of SNr projections revealed that the SNr is organized in specific channels that project to different brainstem targets that have been implicated in the control of different motor actions (McElvain et al., 2021). Interestingly, although these channels seem to be specific, in the sense that different SNr neurons project to different brainstem command centers for specific behaviors, they all send collaterals to the motor thalamic nuclei (therefore accessing the thalamo-cortical loops

for motor control) as well as the PPN and the mesencephalic reticular formation. These findings suggest that the PPN/mRT is not just another channel for a specific motor program (putatively locomotion) but is also informed about many different motor outputs arising from the SNr. This could explain the different patterns of activity of Rbp4 neurons we observed at the single cell level. Furthermore, the topography of the synaptic projections from the SNr to the MLR is specifically directed at the PPN and dorsomedially-adjacent mRT (McElvain et al., 2021) (our own unpublished results – see Figure 1 below), the preferential location of the MLR-Rbp4 neurons we describe. Therefore, this region is fully embedded in the basal ganglia circuitry, receiving inhibitory input from the SNr and GPi and sending excitatory output back to the same structures, and thus contrasting with the more dorsally located CNF region, which only receives sparse input from basal ganglia structures (Caggiano et al., 2018). According to the basal ganglia model of behavioral selection by disinhibition, one could expect that the SNr subpopulation that projects to brainstem regions implicated in forelimb movements (and therefore selects them as the motor program to be executed, by disinhibiting local neurons), would be the one collateralizing and contacting MLR-Rbp4 neurons that fire during the execution of such movements. This MLR-Rbp4 activity would, in turn, signal back to the SNr (and other levels of the basal ganglia) and excite inhibitory neurons to shape motor output, possibly by leading to the silencing of competitive motor programs not compatible with the execution of the ongoing forelimb movement. This is a speculative scenario; testing it requires technology to specifically interrogate if specific neurons in two bidirectionally interconnected structures project back to the same neurons that provide direct input to them. Interestingly, and in line with our findings of MLR-Rbp4 neurons encoding forelimb activity, a clinical case study

reported improved hand dexterity after PPN-DBS in a Parkinson's disease (PD) patient (Franzini et al., 2011).

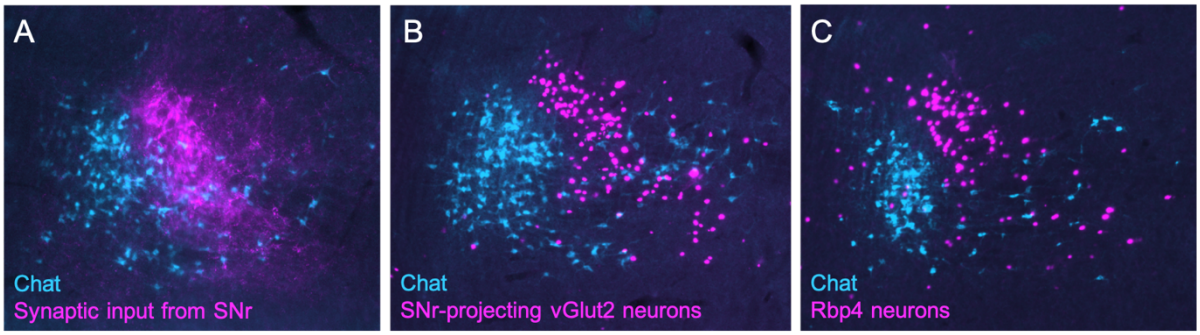

Figure 1. SNr input to the MLR targets the region containing SNr-projecting neurons

(A) Injection of AAV2.9-Flex-Synaptophysin-Tag into the SNr of vGAT-Cre mice to visualize SNr input into the MLR.

(B) Injection of rAAV-flex-H2B-nTag into the SNr of vGlut2-Cre mice to visualize SNr-projecting glutamatergic MLR neurons.

(C) Systemic injection of AAV-PHP.eB-flex-nTag in Rbp4-Cre mice to label Rbp4-positive MLR neurons.

Blue: PPN-Chat positive neurons; Magenta: syn-Tag terminals (A) or nTag (B and C). Note the common topography of the SNr synaptic input and the SNr-projecting neurons in the PPN/mRT region.

Together, these findings clearly demonstrate that "MLR (Mesencephalic Locomotor Region)" is an outdated name, since it implies that this complex mesencephalic territory is dedicated to locomotion control alone, which is clearly too reductive. While it's role in locomotion is indisputable, integrating contextual information from many different upstream structures and recruiting reticulospinal circuits to promote the execution of locomotion in different contexts, current scientific evidence suggests that this function is carried out by medulla-projecting neurons, which are homogeneously distributed throughout the CNF/pre-CNF, PPN and adjacent mRT. However, a more complex network of glutamatergic neurons residing in the PPN/mRT junction is intimately involved with the basal ganglia circuitry and is in a privileged position to influence basal ganglia processing and, consequently, motor program selection. In addition, a spinally-projecting population, which also sends

collaterals to the medulla but not to the SNr, provides a descending signal for postural adjustments not restricted to locomotor activity.

The fact that these segregated populations of rostrally- and caudally-projecting neurons share an overlapping topography in the midbrain but have completely different projection maps and functional roles raises the question of whether they represent two completely different circuits (one concerned with action selection and the other with motor command for locomotion and posture) that just happen to share a common topography or whether there is local communication between these populations. Importantly, our work did not address possible interactions between the described neuronal populations at the microcircuit level within the PPN/mRT area, but it is possible that these neurons residing in close proximity establish local synaptic connectivity between them, either directly or through local interneurons. In fact, local axonal collaterals have been described within the PPN, originating both from cholinergic and non-cholinergic neurons (Ros et al., 2010). Also, the presence of GABAergic neurons within the MLR that suppress the activity of local non-GABAergic neurons (Roseberry et al., 2016) argues in favor of the existence of microcircuits within this complex region. Based on our findings that glutamatergic neurons from SNr-projecting and SC-projecting populations have mostly non-overlapping patterns of activity during naturalistic behavior, the prediction for these putative local circuits would be that most of them are not direct, via local excitatory collaterals, but occur through inhibitory interneurons, which would be responsible for silencing locomotion- and posture-correlated neurons during the execution of forelimb movements and vice versa. Therefore, the suppression of unintended movements to allow the execution of the selected motor program, a concept that emerged from studies of the basal ganglia circuits (Hikosaka et al., 2000; Tecuapetla et al., 2016), where the MLR-Rbp4

population impinges, could also occur locally at the PPN/mRT area. The possibility of local signal processing between neurons with different projection targets and endogenous activity adds another layer of complexity to the global role played by this anatomical region in motor control and is certainly an interesting area to explore in the future.

Postural Control in the Brainstem

Maintaining adequate posture requires the concerted regulation of the muscle tone of gravity-antagonizing limb and trunk muscles. Compared to the knowledge on limb muscle role in postural control, little is known about the neuronal circuits governing axial muscle activity, especially in mammals (D'Elia and Dasen, 2018). In fact, axial muscle tone regulation maintains adequate posture and balance during virtually all behavior transitions and is especially important during the execution of locomotion, a state where the constant oscillation of limb position poses a particular challenge to postural adjusting mechanisms. Trunk muscular activity adjustments mobilize the axial skeleton, allowing the animal body to contract, extend, twist, turn, thus displacing the center of body mass in order to adjust its position to the ongoing behavior.

The first MLR studies in the mesencephalic cat also provided interesting insights regarding postural control. In the acute phase after CNS transection, the reliability to induce locomotion with low-intensity MLR stimulation from a stationary position was low (Shik et al., 1966). Electromyographic recordings from hindlimb muscles revealed that MLR stimulation in the stationary state produced strong muscle activity in the ankle plantar flexors gastrocnemius and soleus that behaviorally translated into the animal standing up (Mori et al., 1978). In non-locomotion trials, the

magnitude of postural muscle tone developed was suboptimal, but if an adequate level was achieved the animal would then proceed to initiate a locomotor bout. These observations support the concept that postural adaptations are crucial for an animal to transition into a locomotor state. Furthermore, since both locomotion and postural adjustments alone could be obtained from electrical stimulation of the MLR, a possible role for this structure in postural control was also proposed, raising the question of whether neuronal control of locomotion and posture share common pathways (at least to some degree) or whether they are fully independent, yet interacting, circuits. Of note, as mentioned above, postural adjustments preceding a specific movement are probably not a feature restricted to locomotion; all motor tasks likely entail adaptive postural responses in order to maintain adequate body position to permit the correct execution of the desired movement.

Attempting to further dissect the complexity of the MLR, Takakusaki and colleagues conducted electrical stimulation studies in the cat and reported an interesting dorso-ventral axis of effects over posture and locomotion (Takakusaki et al., 2016). According to this mapping, locomotion-inducing sites were restricted to the CNF nucleus, the CNF-PPN transition and the dorsal PPN (which present mixed locomotion-atonia responses), while ventral PPN stimulations decreased limb muscle tone without producing any limb movement. These results could suggest a simple model where the CNF controls locomotion and the PPN controls posture, and the mixed response obtained with dorsal PPN stimulation results from current propagation and co-activation of locomotor-promoting CNF neurons. Alternatively, locomotion-promoting neurons could be present in both PPN and CNF, but co-activation of intermingled populations could explain the variable results of PPN stimulation. Since the atonia and mixed response sites closely match the dorso-ventral distribution of

cholinergic neuron density, the authors hypothesized that postural changes could be mediated by this population. In line with the electrical stimulation work, a 2018 study revealed that optogenetic stimulation of glutamatergic CnF neurons increased hindlimb postural muscle tone prior to eliciting the alternating flexor-extensor muscle activity that characterized locomotion, while glutamatergic (and cholinergic) PPN activation produced phasic muscle activity without locomotion (Josset et al., 2018).

Analyzing these results in light of our findings, it is conceivable that straight activation of glutamatergic PPN neurons did not produce locomotion because of the simultaneous recruitment of all resident subpopulations, including the SNr-projecting population. According to our data, spinally-projecting neurons residing mostly within the PPN/mRT region are largely tuned to rearing (over locomotion), a behavior where mice acquire a more vertical position by contracting spinal column extensor muscles, raising themselves in their hindlimbs and, therefore increasing body weight load on them. Accordingly, their optogenetic activation produced body stretching, failing to produce reliable locomotion Thus, our findings point towards a segregation of locomotion- and postural-controlling populations at the level of the MLR. However, spinally-projecting PPN/mRT neurons could signal postural changes and interact with locomotion-promoting neurons in the caudal brainstem by means of their medullary collaterals and, potentially, with medulla-projecting MLR neurons via intra-MLR local circuitry. In addition, it is also possible that the SNr pathways for specific behaviors, that universally collateralize to the PPN (McElvain et al., 2021), contact spinally-projecting neurons, contributing to recruit the postural adaptations required for the execution of a desired behavior.

Implications for the clinical application of PPN-DBS

How can this knowledge on brainstem circuitry organization be translated into clinical application to treat movement disorders in humans? Before answering this question, a fundamental one needs to be addressed first: are human and mice motor systems similar enough so that these findings can be applied? My answer is: yes, they most likely are, even though it is impossible to study human circuits with a similar level of detail, for ethical and technical reasons. I'll provide some arguments over the next paragraph, first considering what makes mice and human different locomotion-wise, and afterwards discussing evidence pointing to similarities between them.

Firstly, there are obvious musculoskeletal and mechanical differences between the locomotor and postural systems of human and mice, that stem from the bipedalism vs quadrupedalism differences. At the neuronal control level, compared to other mammals, humans rely much more on corticospinal signals to activate spinal cord circuitry and engage in movement, as it is obvious by the dramatic motor deficits caused by injury to the corticospinal and corticobulbar tracts in humans, while mice and cats can still perform fully coordinated movements, including locomotion, even after a precollicular CNS transection, as discussed in a previous section pertaining to the "mesencephalic cat" model. It has been proposed that this progressive increase of cortical importance for motor control that accompanies the evolution of the motor system is a reflection of the need for higher computational power in order to encode progressively more complex behaviors (striking examples include the development of Broca's area for speech control and the increased cortical representation of hand movements that follows the evolution of dexterity), as well as the integration of progressively more complex sensory information that shapes motor output (one

example is the increasingly more complex visual information that comes with a foveate retina in anthropoids) (Mendoza and Merchant, 2014).

Despite these adaptations, compared to the wonders of speech control and hand dexterity (allowing us to enjoy the best opera singers or the most skilled piano players), the basic locomotor pattern is a more stereotyped behavior across mammals, entailing the fully coordinated activity between each limb, the flexors/extensors within each limb and the upper and lower body, and there is evidence that the fundamental principles governing motor control of locomotion at the level of the spinal cord and the brainstem are highly preserved across mammals (Alam et al., 2011). In line with this, studies comparing rodents and non-human primates (NHP) revealed that the major locomotion-related anatomical structures, including the PPN, are topographically and morphologically conserved between quadrupedal and bipedal animals, but the connectivity among them may be different (Barton and Harvey, 2000; Courtine et al., 2005; Onodera and Hicks, 2009). Only by having the possibility to study human deep brain microcircuitry with a similar level of resolution as in mice would we be able to definitely establish these putative differences. While current technology doesn't allow us to have such detailed information, we rely on literature from non-invasive functional imaging studies (with low spatial resolution and no cell type specificity), invasive electrophysiological recordings from patients that underwent PPN-DBS and case reports describing focal injuries to the midbrain (where once again the spatial resolution is weak and there is no neuronal specificity). On this note, functional MRI studies asking voluntary human subjects to imagine gait at normal and fast speed (Jahn et al., 2008; Karachi et al., 2010) or to perform alternating ankle dorsiflexion/plantar flexion simulating walking (Wei et al., 2020) revealed activation of brainstem areas including the PPN and CNF during simulated gait and imagined fast

speed locomotion. Moreover, studies employing electrophysiological recordings of PPN neuronal activity (and its surroundings) in PD patients that underwent DBS described increased single unit activity during imagined locomotion (Piallat et al., 2009). Finally, clinical case reports of patients with ischemic injury to the mesopontine tegmentum describe major gait phenotypes such as freezing and ataxia (Bhidayasiri et al., 2003; Kuo et al., 2008; Masdeu et al., 1994). Therefore, evidence from human studies points towards the presence of a locomotion hotspot within the PPN/CNF region of the midbrain. Dissecting this region further, including probing for a potential connectivity with the basal ganglia, is certainly not possible with current human technology to investigate neuronal circuits. However, our and other recent studies have provided much more information on the organization and function of this complex mesencephalic region in the mouse and our findings explain the highly-variable and mostly disappointing outcomes reported for human PPN-DBS in PD.

According to our data and model for the organization of the PPN/mRT region, indiscriminate electrical stimulation of this region is not expected to produce relevant clinical benefit. Even overcoming the important question regarding the effects of electrical stimulation on the firing rate of local neurons and passing axons (Jakobs et al., 2019), the result of locally activating a region containing intermingled populations of projection neurons with different roles in naturalistic behavior is unlikely to produce a reliable, predictable outcome. Our data suggests that, in order to treat axial posture symptoms, the spinally-projecting neurons residing specifically within the PPN/mRT should be targeted. However, gait impairment improvement would require manipulation of locomotion-promoting medulla-projecting neurons, which spread across both the PPN/mRT and the CNF/pre-CNF regions. The outcome of manipulating the SNr-projecting neurons as a whole would be way more complex,

since many behaviors are encoded within this population. Interestingly, our optogenetic stimulation and inhibition experiments produced movement halt or uncontrolled multi-segment movements, respectively resembling the freezing and dyskinetic episodes, located oppositely in the spectrum of motor symptoms of PD. Therefore, studies investigating the effect of the parkinsonic state in the physiology of these neurons would be extremely important. If indeed freezing episodes entail transient overactivation of the SNr-projecting population in the PPN/mRT or dyskinesias correlate with their suppression, these would constitute new entry-points to treat these symptoms.

Outlook

The current era of basic neurosciences research, where it is possible to use genetic entry points to probe neuronal circuits, is allowing the scientific community to uncover new circuits and to revisit previously known ones and describe them with further detail. This is simultaneously providing solutions to previously unanswered questions and revealing new layers of complexity of the CNS organization that lead to new questions. While clinical neurosciences are also evolving, they are not able to keep up with the exploding knowledge that basic sciences are producing. PD is a circuit disorder that, like many movement, neuropsychiatric or other pathologies whose symptoms arise from neuronal circuit malfunctioning, is desperately waiting for more effective therapeutic tools to emerge from basic research that go beyond chemical or electric interventions and allow targeted manipulation of desired circuits/neuronal populations. The solution likely resides on genetic access to specific neurons. On this front, the most promising vectors to deliver genetic tools to manipulate human cells *in vivo* are adeno-associated viruses (AAVs) (Kotterman et

al., 2015; Lentz et al., 2012). However, a major limiting factor for this translation is the lack of genetic tools to apply the information gathered in animal studies to the clinical practice. In fact, some obstacles arise during the design of safe genetic tools for human use. Even circumventing common difficulties in the human gene therapy field, such as the immune response (Rabinowitz et al., 2019), the target tissue size or the difficulties assessing the efficiency and time course of gene expression, specific problems occur in the attempt to manipulate human neuronal circuits (Galvan et al., 2017). Firstly, the absence of a transgenic approach to express recombinases in specific populations makes selective neuronal targeting more challenging. Possible strategies might rely on cell-type specific gene promoters and retrograde labeling based on target specificity. Secondly, the existence of a blood-brain barrier highly conditions the delivery strategy. While stereotaxic injections can be a solution to deliver AAVs to a specific location, such as the STN in PD (LeWitt et al., 2011; Niethammer et al., 2017), targeting bigger structures or neurons diffusely spread across the CNS requires a different approach. On this note, AAV variants able to cross the blood-brain barrier are being developed and may be appropriate for intravenous administration, allowing for AAV delivery across the CNS (Chan et al., 2017; Deverman et al., 2016). Thirdly, it is possible that AAVs that effectively target specific mouse neuronal populations do not display the same specificity in targeting human cells. Given that the mouse is the mammal model with the widest array of genetic tools developed, this can be a serious issue, when pursuing clinical translation of this technology. In fact, evidence from the retina shows that the ability of an AAV to target a specific neuronal population in mice does not predict the same specificity in the human retina; however, the efficiency in targeting NHP neuronal populations is a good predictor of the outcome in the human retina (Juttner et al., 2019). Therefore, one

important step in the quest to apply the cell-type specific interventions developed in murine models to human patients seems to be the validation of the genetic tools in NHP models and, in fact, the community developing optogenetic tools for NHP is collaborating in an attempt to accelerate the process (Tremblay et al., 2020).

While the clinical translation of all the vast knowledge acquired with cell-type specific access to neuronal circuits is still not available, progress is being made on this front. As of May 2021, there are 152 clinical trials testing AAVs registered at the NIH database ClinicalTrials.gov, approximately 20% of them targeting the human brain. Specifically for movement disorders, novel techniques for future gene therapy are being developed (Kaplitt, 2019). Of note, the first gene therapy trial for the treatment of neurological diseases in humans was for PD patients (Kaplitt et al., 2007).

One possible metaphor for the current state of basic and clinical neuroscientific research is the scenario of a castle surrounded by water and infested with a mosquito plague. All the inhabitants have to protect themselves from mosquito bites are poorly effective little swatters and dynamite sticks. Even though people inside the castle have to survive juggling between using ineffective and dangerous tools, there are highly qualified extermination squads outside the castle, equipped with selective insecticide sprays that only target mosquitoes, but there is no bridge they can use to access the castle. As time goes by, new and more elegant insecticides are being developed that also target fleas or all kinds of insects, and perhaps someone discovered a new insecticide that repurposes the insects towards disliking human blood and attacking each other, but the bridge that will deliver these tools to the castle is still incomplete. It is expected that the arsenal of genetic tools will be developed and validated for use in human patients in the near future, therefore completing the missing bridge that will allow us to selectively target the plague/have better control over neurological diseases.

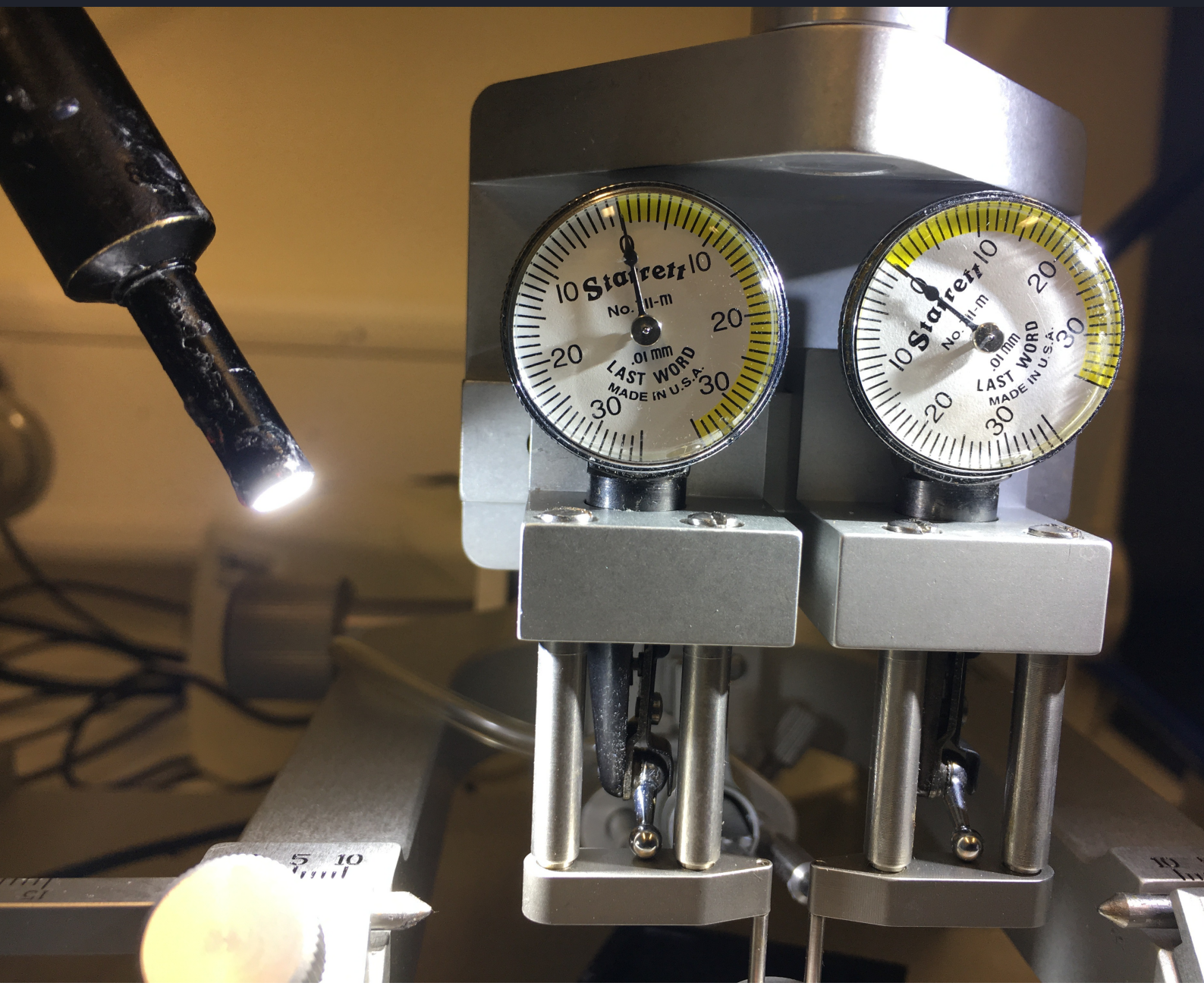

References

Alam, M., Schwabe, K., and Krauss, J.K. (2011). The pedunculopontine nucleus area: critical evaluation of interspecies differences relevant for its use as a target for deep brain stimulation. Brain *134*, 11-23.

Alaynick, W.A., Jessell, T.M., and Pfaff, S.L. (2011). SnapShot: spinal cord development. Cell *146*, 178-178 e171.

Albin, R.L., Young, A.B., and Penney, J.B. (1989). The functional anatomy of basal ganglia disorders. Trends Neurosci *12*, 366-375.

Ampatzis, K., Song, J., Ausborn, J., and El Manira, A. (2013). Pattern of innervation and recruitment of different classes of motoneurons in adult zebrafish. J Neurosci *33*, 10875-10886.

Ampatzis, K., Song, J., Ausborn, J., and El Manira, A. (2014). Separate microcircuit modules of distinct v2a interneurons and motoneurons control the speed of locomotion. Neuron *83*, 934-943.

Arber, S. (2012). Motor Circuits in Action: Specification, Connectivity, and Function. Neuron *74*, 975-989.

Arber, S., and Costa, R.M. (2018). Connecting neuronal circuits for movement. Science *360*, 1403-1404.

Assous, M., Dautan, D., Tepper, J.M., and Mena-Segovia, J. (2019). Pedunculopontine glutamatergic neurons provide a novel source of feedforward inhibition in the striatum by selectively targeting interneurons. J Neurosci *39*, 4727-4737.

Barbera, G., Liang, B., Zhang, L., Gerfen, C.R., Culurciello, E., Chen, R., Li, Y., and Lin, D.T. (2016). Spatially Compact Neural Clusters in the Dorsal Striatum Encode Locomotion Relevant Information. Neuron *92*, 202-213.

Bard, P., and Macht, M.B. (1958). The Behaviour of Chronically Decerebrate Cats. In Neurological Basis of Behaviour, M.A. G. E. W. Wolstenholme O.B.E., M.B., B.Ch. Cecilia M. O'Connor B.Sc., ed., pp. 55-71.

Barton, R.A., and Harvey, P.H. (2000). Mosaic evolution of brain structure in mammals. Nature *405*, 1055-1058.

Basaldella, E., Takeoka, A., Sigrist, M., and Arber, S. (2015). Multisensory Signaling Shapes Vestibulo-Motor Circuit Specificity. Cell *163*, 301-312.

Bellardita, C., and Kiehn, O. (2015). Phenotypic characterization of speed-associated gait changes in mice reveals modular organization of locomotor networks. Curr Biol *25*, 1426-1436.

Bhidayasiri, R., Hathout, G., Cohen, S.N., and Tourtellotte, W.W. (2003). Midbrain ataxia: possible role of the pedunculopontine nucleus in human locomotion. Cerebrovasc Dis *16*, 95-96.

Bikoff, J.B., Gabitto, M.I., Rivard, A.F., Drobac, E., Machado, T.A., Miri, A., Brenner-Morton, S., Famojure, E., Diaz, C., Alvarez, F.J.*, et al.* (2016). Spinal Inhibitory Interneuron Diversity Delineates Variant Motor Microcircuits. Cell *165*, 207-219.

Bouvier, J., Caggiano, V., Leiras, R., Caldeira, V., Bellardita, C., Balueva, K., Fuchs, A., and Kiehn, O. (2015). Descending Command Neurons in the Brainstem that Halt Locomotion. Cell *163*, 1191-1203.

Braak, H., Del Tredici, K., Bratzke, H., Hamm-Clement, J., Sandmann-Keil, D., and Rub, U. (2002). Staging of the intracerebral inclusion body pathology associated with idiopathic Parkinson's disease (preclinical and clinical stages). J Neurol *249 Suppl 3*, III/1-5.

Bretzner, F., and Drew, T. (2005). Contribution of the motor cortex to the structure and the timing of hindlimb locomotion in the cat: a microstimulation study. Journal of neurophysiology *94*, 657-672.

Brocard, F., and Dubuc, R. (2003). Differential contribution of reticulospinal cells to the control of locomotion induced by the mesencephalic locomotor region. Journal of neurophysiology *90*, 1714-1727.

Brownstone, R.M., and Chopek, J.W. (2018). Reticulospinal Systems for Tuning Motor Commands. Front Neural Circuits *12*, 30.

Caggiano, V., Leiras, R., Goñi-Erro, H., Masini, D., Bellardita, C., Bouvier, J., Caldeira, V., Fisone, G., and Kiehn, O. (2018). Midbrain circuits that set locomotor speed and gait selection. Nature *553*, 455-460.

Capelli, P., Pivetta, C., Soledad Esposito, M., and Arber, S. (2017). Locomotor speed control circuits in the caudal brainstem. Nature *551*, 373-377.

Carvalho, M.M., Tanke, N., Kropff, E., Witter, M.P., Moser, M.B., and Moser, E.I. (2020). A Brainstem Locomotor Circuit Drives the Activity of Speed Cells in the Medial Entorhinal Cortex. Cell Rep *32*, 108123.

Cazorla, M., de Carvalho, F.D., Chohan, M.O., Shegda, M., Chuhma, N., Rayport, S., Ahmari, S.E., Moore, H., and Kellendonk, C. (2014). Dopamine D2 receptors regulate the anatomical and functional balance of basal ganglia circuitry. Neuron *81*, 153-164.

Chakravarthy, V.S., Joseph, D., and Bapi, R.S. (2010). What do the basal ganglia do? A modeling perspective. Biol Cybern *103*, 237-253.

Challis, R.C., Ravindra Kumar, S., Chan, K.Y., Challis, C., Beadle, K., Jang, M.J., Kim, H.M., Rajendran, P.S., Tompkins, J.D., Shivkumar, K.*, et al.* (2019). Systemic AAV vectors for widespread and targeted gene delivery in rodents. Nat Protoc *14*, 379-414.

Chan, K.Y., Jang, M.J., Yoo, B.B., Greenbaum, A., Ravi, N., Wu, W.L., Sanchez-Guardado, L., Lois, C., Mazmanian, S.K., Deverman, B.E.*, et al.* (2017). Engineered AAVs for efficient noninvasive gene delivery to the central and peripheral nervous systems. Nat Neurosci *20*, 1172-1179.

Chang, S.J., Cajigas, I., Opris, I., Guest, J.D., and Noga, B.R. (2020). Dissecting Brainstem Locomotor Circuits: Converging Evidence for Cuneiform Nucleus Stimulation. Front Syst Neurosci *14*, 64.

Choi, J.T., and Bastian, A.J. (2007). Adaptation reveals independent control networks for human walking. Nat Neurosci *10*, 1055-1062.

Cohen, J.Y., Haesler, S., Vong, L., Lowell, B.B., and Uchida, N. (2012). Neuron-type-specific signals for reward and punishment in the ventral tegmental area. Nature *482*, 85-88.

Costa, R.M., Lin, S.-C., Sotnikova, T.D., Cyr, M., Gainetdinov, R.R., Caron, M.G., and Nicolelis, M.A.L. (2006). Rapid Alterations in Corticostriatal Ensemble Coordination during Acute Dopamine-Dependent Motor Dysfunction. Neuron *52*, 359-369.

Courtine, G., Roy, R.R., Raven, J., Hodgson, J., McKay, H., Yang, H., Zhong, H., Tuszynski, M.H., and Edgerton, V.R. (2005). Performance of locomotion and foot grasping following a unilateral thoracic corticospinal tract lesion in monkeys (Macaca mulatta). Brain *128*, 2338-2358.

Crone, S.A., Zhong, G., Harris-Warrick, R., and Sharma, K. (2009). In mice lacking V2a interneurons, gait depends on speed of locomotion. J Neurosci *29*, 7098-7109.

Cui, G., Jun, S.B., Jin, X., Pham, M.D., Vogel, S.S., Lovinger, D.M., and Costa, R.M. (2013). Concurrent activation of striatal direct and indirect pathways during action initiation. Nature *494*, 238-242.

D'Elia, K.P., and Dasen, J.S. (2018). Development, functional organization, and evolution of vertebrate axial motor circuits. Neural Dev *13*, 10.

da Silva, J.A., Tecuapetla, F., Paixao, V., and Costa, R.M. (2018). Dopamine neuron activity before action initiation gates and invigorates future movements. Nature *554*, 244-248.

Dana, H., Sun, Y., Mohar, B., Hulse, B.K., Kerlin, A.M., Hasseman, J.P., Tsegaye, G., Tsang, A., Wong, A., Patel, R.*, et al.* (2019). High-performance calcium sensors for imaging activity in neuronal populations and microcompartments. Nat Methods *16*, 649-657.

Dauer, W., and Przedborski, S. (2003). Parkinson's disease: mechanisms and models. Neuron *39*, 889-909.

Dautan, D., Souza, A.S., Huerta-Ocampo, I., Valencia, M., Assous, M., Witten, I.B., Deisseroth, K., Tepper, J.M., Bolam, J.P., Gerdjikov, T.V.*, et al.* (2016). Segregated cholinergic transmission modulates dopamine neurons integrated in distinct functional circuits. Nat Neurosci *19*, 1025-1033.

Deliagina, T.G., Zelenin, P.V., Fagerstedt, P., Grillner, S., and Orlovsky, G.N. (2000). Activity of reticulospinal neurons during locomotion in the freely behaving lamprey. Journal of neurophysiology *83*, 853-863.

DeLong, M.R. (1990). Primate models of movement disorders of basal ganglia origin. Trends Neurosci *13*, 281-285.

Depoortere, R., Sandner, G., and Di Scala, G. (1990). Aversion induced by electrical stimulation of the mesencephalic locomotor region in the intact and freely moving rat. Physiol Behav *47*, 561-567.

Deverman, B.E., Pravdo, P.L., Simpson, B.P., Kumar, S.R., Chan, K.Y., Banerjee, A., Wu, W.L., Yang, B., Huber, N., Pasca, S.P.*, et al.* (2016). Cre-dependent selection yields AAV variants for widespread gene transfer to the adult brain. Nat Biotechnol *34*, 204-209.

Dietz, C., and Berthold, M.R. (2016). KNIME for Open-Source Bioimage Analysis: A Tutorial. Advances in anatomy, embryology, and cell biology *219*, 179-197.

Dietz, V. (2010). Behavior of spinal neurons deprived of supraspinal input. Nature Rev Neurol *6*, 167-174.

Dodson, P.D., Dreyer, J.K., Jennings, K.A., Syed, E.C.J., Wade-Martins, R., Cragg, S.J., Bolam, J.P., and Magill, P.J. (2016). Representation of spontaneous movement by dopaminergic neurons is cell-type selective and disrupted in parkinsonism. PNAS *113*, E2180-E2188.

Drew, T., Andujar, J.E., Lajoie, K., and Yakovenko, S. (2008). Cortical mechanisms involved in visuomotor coordination during precision walking. Brain Res Rev *57*, 199-211.

Drew, T., and Marigold, D.S. (2015). Taking the next step: cortical contributions to the control of locomotion. Curr Opin Neurobiol *33*, 25-33.

Drew, T., and Rossignol, S. (1990). Functional organization within the medullary reticular formation of intact unanesthetized cat. I. Movements evoked by microstimulation. Journal of neurophysiology *64*, 767-781.

Esposito, M.S., Capelli, P., and Arber, S. (2014). Brainstem nucleus MdV mediates skilled forelimb motor tasks. Nature *508*, 351-356.

Evans, D.A., Stempel, A.V., Vale, R., Ruehle, S., Lefler, Y., and Branco, T. (2018). A synaptic threshold mechanism for computing escape decisions. Nature *558*, 590-594.

Fadok, J.P., Markovic, M., Tovote, P., and Luthi, A. (2018). New perspectives on central amygdala function. Curr Opin Neurobiol *49*, 141-147.

Fenno, L.E., Mattis, J., Ramakrishnan, C., Hyun, M., Lee, S.Y., He, M., Tucciarone, J., Selimbeyoglu, A., Berndt, A., Grosenick, L.*, et al.* (2014). Targeting cells with single vectors using multiple-feature Boolean logic. Nat Methods *11*, 763-772.

Ferraye, M.U., Debu, B., Fraix, V., Goetz, L., Ardouin, C., Yelnik, J., Henry-Lagrange, C., Seigneuret, E., Piallat, B., Krack, P.*, et al.* (2010). Effects of pedunculopontine nucleus area stimulation on gait disorders in Parkinson's disease. Brain *133*, 205-214.

Ferreira-Pinto, M.J., Ruder, L., Capelli, P., and Arber, S. (2018). Connecting Circuits for Supraspinal Control of Locomotion. Neuron *100*, 361-374.

Forssberg, H., Grillner, S., Halbertsma, J., and Rossignol, S. (1980). The locomotion of the low spinal cat. II. Interlimb coordination. Acta physiologica Scandinavica *108*, 283-295.

Francius, C., Harris, A., Rucchin, V., Hendricks, T.J., Stam, F.J., Barber, M., Kurek, D., Grosveld, F.G., Pierani, A., Goulding, M.*, et al.* (2013). Identification of multiple subsets of ventral interneurons and differential distribution along the rostrocaudal axis of the developing spinal cord. PloS one *8*, e70325.

Franklin, K.B., and Paxinos, G. (2007). The Mouse Brain in Stereotaxic Coordinates, 3rd edn (San Diego: Elsevier).

Franzini, A., Messina, G., Zekaj, E., Romito, L., and Cordella, R. (2011). Improvement of hand dexterity induced by stimulation of the peduncolopontine nucleus in a patient with advanced Parkinson's disease and previous long-lasting bilateral subthalamic DBS. Acta Neurochir (Wien) *153*, 1587-1590.

Freeze, B.S., Kravitz, A.V., Hammack, N., Berke, J.D., and Kreitzer, A.C. (2013). Control of basal ganglia output by direct and indirect pathway projection neurons. J Neurosci *33*, 18531-18539.

Gahtan, E., and Baier, H. (2004). Of lasers, mutants, and see-through brains: functional neuroanatomy in zebrafish. J Neurobiol *59*, 147-161.

Galvan, A., Stauffer, W.R., Acker, L., El-Shamayleh, Y., Inoue, K.I., Ohayon, S., and Schmid, M.C. (2017). Nonhuman Primate Optogenetics: Recent Advances and Future Directions. J Neurosci *37*, 10894-10903.

Garcia-Rill, E., Houser, C.R., Skinner, R.D., Smith, W., and Woodward, D.J. (1987). Locomotion-inducing sites in the vicinity of the pedunculopontine nucleus. Brain Res Bull *18*, 731-738.

Garcia-Rill, E., Saper, C.B., Rye, D.B., Kofler, M., Nonnekes, J., Lozano, A., Valls-Sole, J., and Hallett, M. (2019). Focus on the pedunculopontine nucleus. Consensus review from the May 2018 brainstem society meeting in Washington, DC, USA. Clin Neurophysiol *130*, 925-940.

Garcia-Rill, E., and Skinner, R.D. (1987). The mesencephalic locomotor region. I. Activation of a medullary projection site. Brain Res *411*, 1-12.

Garcia-Rill, E., Skinner, R.D., and Fitzgerald, J.A. (1985). Chemical activation of the mesencephalic locomotor region. Brain Res *330*, 43-54.

Gerfen, C.R., Paletzki, R., and Heintz, N. (2013). GENSAT BAC cre-recombinase driver lines to study the functional organization of cerebral cortical and basal ganglia circuits. Neuron *80*, 1368-1383.

Giber, K., Diana, M.A., Plattner, V., Dugue, G.P., Bokor, H., Rousseau, C.V., Magloczky, Z., Havas, L., Hangya, B., Wildner, H.*, et al.* (2015). A subcortical inhibitory signal for behavioral arrest in the thalamus. Nat Neurosci *18*, 562-568.

Goedert, M. (2015). NEURODEGENERATION. Alzheimer's and Parkinson's diseases: The prion concept in relation to assembled Abeta, tau, and alpha-synuclein. Science *349*, 1255555.

Golestanirad, L., Elahi, B., Graham, S.J., Das, S., and Wald, L.L. (2016). Efficacy and Safety of Pedunculopontine Nuclei (PPN) Deep Brain Stimulation in the Treatment of Gait Disorders: A Meta-Analysis of Clinical Studies. Can J Neurol Sci *43*, 120-126.

Goulding, M. (2009). Circuits controlling vertebrate locomotion: moving in a new direction. Nature Rev Neurosci *10*, 507-518.

Grillner, S. (1975). Locomotion in vertebrates: central mechanisms and reflex interaction. Physiol Rev *55*, 247-304.

Grillner, S. (2003). The motor infrastructure: from ion channels to neuronal networks. Nat Rev Neurosci *4*, 573-586.

Grillner, S., Georgopoulos, A.P., and Jordan, L.M. (1997). Selection and initiation of motor behavior. In Neurons, networks, and motor behavior, P.S.G. Stein, S. Grillner, A.I. Selverston, and D.G. Stuart, eds. (Cambridge: The MIT Press), pp. 3-19.

Grillner, S., and Jessell, T.M. (2009). Measured motion: searching for simplicity in spinal locomotor networks. Curr Opin Neurobiol *19*, 572-586.

Halbertsma, J.M. (1983). The stride cycle of the cat: the modelling of locomotion by computerized analysis of automatic recordings. Acta physiologica Scandinavica *521*, 1-75.

Hale, M.E., Katz, H.R., Peek, M.Y., and Fremont, R.T. (2016). Neural circuits that drive startle behavior, with a focus on the Mauthner cells and spiral fiber neurons of fishes. J Neurogenet *30*, 89-100.

Han, W., Tellez, L.A., Rangel, M.J., Jr., Motta, S.C., Zhang, X., Perez, I.O., Canteras, N.S., Shammah-Lagnado, S.J., van den Pol, A.N., and de Araujo, I.E. (2017). Integrated Control of Predatory Hunting by the Central Nucleus of the Amygdala. Cell *168*, 311-324 e318.

Hayashi, M., Hinckley, C.A., Driscoll, S.P., Moore, N.J., Levine, A.J., Hilde, K.L., Sharma, K., and Pfaff, S.L. (2018). Graded Arrays of Spinal and Supraspinal V2a Interneuron Subtypes Underlie Forelimb and Hindlimb Motor Control. Neuron *97*, 869-884.e865.

Hikosaka, O. (2007). GABAergic output of the basal ganglia. Prog Brain Res *160*, 209-226.

Hikosaka, O., Takikawa, Y., and Kawagoe, R. (2000). Role of the basal ganglia in the control of purposive saccadic eye movements. Physiol Rev *80*, 953-978.

Hirsch, E.C., Graybiel, A.M., Duyckaerts, C., and Javoy-Agid, F. (1987). Neuronal loss in the pedunculopontine tegmental nucleus in Parkinson disease and in progressive supranuclear palsy. Proc Natl Acad Sci U S A *84*, 5976-5980.

Howe, M.W., and Dombeck, D.A. (2016). Rapid signalling in distinct dopaminergic axons during locomotion and reward. Nature *535*, 505-510.

Jahn, K., Deutschlander, A., Stephan, T., Kalla, R., Wiesmann, M., Strupp, M., and Brandt, T. (2008). Imaging human supraspinal locomotor centers in brainstem and cerebellum. Neuroimage *39*, 786-792.

Jakobs, M., Fomenko, A., Lozano, A.M., and Kiening, K.L. (2019). Cellular, molecular, and clinical mechanisms of action of deep brain stimulation-a systematic review on established indications and outlook on future developments. EMBO Mol Med *11*.

Jessell, T.M. (2000). Neuronal specification in the spinal cord: inductive signals and transcriptional codes. Nature Rev Genetics *1*, 20-29.

Jin, X., Tecuapetla, F., and Costa, R.M. (2014). Basal ganglia subcircuits distinctively encode the parsing and concatenation of action sequences. Nat Neurosci *17*, 423-430.

Jordan, L.M. (1998). Initiation of locomotion in mammals. Ann N Y Acad Sci *860*, 83-93.

Josset, N., Roussel, M., Lemieux, M., Lafrance-Zoubga, D., Rastqar, A., and Bretzner, F. (2018). Distinct Contributions of Mesencephalic Locomotor Region Nuclei to Locomotor Control in the Freely Behaving Mouse. Curr Biol *28*, 884-901 e883.

Juttner, J., Szabo, A., Gross-Scherf, B., Morikawa, R.K., Rompani, S.B., Hantz, P., Szikra, T., Esposti, F., Cowan, C.S., Bharioke, A.*, et al.* (2019). Targeting neuronal and glial cell types with synthetic promoter AAVs in mice, non-human primates and humans. Nat Neurosci *22*, 1345-1356.

Juvin, L., Gratsch, S., Trillaud-Doppia, E., Gariepy, J.F., Buschges, A., and Dubuc, R. (2016). A Specific Population of Reticulospinal Neurons Controls the Termination of Locomotion. Cell Rep *15*, 2377-2386.

Kaplitt, M.G. (2019). Gene-targeting approaches for movement disorders: recent advances. Curr Opin Neurol *32*, 566-570.

Kaplitt, M.G., Feigin, A., Tang, C., Fitzsimons, H.L., Mattis, P., Lawlor, P.A., Bland, R.J., Young, D., Strybing, K., Eidelberg, D.*, et al.* (2007). Safety and tolerability of gene therapy with an adeno-associated virus (AAV) borne GAD gene for Parkinson's disease: an open label, phase I trial. Lancet *369*, 2097-2105.

Karachi, C., Grabli, D., Bernard, F.A., Tande, D., Wattiez, N., Belaid, H., Bardinet, E., Prigent, A., Nothacker, H.P., Hunot, S.*, et al.* (2010). Cholinergic mesencephalic neurons are involved in gait and postural disorders in Parkinson disease. J Clin Invest *120*, 2745-2754.

Karigo, T., Kennedy, A., Yang, B., Liu, M., Tai, D., Wahle, I.A., and Anderson, D.J. (2021). Distinct hypothalamic control of same- and opposite-sex mounting behaviour in mice. Nature *589*, 258-263.

Kiehn, O. (2016). Decoding the organization of spinal circuits that control locomotion. Nature reviews Neuroscience *17*, 224-238.

Kinjo, N., Atsuta, Y., Webber, M., Kyle, R., Skinner, R.D., and Garcia-Rill, E. (1990). Medioventral medulla-induced locomotion. Brain Res Bull *24*, 509-516.

Klaus, A., Martins, G.J., Paixao, V.B., Zhou, P., Paninski, L., and Costa, R.M. (2017a). The Spatiotemporal Organization of the Striatum Encodes Action Space. Neuron *96*, 949.

Klaus, A., Martins, G.J., Paixao, V.B., Zhou, P., Paninski, L., and Costa, R.M. (2017b). The Spatiotemporal Organization of the Striatum Encodes Action Space. Neuron *95*, 1171-1180 e1177.

Koch, S.C., Del Barrio, M.G., Dalet, A., Gatto, G., Günther, T., Zhang, J., Seidler, B., Saur, D., Schüle, R., and Goulding, M. (2017). RORβ Spinal Interneurons Gate Sensory Transmission during Locomotion to Secure a Fluid Walking Gait. Neuron *96*, 1419-1431.e1415.

Kotterman, M.A., Chalberg, T.W., and Schaffer, D.V. (2015). Viral Vectors for Gene Therapy: Translational and Clinical Outlook. Annu Rev Biomed Eng *17*, 63-89.

Kravitz, A.V., Freeze, B.S., Parker, P.R., Kay, K., Thwin, M.T., Deisseroth, K., and Kreitzer, A.C. (2010). Regulation of parkinsonian motor behaviours by optogenetic control of basal ganglia circuitry. Nature *466*, 622-626.

Kreitzer, A.C., and Malenka, R.C. (2008). Striatal plasticity and basal ganglia circuit function. Neuron *60*, 543-554.

Kuo, S.H., Kenney, C., and Jankovic, J. (2008). Bilateral pedunculopontine nuclei strokes presenting as freezing of gait. Mov Disord *23*, 616-619.

Le Ray, D., Brocard, F., Bourcier-Lucas, C., Auclair, F., Lafaille, P., and Dubuc, R. (2003). Nicotinic activation of reticulospinal cells involved in the control of swimming in lampreys. Eur J Neurosci *17*, 137-148.

Le Ray, D., Juvin, L., Ryczko, D., and Dubuc, R. (2011). Chapter 4--supraspinal control of locomotion: the mesencephalic locomotor region. Prog Brain Res *188*, 51-70.

Lee, A.M., Hoy, J.L., Bonci, A., Wilbrecht, L., Stryker, M.P., and Niell, C.M. (2014). Identification of a brainstem circuit regulating visual cortical state in parallel with locomotion. Neuron *83*, 455-466.

Lemieux, M., Josset, N., Roussel, M., Couraud, S., and Bretzner, F. (2016). Speed-Dependent Modulation of the Locomotor Behavior in Adult Mice Reveals Attractor and Transitional Gaits. Frontiers in Neurosci *10*, 42.

Lentz, T.B., Gray, S.J., and Samulski, R.J. (2012). Viral vectors for gene delivery to the central nervous system. Neurobiol Dis *48*, 179-188.

LeWitt, P.A., Rezai, A.R., Leehey, M.A., Ojemann, S.G., Flaherty, A.W., Eskandar, E.N., Kostyk, S.K., Thomas, K., Sarkar, A., Siddiqui, M.S.*, et al.* (2011). AAV2-GAD gene therapy for advanced Parkinson's disease: a double-blind, sham-surgery controlled, randomised trial. Lancet Neurol *10*, 309-319.

Li, Y., Zeng, J., Zhang, J., Yue, C., Zhong, W., Liu, Z., Feng, Q., and Luo, M. (2018). Hypothalamic Circuits for Predation and Evasion. Neuron *97*, 911-924 e915.

Liang, H., Paxinos, G., and Watson, C. (2012). Spinal projections from the presumptive midbrain locomotor region in the mouse. Brain Struct Funct *217*, 211-219.

Lin, J.Y., Knutsen, P.M., Muller, A., Kleinfeld, D., and Tsien, R.Y. (2013). ReaChR: a red-shifted variant of channelrhodopsin enables deep transcranial optogenetic excitation. Nat Neurosci *16*, 1499-1508.

Lozano, A.M., Hutchison, W.D., and Kalia, S.K. (2017). What Have We Learned About Movement Disorders from Functional Neurosurgery? Annu Rev Neurosci *40*, 453-477.

Mahn, M., Gibor, L., Patil, P., Cohen-Kashi Malina, K., Oring, S., Printz, Y., Levy, R., Lampl, I., and Yizhar, O. (2018). High-efficiency optogenetic silencing with soma-targeted anion-conducting channelrhodopsins. Nat Commun *9*, 4125.

Mallet, N., Micklem, B.R., Henny, P., Brown, M.T., Williams, C., Bolam, J.P., Nakamura, K.C., and Magill, P.J. (2012). Dichotomous organization of the external globus pallidus. Neuron *74*, 1075-1086.

Martinez-Gonzalez, C., Bolam, J.P., and Mena-Segovia, J. (2011). Topographical organization of the pedunculopontine nucleus. Front Neuroanat *5*, 22.

Masdeu, J.C., Alampur, U., Cavaliere, R., and Tavoulareas, G. (1994). Astasia and gait failure with damage of the pontomesencephalic locomotor region. Ann Neurol *35*, 619-621.

Mathis, A., Mamidanna, P., Cury, K.M., Abe, T., Murthy, V.N., Mathis, M.W., and Bethge, M. (2018). DeepLabCut: markerless pose estimation of user-defined body parts with deep learning. Nat Neurosci *21*, 1281-1289.

Matsuyama, K., and Drew, T. (2000). Vestibulospinal and reticulospinal neuronal activity during locomotion in the intact cat. I. Walking on a level surface. Journal of neurophysiology *84*, 2237-2256.

Mazzone, P., Lozano, A., Stanzione, P., Galati, S., Scarnati, E., Peppe, A., and Stefani, A. (2005). Implantation of human pedunculopontine nucleus: a safe and clinically relevant target in Parkinson's disease. Neuroreport *16*, 1877-1881.

McElvain, L.E., Chen, Y., Moore, J.D., Brigidi, G.S., Bloodgood, B.L., Lim, B.K., Costa, R.M., and Kleinfeld, D. (2021). Specific populations of basal ganglia output neurons target distinct

brain stem areas while collateralizing throughout the diencephalon. Neuron *109*, 1721-1738 e1724.

Mena-Segovia, J., and Bolam, J.P. (2017). Rethinking the Pedunculopontine Nucleus: From Cellular Organization to Function. Neuron *94*, 7-18.

Mena-Segovia, J., Sims, H.M., Magill, P.J., and Bolam, J.P. (2008). Cholinergic brainstem neurons modulate cortical gamma activity during slow oscillations. J Physiol *586*, 2947-2960.

Mendoza, G., and Merchant, H. (2014). Motor system evolution and the emergence of high cognitive functions. Prog Neurobiol *122*, 73-93.

Miller, S., and van der Meché, F.G.A. (1976). Coordinated stepping of all four limbs in the high spinal cat. Brain research *109*, 395-398.

Miri, A., Warriner, C.L., Seely, J.S., Elsayed, G.F., Cunningham, J.P., Churchland, M.M., and Jessell, T.M. (2017). Behaviorally Selective Engagement of Short-Latency Effector Pathways by Motor Cortex. Neuron *95*, 683-696 e611.

Moehle, M.S., Pancani, T., Byun, N., Yohn, S.E., Wilson, G.H., 3rd, Dickerson, J.W., Remke, D.H., Xiang, Z., Niswender, C.M., Wess, J.*, et al.* (2017). Cholinergic Projections to the Substantia Nigra Pars Reticulata Inhibit Dopamine Modulation of Basal Ganglia through the M4 Muscarinic Receptor. Neuron *96*, 1358-1372 e1354.

Mori, S. (1987). Integration of posture and locomotion in acute decerebrate cats and in awake, freely moving cats. Prog Neurobiol *28*, 161-195.

Mori, S. (1989). Contribution of postural muscle tone to full expression of posture and locomotor movements: multi-faceted analyses of its setting brainstem-spinal cord mechanisms in the cat. Jpn J Physiol *39*, 785-809.

Mori, S., Kawahara, K., and Sakamoto, T. (1983). Supraspinal aspects of locomotion in the mesencephalic cat. Symp Soc Exp Biol *37*, 445-468.

Mori, S., Matsuyama, K., Kohyama, J., Kobayashi, Y., and Takakusaki, K. (1992). Neuronal constituents of postural and locomotor control systems and their interactions in cats. Brain Dev *14 Suppl*, S109-120.

Mori, S., Nishimura, H., Kurakami, C., Yamamura, T., and Aoki, M. (1978). Controlled locomotion in the mesencephalic cat: distribution of facilitatory and inhibitory regions within pontine tegmentum. J Neurophysiol *41*, 1580-1591.

Mori, S., Sakamoto, T., Ohta, Y., Takakusaki, K., and Matsuyama, K. (1989). Site-specific postural and locomotor changes evoked in awake, freely moving intact cats by stimulating the brainstem. Brain Res *505*, 66-74.

Niell, C.M., and Stryker, M.P. (2010). Modulation of visual responses by behavioral state in mouse visual cortex. Neuron *65*, 472-479.

Niethammer, M., Tang, C.C., LeWitt, P.A., Rezai, A.R., Leehey, M.A., Ojemann, S.G., Flaherty, A.W., Eskandar, E.N., Kostyk, S.K., Sarkar, A.*, et al.* (2017). Long-term follow-up of a randomized AAV2-GAD gene therapy trial for Parkinson's disease. JCI Insight *2*, e90133.

Noda, T., and Oka, H. (1984). Nigral inputs to the pedunculopontine region: intracellular analysis. Brain Res *322*, 332-336.

Noga, B.R., Kettler, J., and Jordan, L.M. (1988). Locomotion produced in mesencephalic cats by injections of putative transmitter substances and antagonists into the medial reticular formation and the pontomedullary locomotor strip. J Neurosci *8*, 2074-2086.

Noga, B.R., Turkson, R.P., Xie, S., Taberner, A., Pinzon, A., and Hentall, I.D. (2017). Monoamine Release in the Cat Lumbar Spinal Cord during Fictive Locomotion Evoked by the Mesencephalic Locomotor Region. Front Neural Circuits *11*, 59.

Nowacki, A., Galati, S., Ai-Schlaeppi, J., Bassetti, C., Kaelin, A., and Pollo, C. (2018). Pedunculopontine nucleus: An integrative view with implications on Deep Brain Stimulation. Neurobiol Dis *128*, 75-85.

Onodera, S., and Hicks, T.P. (2009). A comparative neuroanatomical study of the red nucleus of the cat, macaque and human. PLoS One *4*, e6623.

Oorschot, D.E. (1996). Total number of neurons in the neostriatal, pallidal, subthalamic, and substantia nigral nuclei of the rat basal ganglia: a stereological study using the cavalieri and optical disector methods. J Comp Neurol *366*, 580-599.

Opris, I., Dai, X., Johnson, D.M.G., Sanchez, F.J., Villamil, L.M., Xie, S., Lee-Hauser, C.R., Chang, S., Jordan, L.M., and Noga, B.R. (2019). Activation of Brainstem Neurons During Mesencephalic Locomotor Region-Evoked Locomotion in the Cat. Front Syst Neurosci *13*, 69.

Orlovsky, G.N., Deliagina, T.G., and Grillner, S. (1999). Neuronal control of locomotion: From mollusc to man, Vol Chapter 12 (Oxford: Oxford University Press).

Pamukcu, A., Cui, Q., Xenias, H.S., Berceau, B.L., Augustine, E.C., Fan, I., Chalasani, S., Hantman, A.W., Lerner, T.N., Boca, S.M.*, et al.* (2020). Parvalbumin(+) and Npas1(+) Pallidal Neurons Have Distinct Circuit Topology and Function. J Neurosci *40*, 7855-7876.

Parker, J.G., Marshall, J.D., Ahanonu, B., Wu, Y.W., Kim, T.H., Grewe, B.F., Zhang, Y., Li, J.Z., Ding, J.B., Ehlers, M.D.*, et al.* (2018). Diametric neural ensemble dynamics in parkinsonian and dyskinetic states. Nature *557*, 177-182.

Perreault, M.C., Drew, T., and Rossignol, S. (1993). Activity of medullary reticulospinal neurons during fictive locomotion. Journal of neurophysiology *69*, 2232-2247.

Philippidou, P., and Dasen, J.S. (2013). Hox genes: choreographers in neural development, architects of circuit organization. Neuron *80*, 12-34.

Piallat, B., Chabardes, S., Torres, N., Fraix, V., Goetz, L., Seigneuret, E., Bardinet, E., Ferraye, M., Debu, B., Krack, P.*, et al.* (2009). Gait is associated with an increase in tonic firing of the sub-cuneiform nucleus neurons. Neuroscience *158*, 1201-1205.

Pivetta, C., Esposito, M.S., Sigrist, M., and Arber, S. (2014). Motor-circuit communication matrix from spinal cord to brainstem neurons revealed by developmental origin. Cell *156*, 537-548.

Plaha, P., and Gill, S.S. (2005). Bilateral deep brain stimulation of the pedunculopontine nucleus for Parkinson's disease. Neuroreport *16*, 1883-1887.

Pnevmatikakis, E.A., Soudry, D., Gao, Y., Machado, T.A., Merel, J., Pfau, D., Reardon, T., Mu, Y., Lacefield, C., Yang, W.*, et al.* (2016). Simultaneous Denoising, Deconvolution, and Demixing of Calcium Imaging Data. Neuron *89*, 285-299.

Pocratsky, A.M., Burke, D.A., Morehouse, J.R., Beare, J.E., Riegler, A.S., Tsoulfas, P., States, G.J.R., Whittemore, S.R., and Magnuson, D.S.K. (2017). Reversible silencing of lumbar spinal interneurons unmasks a task-specific network for securing hindlimb alternation. Nat Commun *8*, 1963.

Rabinowitz, J., Chan, Y.K., and Samulski, R.J. (2019). Adeno-associated Virus (AAV) versus Immune Response. Viruses *11*.

Rajasethupathy, P., Sankaran, S., Marshel, J.H., Kim, C.K., Ferenczi, E., Lee, S.Y., Berndt, A., Ramakrishnan, C., Jaffe, A., Lo, M.*, et al.* (2015). Projections from neocortex mediate top-down control of memory retrieval. Nature *526*, 653-659.

Romanes, G.J. (1951). The motor cell columns of the lumbo-sacral spinal cord of the cat. J Comp Neurol *94*, 313-363.

Ros, H., Magill, P.J., Moss, J., Bolam, J.P., and Mena-Segovia, J. (2010). Distinct types of non-cholinergic pedunculopontine neurons are differentially modulated during global brain states. Neuroscience *170*, 78-91.

Roseberry, T.K., Lee, A.M., Lalive, A.L., Wilbrecht, L., Bonci, A., and Kreitzer, A.C. (2016). Cell-Type-Specific Control of Brainstem Locomotor Circuits by Basal Ganglia. Cell *164*, 526-537.

Ross, G.S., and Sinnamon, H.M. (1984). Forelimb and hindlimb stepping by the anesthetized rat elicited by electrical stimulation of the pons and medulla. Physiol Behav *33*, 201-208.

Rossignol, S. (2006). Dynamic Sensorimotor Interactions in Locomotion. Physiological reviews *86*, 89-154.

Ruder, L., Schina, R., Kanodia, H., Valencia-Garcia, S., Pivetta, C., and Arber, S. (2021). A functional map for diverse forelimb actions within brainstem circuitry. Nature *590*, 445-450.

Ruder, L., Takeoka, A., and Arber, S. (2016). Long-Distance Descending Spinal Neurons Ensure Quadrupedal Locomotor Stability. Neuron *92*, 1063-1078.

Ryczko, D., and Dubuc, R. (2013). The multifunctional mesencephalic locomotor region. Curr Pharm Des *19*, 4448-4470.

Shang, C., Chen, Z., Liu, A., Li, Y., Zhang, J., Qu, B., Yan, F., Zhang, Y., Liu, W., Liu, Z., *et al.* (2018). Divergent midbrain circuits orchestrate escape and freezing responses to looming stimuli in mice. Nat Commun *9*, 1232.

Shefchyk, S.J., Jell, R.M., and Jordan, L.M. (1984). Reversible cooling of the brainstem reveals areas required for mesencephalic locomotor region evoked treadmill locomotion. Exp Brain Res *56*, 257-262.

Shik, M.L., and Orlovsky, G.N. (1976). Neurophysiology of locomotor automatism. Physiological reviews *56*, 465-501.

Shik, M.L., Severin, F.V., and Orlovskii, G.N. (1966). [Control of walking and running by means of electric stimulation of the midbrain]. Biofizika *11*, 659-666.

Sinnamon, H.M. (1993). Preoptic and hypothalamic neurons and the initiation of locomotion in the anesthetized rat. Prog Neurobiol *41*, 323-344.

Skinner, R.D., and Garcia-Rill, E. (1984). The mesencephalic locomotor region (MLR) in the rat. Brain Res *323*, 385-389.

Smith, Y., Bevan, M.D., Shink, E., and Bolam, J.P. (1998). Microcircuitry of the direct and indirect pathways of the basal ganglia. Neuroscience *86*, 353-387.

Stuber, G.D., and Wise, R.A. (2016). Lateral hypothalamic circuits for feeding and reward. Nat Neurosci *19*, 198-205.

Svoboda, K., and Li, N. (2018). Neural mechanisms of movement planning: motor cortex and beyond. Curr Opin Neurobiol *49*, 33-41.

Sweeney, L.B., Bikoff, J.B., Gabitto, M.I., Brenner-Morton, S., Baek, M., Yang, J.H., Tabak, E.G., Dasen, J.S., Kintner, C.R., and Jessell, T.M. (2018). Origin and Segmental Diversity of Spinal Inhibitory Interneurons. Neuron *97*, 341-355.e343.

Takakusaki, K., Chiba, R., Nozu, T., and Okumura, T. (2016). Brainstem control of locomotion and muscle tone with special reference to the role of the mesopontine tegmentum and medullary reticulospinal systems. J Neural Transm (Vienna) *123*, 695-729.

Talpalar, A.E., Bouvier, J., Borgius, L., Fortin, G., Pierani, A., and Kiehn, O. (2013). Dual-mode operation of neuronal networks involved in left-right alternation. Nature *500*, 85-88.

Taverna, S., Ilijic, E., and Surmeier, D.J. (2008). Recurrent collateral connections of striatal medium spiny neurons are disrupted in models of Parkinson's disease. J Neurosci *28*, 5504-5512.

Tecuapetla, F., Jin, X., Lima, S.Q., and Costa, R.M. (2016). Complementary Contributions of Striatal Projection Pathways to Action Initiation and Execution. Cell *166*, 703-715.

Tecuapetla, F., Matias, S., Dugue, G.P., Mainen, Z.F., and Costa, R.M. (2014). Balanced activity in basal ganglia projection pathways is critical for contraversive movements. Nat Commun *5*, 4315.

Tervo, D.G., Hwang, B.Y., Viswanathan, S., Gaj, T., Lavzin, M., Ritola, K.D., Lindo, S., Michael, S., Kuleshova, E., Ojala, D.*, et al.* (2016). A Designer AAV Variant Permits Efficient Retrograde Access to Projection Neurons. Neuron *159*, 121-132.

Thevathasan, W., Debu, B., Aziz, T., Bloem, B.R., Blahak, C., Butson, C., Czernecki, V., Foltynie, T., Fraix, V., Grabli, D.*, et al.* (2018). Pedunculopontine nucleus deep brain stimulation in Parkinson's disease: A clinical review. Mov Disord *33*, 10-20.

Tovote, P., Esposito, M.S., Botta, P., Chaudun, F., Fadok, J.P., Markovic, M., Wolff, S.B., Ramakrishnan, C., Fenno, L., Deisseroth, K.*, et al.* (2016). Midbrain circuits for defensive behaviour. Nature *534*, 206-212.

Tremblay, S., Acker, L., Afraz, A., Albaugh, D.L., Amita, H., Andrei, A.R., Angelucci, A., Aschner, A., Balan, P.F., Basso, M.A.*, et al.* (2020). An Open Resource for Non-human Primate Optogenetics. Neuron *108*, 1075-1090 e1076.

Tubert, C., Galtieri, D., and Surmeier, D.J. (2019). The pedunclopontine nucleus and Parkinson's disease. Neurobiol Dis *128*, 3-8.

Wang, F., Zhu, J., Zhu, H., Zhang, Q., Lin, Z., and Hu, H. (2011). Bidirectional control of social hierarchy by synaptic efficacy in medial prefrontal cortex. Science *334*, 693-697.

Wang, H.L., and Morales, M. (2009). Pedunculopontine and laterodorsal tegmental nuclei contain distinct populations of cholinergic, glutamatergic and GABAergic neurons in the rat. Eur J Neurosci *29*, 340-358.

Wang, J.W., Zhang, Y.Q., Zhang, X.H., Wang, Y.P., Li, J.P., and Li, Y.J. (2017). Deep Brain Stimulation of Pedunculopontine Nucleus for Postural Instability and Gait Disorder After Parkinson Disease: A Meta-Analysis of Individual Patient Data. World Neurosurg *102*, 72-78.

Wang, L., Chen, I.Z., and Lin, D. (2015). Collateral pathways from the ventromedial hypothalamus mediate defensive behaviors. Neuron *85*, 1344-1358.

Wei, P., Zou, T., Lv, Z., and Fan, Y. (2020). Functional MRI Reveals Locomotion-Control Neural Circuits in Human Brainstem. Brain Sci *10*.

Windhorst, U. (2007). Muscle proprioceptive feedback and spinal networks. Brain research bulletin *73*, 155-202.

Xiao, C., Cho, J.R., Zhou, C., Treweek, J.B., Chan, K., McKinney, S.L., Yang, B., and Gradinaru, V. (2016). Cholinergic Mesopontine Signals Govern Locomotion and Reward through Dissociable Midbrain Pathways. Neuron *90*, 333-347.

Yoo, J.H., Zell, V., Wu, J., Punta, C., Ramajayam, N., Shen, X., Faget, L., Lilascharoen, V., Lim, B.K., and Hnasko, T.S. (2017). Activation of Pedunculopontine Glutamate Neurons Is Reinforcing. J Neurosci *37*, 38-46.

Yttri, E.A., and Dudman, J.T. (2016). Opponent and bidirectional control of movement velocity in the basal ganglia. Nature *533*, 402-406.

Yu, K., Ren, Z., Guo, S., Li, J., and Li, Y. (2020). Effects of pedunculopontine nucleus deep brain stimulation on gait disorders in Parkinson's Disease: A meta-analysis of the literature. Clin Neurol Neurosurg *198*, 106108.

Zhou, P., Resendez, S.L., Rodriguez-Romaguera, J., Jimenez, J.C., Neufeld, S.Q., Giovannucci, A., Friedrich, J., Pnevmatikakis, E.A., Stuber, G.D., Hen, R.*, et al.* (2018). Efficient and accurate extraction of in vivo calcium signals from microendoscopic video data. Elife *7*, e28728.